

AD-A119 996

IIT RESEARCH INST CHICAGO IL

F/G 11/4

NONDESTRUCTIVE EVALUATION OF METAL MATRIX COMPOSITES.(U)

MAY 82 S W SCHRAMM, I M DANIEL

DAA646-80-C-0070

UNCLASSIFIED

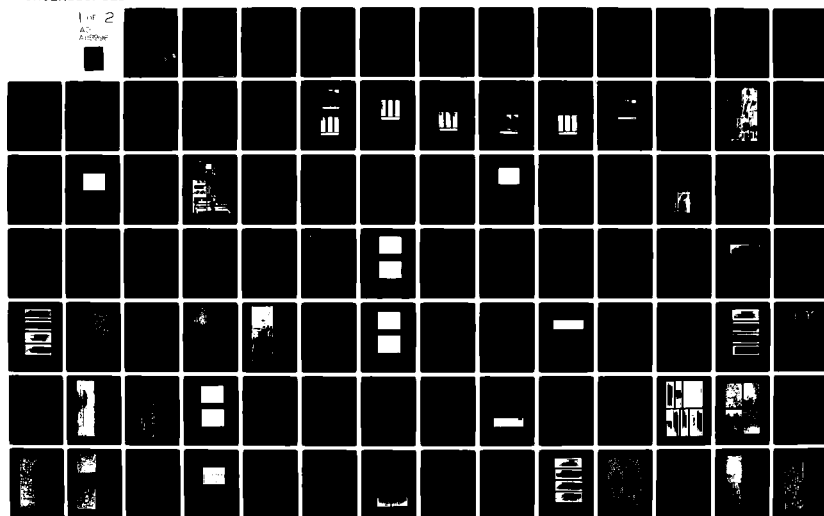
IITRI-M06084-14

AMMRC-TR-82-35

NL

1 of 2

AD
A119996



AD A119996



AD

AMMRC TR 82-35

NONDESTRUCTIVE EVALUATION OF METAL MATRIX COMPOSITES

May 1982

S. W. SCHRAMM and I. M. DANIEL
IIT Research Institute
10 West 35th Street
Chicago, Illinois 60616

FINAL REPORT

Contract No. DAAG46-80-C-0070

Approved for public release; distribution unlimited.

DTIC
ELECTE
OCT 7 1982
S H D

Prepared for

ARMY MATERIALS AND MECHANICS RESEARCH CENTER
Watertown, Massachusetts 02172

DTIC FILE COPY

82 10 07 018

The findings in this report are not to be construed as an official Department of the Army position, unless so designated by other authorized documents.

Mention of any trade names or manufacturers in this report shall not be construed as advertising nor as an official indorsement or approval of such products or companies by the United States Government.

DISPOSITION INSTRUCTIONS

Destroy this report when it is no longer needed.
Do not return it to the originator.

UNCLASSIFIED

SECURITY CLASSIFICATION OF THIS PAGE (When Data Entered)

REPORT DOCUMENTATION PAGE		READ INSTRUCTIONS BEFORE COMPLETING FORM
1. REPORT NUMBER AMMRC TR 82-35	2. GOVT ACCESSION NO. AD-A19796	3. RECIPIENT'S CATALOG NUMBER
4. TITLE (and Subtitle) NONDESTRUCTIVE EVALUATION OF METAL MATRIX COMPOSITES		5. TYPE OF REPORT & PERIOD COVERED Final Report - 1 Oct 80 to 31 Dec 81
		6. PERFORMING ORG. REPORT NUMBER IITRI-M06084-14
7. AUTHOR(s) S. W. Schramm and I. M. Daniel		8. CONTRACT OR GRANT NUMBER(s) DAAG46-80-C-0070
9. PERFORMING ORGANIZATION NAME AND ADDRESS IIT Research Institute 10 West 35th Street Chicago, Illinois 60616		10. PROGRAM ELEMENT, PROJECT, TASK AREA & WORK UNIT NUMBERS D/A Project: 1L263102D071
11. CONTROLLING OFFICE NAME AND ADDRESS Army Materials and Mechanics Research Center ATTN: DRXMR-K Watertown, Massachusetts 02172		12. REPORT DATE May 1982
14. MONITORING AGENCY NAME & ADDRESS (if different from Controlling Office)		13. NUMBER OF PAGES 138
		15. SECURITY CLASS. (of this report) Unclassified
		15a. DECLASSIFICATION/DOWNGRADING SCHEDULE
16. DISTRIBUTION STATEMENT (of this Report) Approved for public release; distribution unlimited.		
17. DISTRIBUTION STATEMENT (of the abstract entered in Block 20, if different from Report)		
18. SUPPLEMENTARY NOTES		
19. KEY WORDS (Continue on reverse side if necessary and identify by block number) Metal matrix composites Alumina Nondestructive testing Magnesium Composites Acoustic velocity		
20. ABSTRACT (Continue on reverse side if necessary and identify by block number) (SEE REVERSE SIDE)		

DD FORM 1 JAN 73 1473

EDITION OF 1 NOV 65 IS OBSOLETE

UNCLASSIFIED

SECURITY CLASSIFICATION OF THIS PAGE (When Data Entered)

UNCLASSIFIED

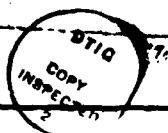
SECURITY CLASSIFICATION OF THIS PAGE(When Data Entered)

Block No. 20

ABSTRACT

The objective of the program was to apply nondestructive evaluation (NDE) methods to assess the integrity of FP/magnesium composites. The material investigated was ZE41A magnesium alloy reinforced with FP (aluminum oxide) fibers. The 21 specimens (three specimens of each of six flaw types and three unflawed specimens) were evaluated using ultrasonic scanning, wave propagation velocity, wave attenuation, and X-ray radiograph inspection techniques. The specimens evaluated were 12.7 cm (5 in.) long x 3.8 cm (1.5 in.) wide x 0.6 cm (0.25 in.) thick, with a fiber volume fraction of 0.50. After the NDE inspections were completed, a representative specimen from each of the seven groups was sectioned and micrographs were made for comparison with the NDE records. It was found that ultrasonic scanning using a 15 MHz compression wave, focused transducer operated in the pulse-echo mode generating an analog C-scan gave the best results. The wave attenuation and wave propagation velocity measurements were found to be very consistent with the ultrasonic C-scans, but X-ray radiography was useful only at locations of gross material defect.

Acco	
NTIS	<input checked="" type="checkbox"/>
DTIC	<input type="checkbox"/>
Uncl	<input type="checkbox"/>
Just	
By	
Dist	
Av	
Dist	



UNCLASSIFIED

SECURITY CLASSIFICATION OF THIS PAGE(When Data Entered)

TABLE OF CONTENTS

	<u>Page</u>
1. INTRODUCTION.....	1
2. EXPERIMENTAL PROCEDURES.....	3
2.1 Specimens.....	3
2.2 Nondestructive Evaluation Methods.....	3
2.2.1 Ultrasonic Inspection.....	10
2.2.2 Ultrasonic Attenuation.....	15
2.2.3 Ultrasonic Backscattering.....	22
2.2.4 Wave Propagation Velocity.....	25
2.2.5 X-Ray Radiography.....	26
2.3 Test Program.....	26
3. RESULTS.....	29
3.1 Type 1 Specimen.....	29
3.1.1 Physical Properties.....	29
3.1.2 Ultrasonic Inspection.....	30
3.1.3 Wave Propagation Velocity.....	30
3.1.4 Wave Attenuation.....	36
3.1.5 X-Ray Radiography.....	39
3.1.6 Ultrasonic Backscattering.....	39
3.1.7 Micrographic Inspection.....	39
3.1.8 Comparison of Inspection Procedures.....	43
3.2 Type 2 Specimen.....	43
3.2.1 Physical Properties.....	43
3.2.2 Ultrasonic Inspection.....	43
3.2.3 Wave Propagation Velocity.....	46
3.2.4 Wave Attenuation.....	49
3.2.5 X-Ray Radiography.....	50
3.2.6 Ultrasonic Backscattering.....	50
3.2.7 Micrographic Inspection.....	52
3.2.8 Comparison of Inspection Procedures.....	52
3.3 Type 3 Specimen.....	55
3.3.1 Physical Properties.....	55
3.3.2 Ultrasonic Inspection.....	55

IIT RESEARCH INSTITUTE

TABLE OF CONTENTS (Cont.)

	<u>Page</u>
3.3.3 Wave Propagation Velocity.....	59
3.3.4 Wave Attenuation.....	61
3.3.5 X-Ray Radiography.....	63
3.3.6 Ultrasonic Backscattering.....	64
3.3.7 Micrographic Inspection.....	64
3.3.8 Comparison of Inspection Procedures.....	64
3.4 Type 4 Specimen.....	68
3.4.1 Physical Properties.....	68
3.4.2 Ultrasonic Inspection.....	68
3.4.3 Wave Propagation Velocity.....	71
3.4.4 Wave Attenuation.....	71
3.4.5 X-Ray Radiography.....	75
3.4.6 Ultrasonic Backscattering.....	76
3.4.7 Micrographic Inspection.....	76
3.4.8 Comparson of Inspection Procedures.....	80
3.5 Type 5 Specimen.....	80
3.5.1 Physical Properties.....	80
3.5.2 Ultrasonic Inspection.....	80
3.5.3 Wave Propagation Velocity.....	85
3.5.4 Wave Attenuation.....	85
3.5.5 X-Ray Radiography.....	88
3.5.6 Ultrasonic Backscattering.....	89
3.5.7 Micrographic Inspection.....	89
3.5.8 Comparison of Inspection Procedures.....	93
3.6 Type 6 Specimen.....	93
3.6.1 Physical Properties.....	94
3.6.2 Ultrasonic Inspection.....	94
3.6.3 Wave Propagation Velocity.....	98
3.6.4 Wave Attenuation.....	101
3.6.5 X-Ray Radiography.....	103
3.6.6 Ultrasonic Backscattering.....	104
3.6.7 Micrographic Inspection.....	104
3.6.8 Comparison of Inspection Procedures.....	108

IIT RESEARCH INSTITUTE

TABLE OF CONTENTS (Cont.)

	<u>Page</u>
3.7 Type 7 Specimen.....	108
3.7.1 Physical Properties.....	108
3.7.2 Ultrasonic Inspection.....	109
3.7.3 Wave Propagation Velocity.....	109
3.7.4 Wave Attenuation.....	114
3.7.5 X-Ray Radiography.....	114
3.7.6 Ultrasonic Backscattering.....	115
3.7.7 Micrographic Inspection.....	115
3.7.8 Comparison of Inspection Procedures.....	119
3.8 Summary of Results.....	119
4. SUMMARY AND CONCLUSIONS.....	122
5. ACKNOWLEDGEMENTS.....	123
REFERENCES.....	124
APPENDIX: Procedures Used to Generate Specimen Defects.....	125

LIST OF TABLES

<u>Table</u>	<u>Page</u>
1 Wave Propagation Velocity Across the Thickness at Various Locations Along Specimen Centerline (Specimen 1-1)	37
2 Ultrasonic Wave Attenuation Coefficients (Specimen 1-1).	38
3 Wave Propagation Velocity Across the Thickness at Various Locations Along Specimen Centerline (Specimen 2-1)	48
4 Wave Propagation Velocity Across the Thickness at Various Locations Along Specimen Centerline (Specimen 3-1)	60
5 Selected Values of Wave Propagation Velocity for FP/Mg Specimen with Porosity (Specimen 3-1).	62
6 Ultrasonic Wave Attenuation for FP/Mg Specimen with Porosity (Specimen 3-1)	62
7 Wave Propagation Velocity Across the Thickness at Various Locations Along Specimen Centerline (Specimen 4-1)	73
8 Ultrasonic Wave Attenuation Coefficients (Specimen 4-1).	74
9 Wave Propagation Velocity Across the Thickness at Various Locations Along Specimen Centerline (Specimen 5-1)	86
10 Selected Values of Wave Propagation Velocity (Specimen 5-1).	87
11 Ultrasonic Wave Attenuation Coefficients (Specimen 5-1).	87
12 Wave Propagation Velocity Across the Thickness at Various Locations Along Specimen Centerline (Specimen 6-2)	100
13 Ultrasonic Wave Attenuation Coefficients (Specimen 6-2).	102
14 Wave Propagation Velocity Across the Thickness at Various Locations Along Specimen Centerline (Specimen 7-2)	113
15 Ultrasonic Wave Attenuation Coefficients (Specimen 7-2).	113
16 Summary of Results on NDE Techniques for Detection of Flaws.	120

LIST OF FIGURES

<u>Figure</u>	<u>Page</u>
1 Type 1 FP/Mg specimens with no intentional flaws.....	4
2 Type 2 FP/Mg specimens with fiber-matrix debonding.....	4
3 Type 3 FP/Mg specimens with porosity throughout the volume.....	5
4 Fiber orientation of fourth and fifth layers of Type 4 FP/Mg specimens.....	6
5 Type 4 FP/Mg specimens with fiber misalignment.....	6
6 Fiber fracture of second, fourth, and sixth layers of Type 5 FP/Mg specimens.....	7
7 Type 5 FP/Mg specimens with fiber fracture.....	7
8 Areas where fibers were removed in fourth layer of Type 6 FP/Mg specimens: (a) Specimens 6-1 and 6-3, (b) Specimen 6-2.....	8
9 Type 6 FP/Mg specimens with nonuniform fiber distribution.....	8
10 Type 7 FP/Mg specimens with matrix fracture.....	9
11 Ultrasonic scanning and recording system for nondestructive flaw detection in composite laminates.....	11
12 Pen-lift and analog C-scans of FP/Mg specimen with no intentional flaws (Specimen 1-1).....	13
13 A-scan representation of a FP/Mg laminate using a compressive wave transducer in the pulse-echo mode.....	14
14 Ultrasonic scanning system showing vertical and horizontal drives, vertical position transducer, and ultrasonic transducer scanning arm.....	16
15 Specimen holder for determination of ultrasonic wave attenuation of FP/Mg specimens.....	18
16 Schematic of echoes received by transducer.....	19
17 Ultrasonic attenuation record for FP/Mg specimen without intentional flaws (Specimen 1-1).....	21
18 Detection of fiber orientation by ultrasonic backscattering measurements.....	23

LIST OF FIGURES (Cont.)

Figure		Page
19	Backscattering measurement fixture.....	24
20	Pen-lift C-scan of FP/Mg Specimen 1-1 (no intentional flaws), 15 MHz transducer in pulse-echo mode.....	31
21	Analog C-scan of FP/Mg Specimen 1-1 (no intentional flaws), 15 MHz transducer in pulse-echo mode.....	32
22	Amplitude-time records (A-scans) of ultrasonic pulse at two locations of Specimen 1-1.....	33
23	Pen-lift C-scan of FP/Mg Specimen 1-1 (no intentional flaws), 5 MHz transducer in the pulse-echo mode.....	34
24	Locations of measurements of wave propagation velocity.....	35
25	X-ray radiograph of FP/Mg specimen with no intentional flaws (Specimen 1-1).....	39
26	Ultrasonic backscattering curve of FP/Mg specimen with no intentional flaws (Specimen 1-1).....	40
27	Micrographs (5X) of FP/Mg Specimen 1-1 (no intentional flaws) at four locations.....	41
28	Micrographs (200X) of FP/Mg Specimen 1-1 (no intentional flaws) at four section locations.....	42
29	Pen-lift C-scans of FP/Mg Specimen 2-1 (fiber-matrix debonding), 15 MHz transducer in pulse-echo mode.....	44
30	Analog C-scan of FP/Mg Specimen 2-1 (fiber-matrix debonding), 15 MHz transducer in pulse-echo mode.....	45
31	Amplitude-time records (A-scans) of ultrasonic pulse at two locations of Specimen 2-1 (fiber-matrix debonding).....	47
32	X-ray radiograph of FP/Mg specimen with fiber-matrix debonding/delamination (Specimen 2-1).....	50
33	Ultrasonic backscattering curve of FP/Mg specimen with fiber-matrix debonding (Specimen 2-1).....	51
34	Micrographs (5X) of FP/Mg Specimen 2-1 (fiber-matrix debonding) at four section locations.....	53

LIST OF FIGURES (Cont.)

<u>Figure</u>		<u>Page</u>
35	Micrographs (200X) of FP/Mg Specimen 2-1 (fiber-matrix debonding) at four section locations.....	54
36	Pen-lift C-scan of FP/Mg Specimen 3-1 (porosity), 15 MHz transducer in pulse-echo mode.....	56
37	Analog C-scan of FP/Mg Specimen 3-1 (porosity), 15 MHz transducer in pulse-echo mode.....	57
38	Amplitude-time records (A-scans) of ultrasonic pulse at two locations of Specimen 3-1 (porosity).....	58
39	X-ray radiograph of FP/Mg specimen with porosity (Specimen 3-1).....	63
40	Ultrasonic backscattering curve of FP/Mg specimen with porosity (Specimen 3-1).....	65
41	Micrographs of FP/Mg Specimen 3-1 (porosity) at four section locations.....	66
42	Micrographs (200X) of FP/Mg Specimen 3-1 (porosity) at four section locations.....	67
43	Pen-lift C-scan of FP/Mg Specimen 4-1 (fiber misalignment), 15 MHz transducer in pulse-echo mode.....	69
44	Analog C-scan of FP/Mg Specimen 4-1 (fiber misalignment), 15 MHz transducer in pulse-echo mode.....	70
45	Amplitude-time record (A-scan) of ultrasonic pulse at an unflawed location of Specimen 4-1 (fiber misalignment).....	72
46	X-ray radiograph of FP/Mg specimen with fiber misalignment (Specimen 4-1).....	75
47	Ultrasonic backscattering curve of FP/Mg specimen with fiber misalignment (Specimen 4-1).....	77
48	Micrographs (5X) of FP/Mg Specimen 4-1 (fiber misalignment) at four section locations.....	78
49	Micrographs (200X) of FP/Mg Specimen 4-1 (fiber misalignment) at four section locations.....	79
50	Pen-lift C-scan of FP/Mg Specimen 5-1 (fiber fracture), 15 MHz transducer in pulse-echo mode.....	81

LIST OF FIGURES (Cont.)

<u>Figure</u>		<u>Page</u>
51	Analog C-scan of FP/Mg Specimen 5-1 (fiber fracture), 15 MHz transducer in pulse-echo mode.....	82
52	Amplitude-time records (A-scans) of ultrasonic pulses at two locations of Specimen 5-1 (fiber fracture).....	84
53	X-ray radiograph of FP/Mg specimen with fiber fracture (Specimen 5-1).....	89
54	Ultrasonic backscattering curve of FP/Mg specimen with fiber fracture (Specimen 5-1).....	90
55	Micrographs of FP/Mg Specimen 5-1 (fiber fracture) at four section locations.....	91
56	Micrographs (200X) of FP/Mg Specimen 5-1 (fiber fracture) at four section locations.....	92
57	Pen-lift C-scan of FP/Mg Specimen 6-2 (nonuniform fiber distribution), 15 MHz transducer in pulse-echo mode.....	95
58	Analog C-scan of FP/Mg Specimen 6-2 (nonuniform fiber distribution), 15 MHz transducer in pulse-echo mode.....	96
59	Amplitude-time records (A-scans) of ultrasonic pulse at two locations of Specimen 6-2 (nonuniform fiber distribution).....	97
60	Wave propagation velocity inspection locations for FP/Mg Specimen 6-2 (nonuniform fiber distribution).....	99
61	X-ray radiograph of FP/Mg specimen with nonuniform fiber distribution (Specimen 6-2).....	103
62	Ultrasonic backscattering curve of FP/Mg specimen with nonuniform fiber distribution (Specimen 6-2).....	105
63	Micrographs of FP/Mg Specimen 6-2 (nonuniform fiber distribution).....	106
64	Micrographs (200X) of FP/Mg Specimen 6-2 (nonuniform fiber distribution).....	107
65	Pen-lift C-scan of FP/Mg Specimen 7-2 (matrix fracture), 5 MHz transducer in pulse-echo mode.....	110
66	Analog C-scan of FP/Mg Specimen 7-2 (matrix fracture), 5 MHz transducer in pulse-echo mode.....	111

LIST OF FIGURES (Cont.)

<u>Figure</u>		<u>Page</u>
67	Amplitude-time records (A-scans) of ultrasonic pulse at two locations of Specimen 7-2 (matrix fracture).....	112
68	X-ray radiograph of FP/Mg specimen with matrix fracture (Specimen 7-2).....	115
69	Ultrasonic backscattering curve of FP/Mg specimen with matrix fracture (Specimen 7-2).....	116
70	Micrographs (5X) of FP/Mg Specimen 7-2 (matrix fracture) at four section locations.....	117
71	Micrographs (200X) of FP/Mg Specimen 7-2 (matrix fracture) at four section locations.....	118

FOREWORD

This is the Final Report of IIT Research Institute Project No. M06084, "Nondestructive Evaluation of Metal Matrix Composites," prepared by IITRI for the Army Materials and Mechanics Research Center (AMMRC) under Contract No. DAAG-46-80-C-0070. The work described in this report was conducted in the period 1 October 1980 to 31 December 1981. Mr. John Nunes was the Technical Monitor for AMMRC. IIT Research Institute personnel who contributed to this program include Dr. I. M. Daniel and Messrs. W. G. Hamilton, T. Niro, and S. W. Schramm.

Respectfully submitted,
IIT RESEARCH INSTITUTE

Scott W. Schramm

Scott W. Schramm

O. J. Viergutz

O. J. Viergutz, P.E.
Manager, Mechanics and
Mechanical Engineering Section

APPROVED:

John A. Granath

John A. Granath, P.E.
Director, Engineering Division

IIT RESEARCH INSTITUTE

1. INTRODUCTION

Advanced metal-matrix composite materials possess unique mechanical and physical characteristics which make them highly desirable for specific applications. In addition to the advantages afforded by the anisotropic characteristics common to all composite materials, they have many additional advantages. In general, they exhibit high shear strength and shear modulus, high transverse tensile strength, excellent stability over a wide temperature range, good strength retention, excellent fatigue and creep properties, and high impact strength. They are easily formed and machined, easily repaired, and amenable to typical aerospace sheet metal design and fabrication.

Composite systems that have received the most attention to date are boron/aluminum, boron/aluminum, and graphite/aluminum.¹ More recently, with the advent of aluminum oxide (FP) fibers in continuous form, systems such as FP/aluminum and FP/magnesium have been introduced by DuPont. The basic fabrication (casting) techniques for these composites have been developed by DuPont. However, there is a need for further improvement in the fabrication processes. It is, therefore, of great importance to be able to assess the quality of the composite and to characterize all possible types of flaws that may be introduced during fabrication.

The objective of the program was to apply established nondestructive evaluation (NDE) methods to assess the integrity of FP/magnesium composites utilizing sound and intentionally flawed test coupons.

One of the most common and widely accepted NDE methods is ultrasonic inspection.² Methods and principles for ultrasonic inspection and flaw detection in materials are detailed in the literature.²⁻⁴ Basically, a high frequency sound (1 to 25 MHz) is emitted in periodic bursts from an ultrasonic transducer through a coupling medium into the specimen material being inspected. The resulting attenuated pulse emerging from the specimen is picked up by a receiving transducer; the information from it is electronically processed; and the data are displayed for the evaluation of presence, size, and location of flaws.

The preferred method of flaw identification is by comparison of pulse information obtained from known flawed and unflawed standard specimens. Appropriate standards, especially in laminated composites, are not always easy to produce and sometimes are not feasible. Alternative pulse processing/identification techniques for ultrasonic inspection, such as frequency and phase shift analysis and adaptive learning techniques, are being developed.⁵⁻⁹

The ultrasonic scanning inspections were conducted using ultrasonic transducers of 1, 2.25, 5, 10, and 15 MHz frequencies operated in the pulse-echo mode. The acoustic couplant between the focused, immersion transducers and the specimens was water. The data generated during scanning were recorded on an X-Y plotter as pen-lift and analog C-scans and on oscilloscope photographs of A-scans. The photographs were used as additional information to the C-scans.

Wave attenuation coefficients were determined using two methods. One method used the ultrasonic transducers mentioned above in a water delay line technique. The other method used a 10 MHz shear wave transducer operated in the pulse-echo mode while in intimate contact with the specimen. The data generated were recorded on oscilloscope photographs as amplitudes versus reflection number. The amplitudes were then reduced to a single attenuation coefficient by solving a set of equations, simultaneously.

The wave propagation velocities were determined using an ultrasonic thickness gage. The wave propagation velocities were generated by varying the acoustic wave velocity control on the thickness gage until the indicated specimen thickness was identical to that determined by micrometer.

The X-ray radiographs were generated using a 62 kV/10 mA energy level for a 25 sec exposure time. The radiographs were made without the use of dye penetrant or enhancement media. The micrographs were generated after specimen sectioning and surface polishing using a standard laboratory microscope. The microscope had a maximum magnification factor of 100X and was equipped with a camera adapter unit. The micrographs verified, or refuted, the accuracy of the NDE records.

2. EXPERIMENTAL PROCEDURE

2.1 SPECIMENS

The material investigated was ZE41A magnesium alloy reinforced with FP (aluminum oxide) fibers. The specimens were coupons 12.7 cm (5 in.) long x 3.8 cm (1.5 in.) wide x 0.6 cm (0.25 in.) thick with a 0.50 fiber volume ratio. The following FP/Mg specimens with and without defects were fabricated:

- Type 1: Three FP/Mg specimens with no intentional flaws (Figure 1)
- Type 2: Three FP/Mg specimens with fiber-matrix debonding (Figure 2)
- Type 3: Three FP/Mg specimens with porosity (Figure 3)
- Type 4: Three FP/Mg specimens with fiber misalignment (Figures 4 and 5)
- Type 5: Three FP/Mg specimens with fiber fracture (Figures 6 and 7)
- Type 6: Three FP/Mg specimens with nonuniform fiber distribution (Figures 8 and 9)
- Type 7: Three FP/Mg specimens with matrix fracture (Figure 10).

2.2 NONDESTRUCTIVE EVALUATION METHODS

During the course of the program, at least one specimen from each of the seven specimen types was subjected to the five NDE methods investigated in the program. The five NDE methods used were:

- Ultrasonic inspection, including A-scans, C-scans (conventional pen-lift), and C-scans (analog)
- Ultrasonic attenuation, including contact transducer and water delay line
- Ultrasonic backscattering

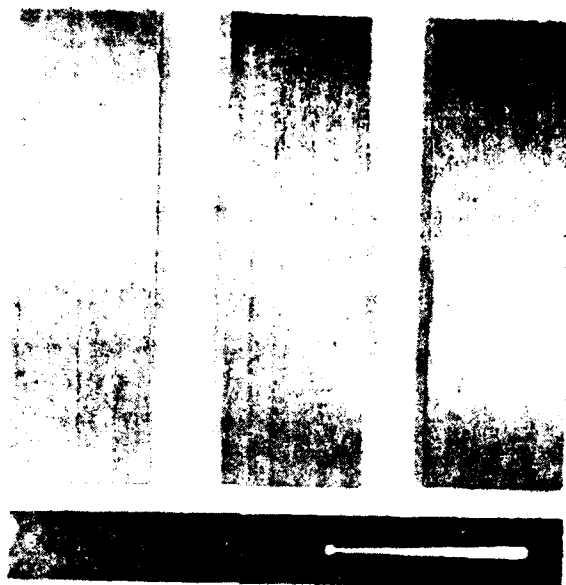


Figure 1. Type 1 FP/Mg specimens with no intentional flaws.



Figure 2. Type 2 FP/Mg specimens with fiber-matrix debonding.

IIT RESEARCH INSTITUTE

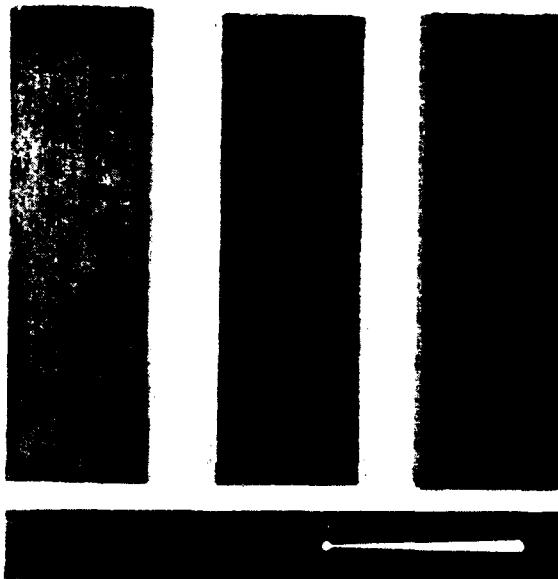


Figure 3. Type 3 FP/Mg specimens with porosity throughout the volume.

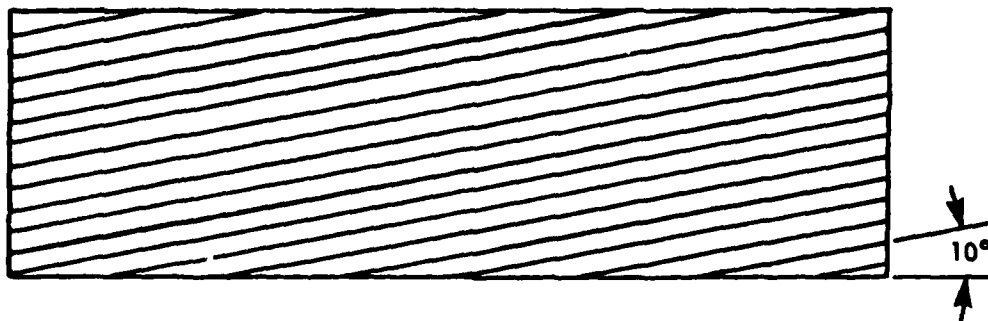


Figure 4. Fiber orientation of fourth and fifth layers of Type 4 FP/Mg specimens.



Figure 5. Type 4 FP/Mg specimens with fiber misalignment.

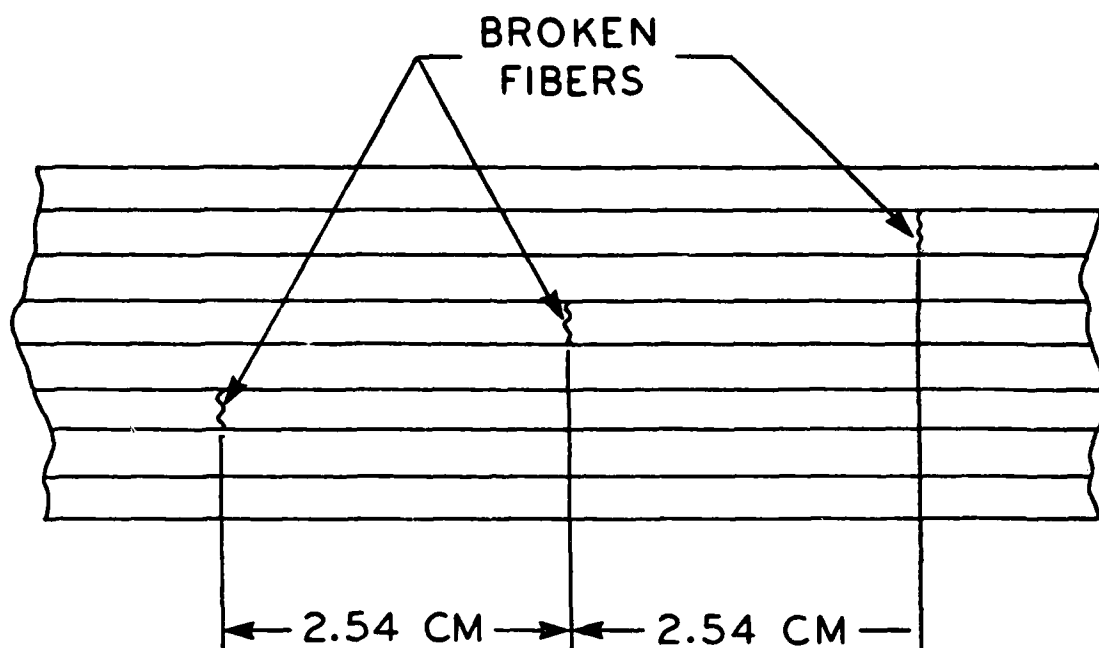
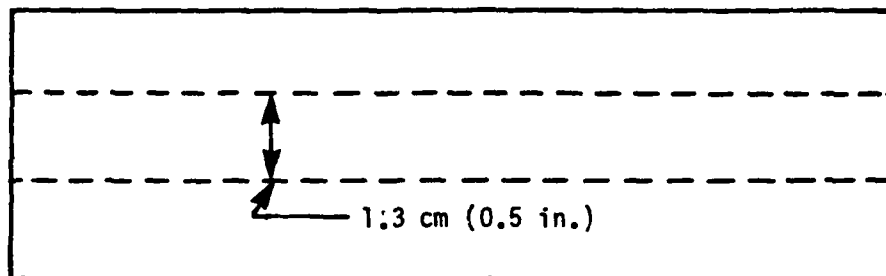


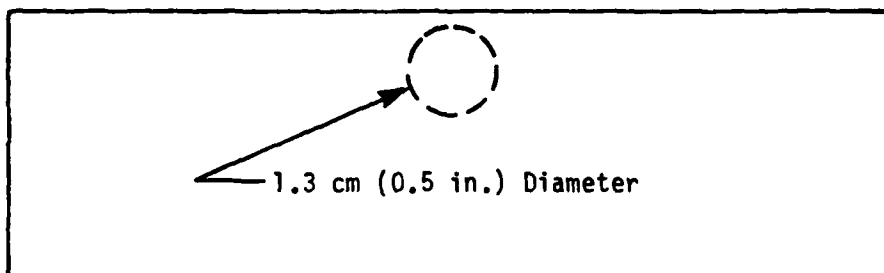
Figure 6. Fiber fracture of second, fourth, and sixth layers of Type 5 FP/Mg specimens.



Figure 7. Type 5 FP/Mg specimens with fiber fracture.



(a)



(b)

Figure 8. Areas where fibers were removed in fourth layer
Type 6 FP/Mg specimens: (a) specimens 6-1 and 6-3,
(b) specimen 6-2.

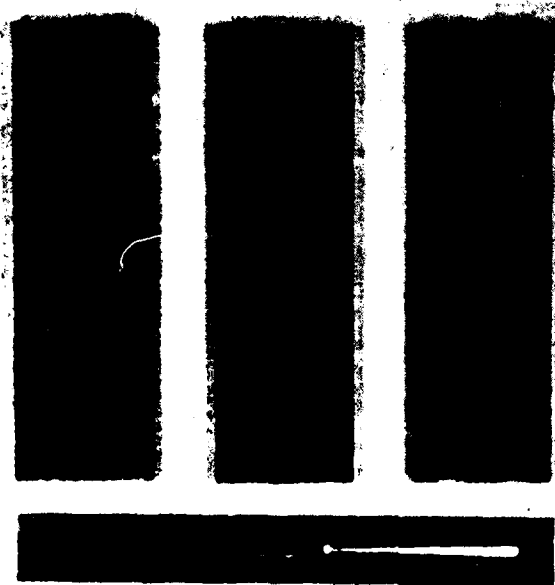


Figure 9. Type 6 FP/Mg specimens with non-uniform fiber distribution.

IIT RESEARCH INSTITUTE



Figure 10. Type 7 FP/Mg specimens with matrix fracture.

- Wave propagation velocity
- X-ray radiography.

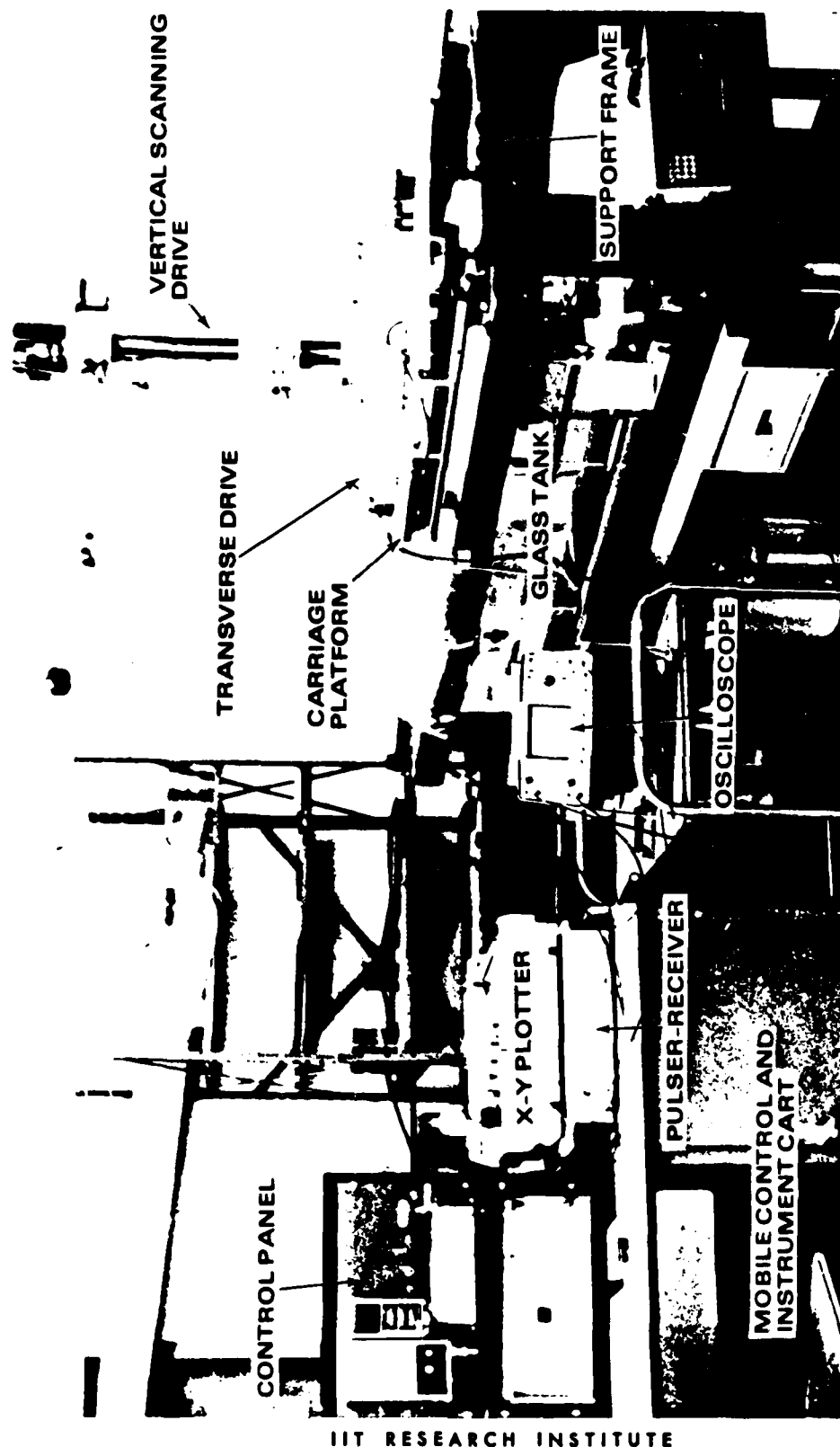
Each of these methods is described in detail in the following sections.

2.2.1 Ultrasonic Inspection

Figure 11 shows the overall setup of the ultrasonic scanning and recording system used in this program. The ultrasonic transducer system is operated by a Model 5052 UA pulser-receiver manufactured by Panametrics, Inc. It is capable of driving the transducers in either pulse-echo or in through-transmission mode.^{2,3} The pulser-receiver is a broad-band device which can readily operate transducers in the range of 1 MHz to 20 MHz. It has independent controls for input energy, signal repetition rate, high pass filter gain, and attenuation all of which control the final transducer signal. It provides a time domain output for reviewing the RF signal on an oscilloscope or spectrum analyzer. It also has a gated peak output detector which can operate one axis of an X-Y recorder pen for plotting the ultrasonic information contained in the variation of the peak output signal.

The pulser-receiver was used to drive transducers of 1, 2.25, 5, 10, and 15 MHz frequency. All the transducers were immersion type, focused transducers; 2.5 cm (1 in.) in diameter for the 1, 2.25, and 5 MHz frequencies and 1.3 cm (0.5 in.) in diameter for the 10 and 15 MHz frequencies, respectively. The requirements for determining the transducer selection were: a standoff distance of at least 5.1 cm (2 in.) to clear hardware associated with specimen mounting; high damping and broad bandwidth to provide resolving power for the detection of subsurface flaws; and a small sound-beam cross-section for good definition of flaw boundaries in the plane of the specimen. The nominal focal length in water of the transducers was 6.4 cm (2.5 in.). The focal spot size was 1.3 mm (0.05 in.), which made it possible to outline the boundary of a flaw in the plane of the specimen to within ± 0.64 mm (± 0.025 in.).

In addition to the transducers and pulser-receiver, three pieces of equipment are required to get a complete picture of the specimen integrity. They are an X-Y recorder, an oscilloscope, and an oscilloscope camera.



IIT RESEARCH INSTITUTE

Figure 11. Ultrasonic scanning and recording system for nondestructive flaw detection in composite laminates.

The X-Y plotter was a Hewlett-Packard Model 7044A X-Y recorder. The X and Y control sensitivities range from 0.25 mV/cm to 5 V/cm. The recorded C-scan could be smaller, equal to or larger than the actual specimen up to a size of 25 cm (10 in.) x 38 cm (15 in.). The X-Y recorder could operate in either the pen-lift or analog mode (see Figure 12). In the pen-lift mode the output from the peak detector was channeled through an electronic alarm unit into the pen-lift control of the recorder. The alarm unit was set to trigger the pen-lift whenever the amplitude of the peak detector fell below a prescribed level, indicating a flaw; otherwise, the pen stayed in contact with the paper tracing a line. This gives detailed flaw locations in the plane of the specimen with definite outlines of the flaw boundaries. The analog mode supplements this information by giving a continuous record of the amplitude of the gated pulse. It was obtained by scanning the specimen with the (alarm) unit bypassed. The horizontal and vertical motion of the pen was effected by information fed to the X-Y recorder by displacement transducers used on the scanning drive mechanism. The scanning drive mechanism (which will be described later), like the X-Y recorder, was used in conjunction with the compression wave immersion transducers only.

The oscilloscope used was a Tektronix Model 445/A2/B2. This was a 50 MHz, dual channel portable oscilloscope with deflection factors calibrated from 5 mV to 5 V/division. The horizontal deflection system provides stable triggering over the full bandwidth capabilities of the vertical system. The oscilloscope was fed with information processed by the pulser-receiver. The upper trace (Figure 13) is a voltage/time representation of the ultrasonic signal as it passed through the specimen. This trace was generated off the marked RF terminal of the pulser-receiver with the W-shaped pulse on the left representing the front face reflection and the smaller M-shaped pulse on the right representing the back face reflection.

The lower trace in Figure 13 is a voltage/time representation of the gated portion of the pulse reflected from the back face. This trace was generated off the gated RF terminal of the pulser-receiver. The gate window may be moved to any position.

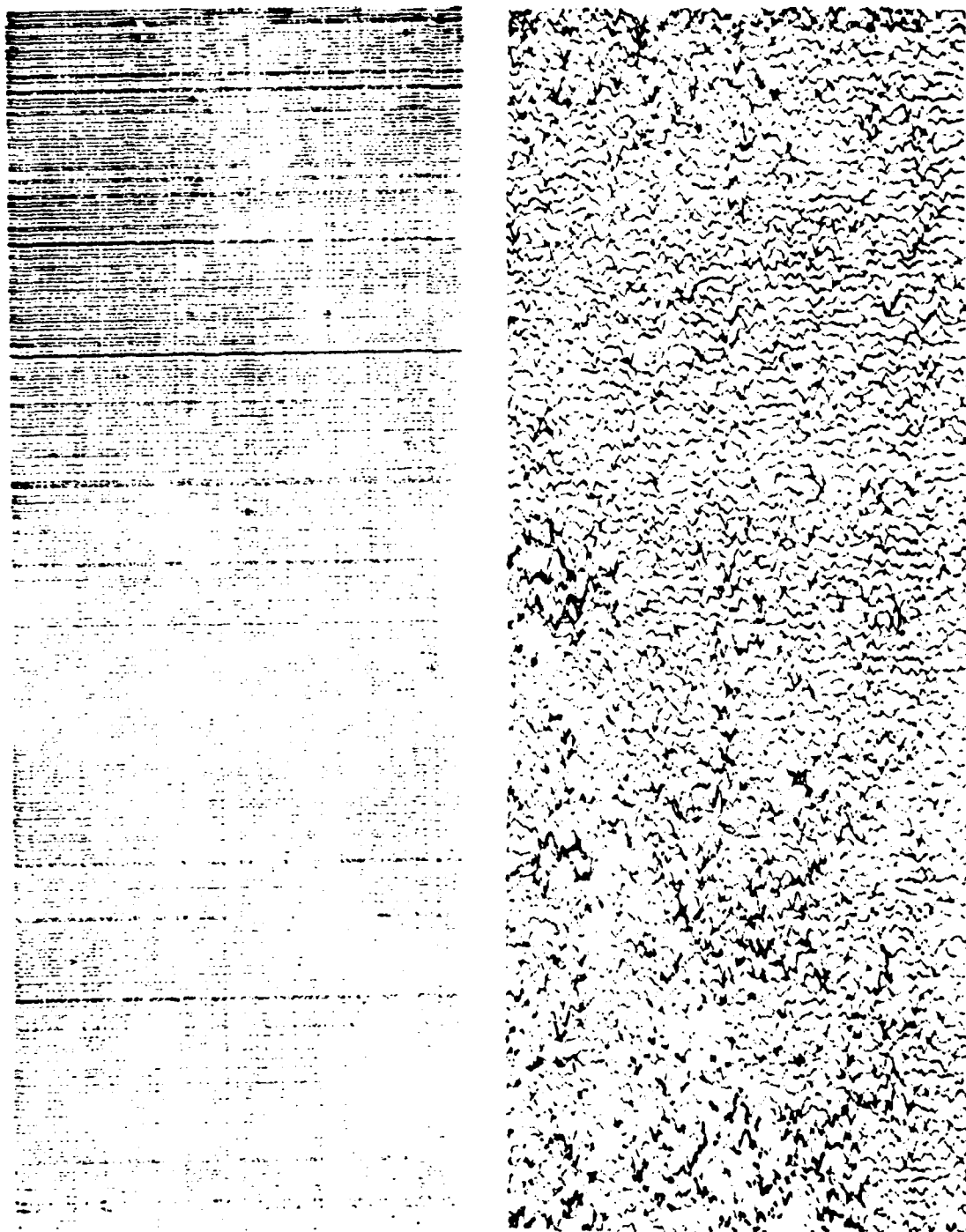


Figure 12. Pen-lift (upper) and analog (lower) C-scans of FP/Mg specimen with no intentional flaws (specimen 1-1).

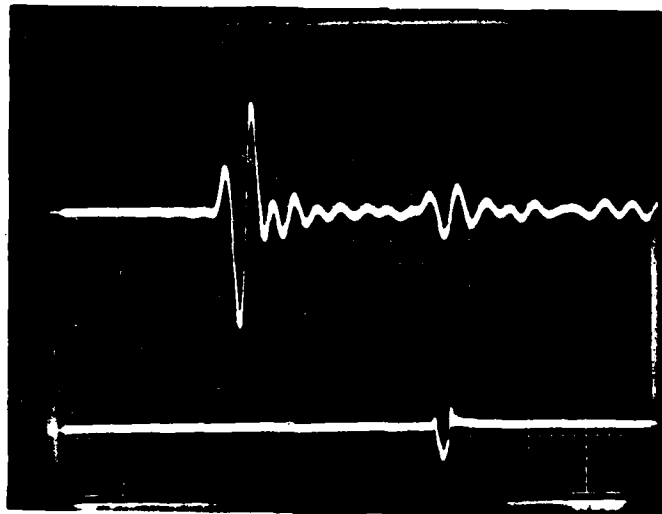


Figure 13. A-scan representation of a FP/Mg laminate using a compressive wave transducer in the pulse-echo mode.

Figure 14 shows the ultrasonic scanning system used with the compressive wave immersion transducers. This system is a subsystem of the total ultrasonic scanning and recording system as shown in Figure 11.

The system shown in Figure 11 consists of an all glass immersion tank 45.7 cm (18 in.) wide, 45.7 cm (18 in.) high, and 183 cm (72 in.) long resting on a support table. The transparent glass tank affords distortion-free visual observation through the tank sides during aligning of specimens and transducers and during scanning. A sturdy steel frame resting on the support table surrounds the glass tank which is accurately positioned relative to the frame. The frame supports the mechanical system for scanning the specimens.

The mechanical system has a scanning carriage platform with three precision screw drives which move the ultrasonic transducer along three mutually perpendicular axes. It is guided along the tank length on steel shafts attached to the support frame. The platform is elevated above the tank and can be traversed and positioned at any tank location.

Figure 14 shows the motorized screw drive for vertical motion and the vertical scanning arm holding the ultrasonic transducer at its lower end. The drive is capable of moving the arm in up and down scanning strokes of any adjustable length up to 35.6 cm (14 in.) at rates up to 127 cm/min (50 in./min). The strokes are monitored by the cable-type electromechanical position transducer attached to the vertical drive. Figure 14 shows also the horizontal transverse screw drive. It is manually operated and is used only for locating or focusing the ultrasonic transducer each time a new specimen is scanned.

2.2.2 Ultrasonic Attenuation

A method of specimen inspection complementary to the determination of wave propagation velocity is the determination of ultrasonic attenuation coefficients. The attenuation results from geometric dispersion due to material heterogeneity (such as the porosity of the Type 3 specimens), geometric attenuation due to internal defects such as fiber fracture (Type 5), fiber debonding (Type 2), delaminations and matrix cracks (Type 7), and energy dissipation due to viscoelastic or other dissipative nature of the material.

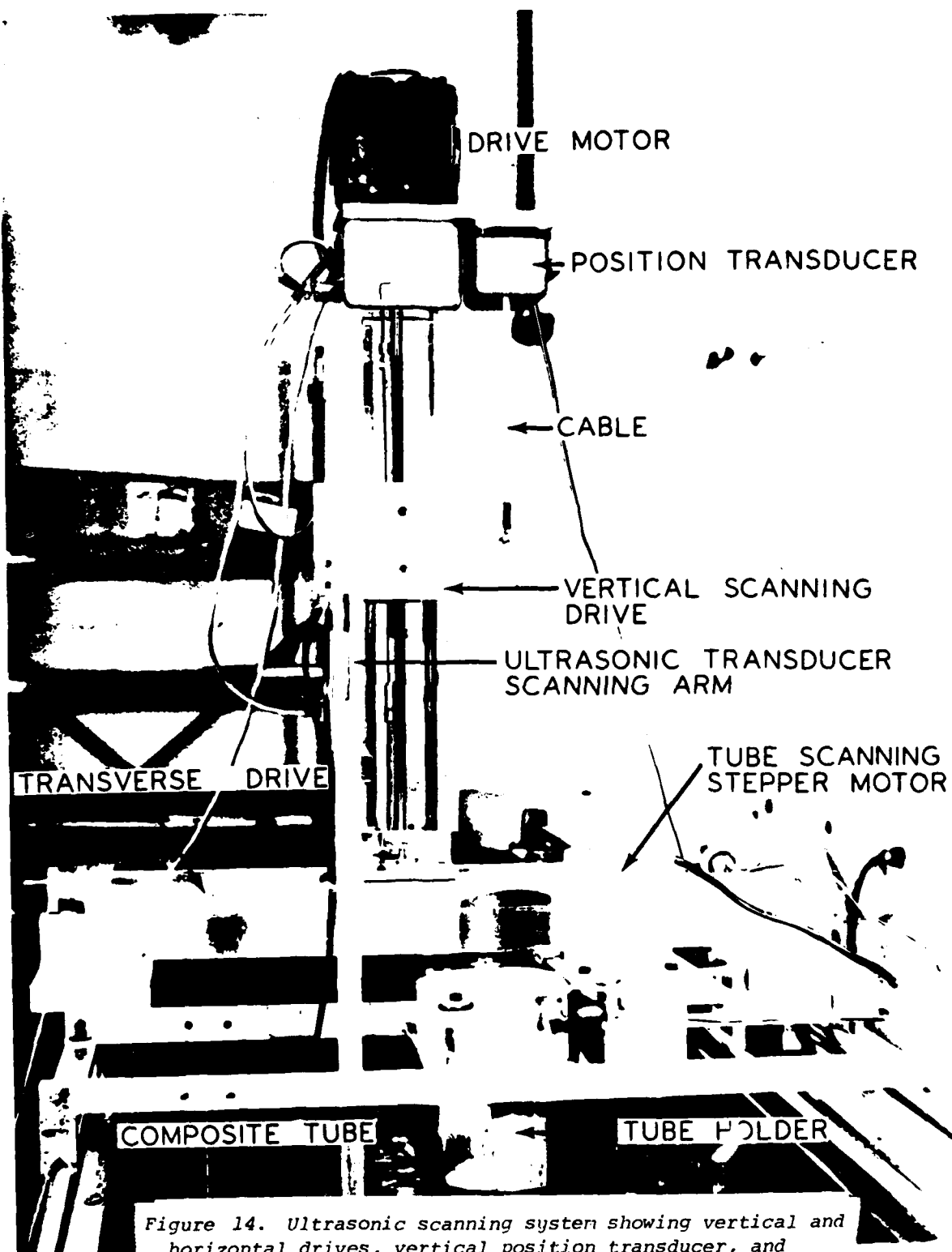


Figure 14. Ultrasonic scanning system showing vertical and horizontal drives, vertical position transducer, and ultrasonic transducer scanning arm.

The objective of the attenuation measurements was to correlate, if possible, the measured attenuation with the condition of the material being evaluated. Since it was important to make the amplitude measurements in a reliable, quantitative, and reproducible manner, a special specimen holder was fabricated (Figure 15). Absolute measurements of attenuation were difficult because the amplitude of the reflected or transmitted pulse depends not only on material attenuation, but also on the energy dissipation in the coupling between transducer and specimen, and on reflection losses. The specimen holder shown in Figure 15 was designed to minimize ultrasonic wave energy losses associated with the transmission of ultrasound to the water through the back-face of the specimen during immersed ultrasonic inspection. The special specimen holder had a watertight seal which when immersed in water formed an air pocket adjacent to the back-face of the specimen. Since the impedance mismatch was greater between FP/Mg and air than between FP/Mg and water, less wave energy was lost through the back-face to the air than would be if the specimen were totally surrounded by water.

Figure 16 shows schematically the various pulses received by the transducer where:

$$t_2 = \text{travel time in water delay line}$$

$$t_1 = \text{travel time in specimen}$$

$$R_{21} = \frac{Z_1 - Z_2}{Z_1 + Z_2} \text{ reflection coefficient in water/specimen interface}$$

$$R_{12} = \frac{Z_2 - Z_1}{Z_1 + Z_2} \text{ reflection coefficient in specimen/water interface}$$

$$T_{12} = \frac{2Z_2}{Z_1 + Z_2} \text{ transmission coefficient from specimen to water}$$

$$T_{21} = \frac{2Z_1}{Z_1 + Z_2} \text{ transmission coefficient from water to specimen}$$

$$Z_1, Z_2 = \text{acoustic impedances of specimen and water, respectively (product of material density and wave propagation velocity)}$$

$$R_{10} = \text{reflection coefficient from dry specimen surface } (\approx 1)$$

$$10^{-\alpha_1}, 10^{-\alpha_2} = \text{attenuation per echo for specimen and water, respectively.}$$

IIT RESEARCH INSTITUTE

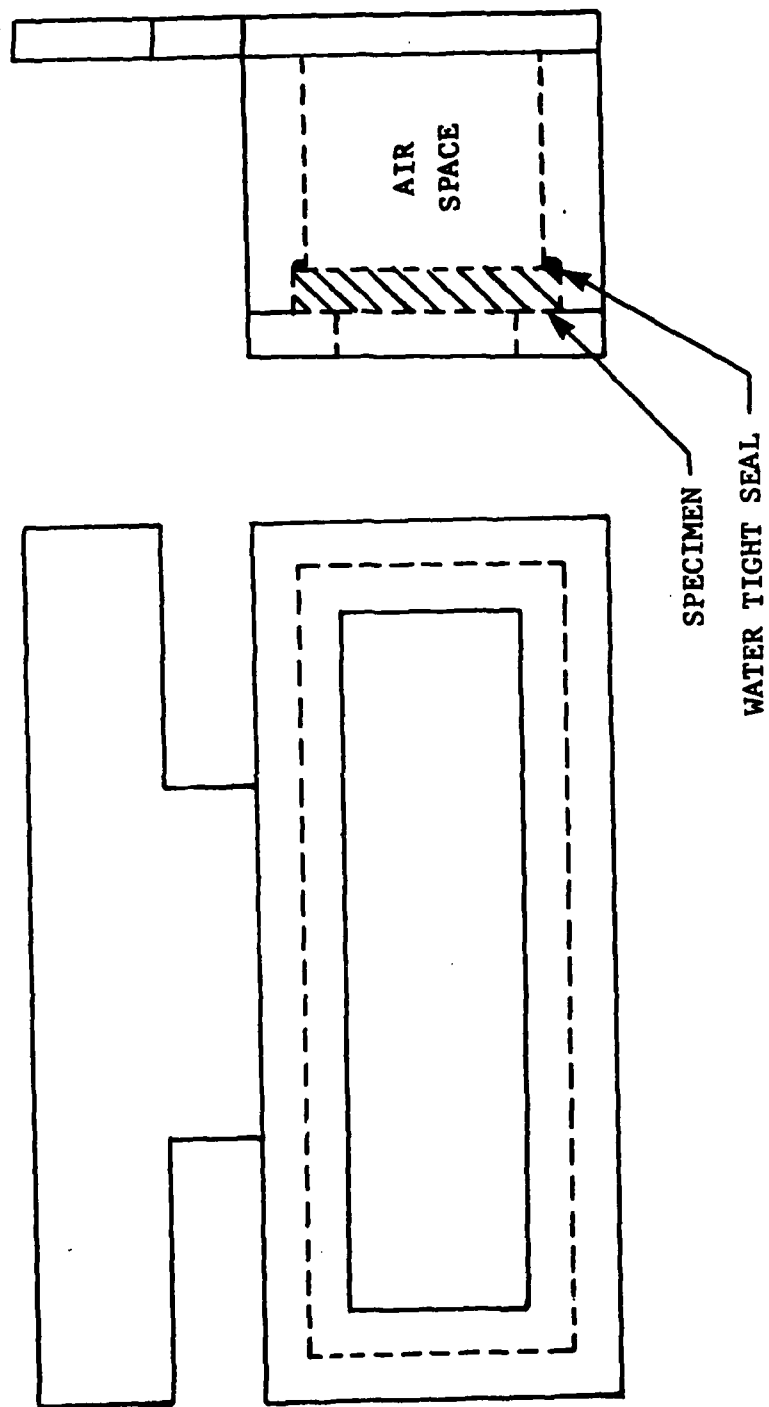
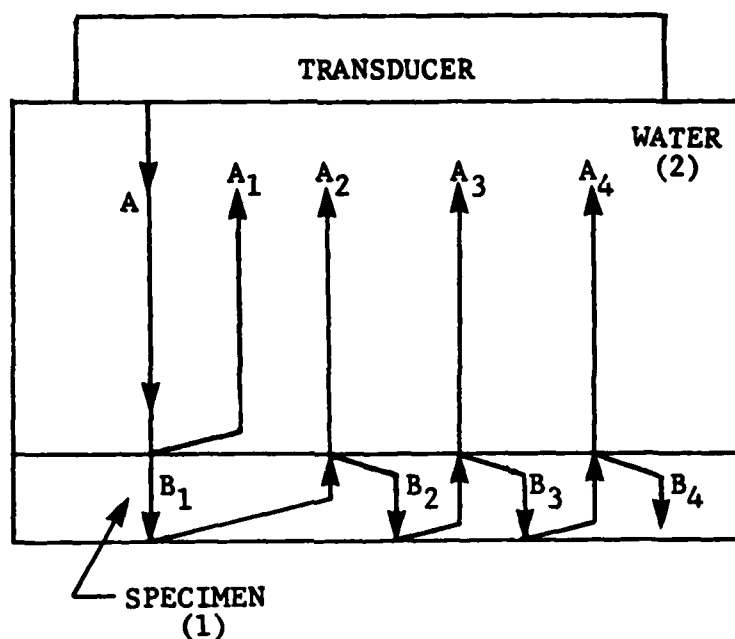


Figure 15. Specimen holder for determination of ultrasonic wave attenuation of FP/Mg specimens.



<u>Time After Initial Pulse</u>	<u>Pulse</u>	<u>Magnitude</u>
0	A	A
$2t_2$	A_1	$AR_{21}10^{-\alpha_2}$
$2t_2+2t_1$	A_2	$AT_{21}T_{12}R_{10}10^{-\alpha_2-\alpha_1}$
$2t_2+4t_1$	A_3	$AT_{21}T_{12}R_{10}^2R_{12}10^{-\alpha_2-2\alpha_1}$
$2t_2+6t_1$	A_4	$AT_{21}T_{12}R_{10}^3R_{12}^210^{-\alpha_2-3\alpha_1}$

Figure 16. Schematic of echoes received by transducer.

The attenuation of the specimen material in decibels per unit length is then expressed as:

$$\alpha = \frac{20}{2d_1} \alpha_1 = \frac{10}{d_1} \alpha_1$$

where d_1 is the specimen thickness.

Taking the logarithms of the amplitude ratios of the various echoes shown in Figure 2 and setting $R_{10} = 1$, we obtain:

$$\log \frac{A_1}{A_2} = \alpha_1 + \log |R_{21}| - \log (T_{12}T_{21})$$

$$\log \frac{A_1}{A_3} = 2\alpha_1 + \log \left| \frac{R_{21}}{R_{12}} \right| - \log (T_{12}T_{21})$$

$$\log \frac{A_1}{A_4} = 3\alpha_1 + \log |R_{21}| - 2 \log |R_{12}| - \log (T_{12}T_{21}).$$

The equations above can be simplified by noting that:

$$|R_{21}| = |R_{12}| = R$$

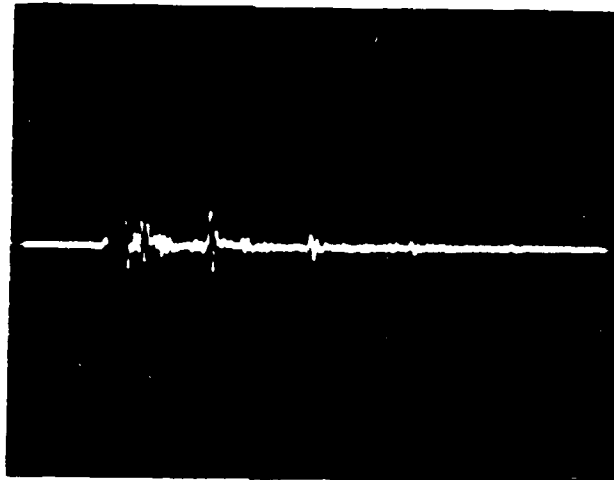
$$T_{12}T_{21} = 1 - R^2.$$

Then, any two of the equations above can be solved for R and α_1 , the only two unknowns.

The acoustic impedance for water is considered constant at $Z_2 = 1.5 \times 10^6$ kg/m²s. The acoustic impedance for each specimen was calculated using density and wave propagation velocity values determined earlier.

A minimum of three measurements were made on one specimen from each of the seven specimen types. The measurements were made using a 15 MHz focused, compression wave, immersion transducer operated in the pulse-echo mode. Figure 17 shows a typical ultrasonic attenuation measurement record (A-scan) and corresponding amplitudes. The amplitudes were determined using a digital voltmeter, variable voltage power supply, and a dual beam oscilloscope. The amplitude voltages were determined by using one beam of the oscilloscope as a cursor and moving it with the power supply to pass through the peak of the various pulses. The voltages were read off the digital voltmeter.

IIT RESEARCH INSTITUTE



Inspection Location	Amplitude (Volts)	Time (10^{-6} sec)
1	1.90	0.00
2	0.49	1.75
3	0.10	3.50
4	0.05	5.25

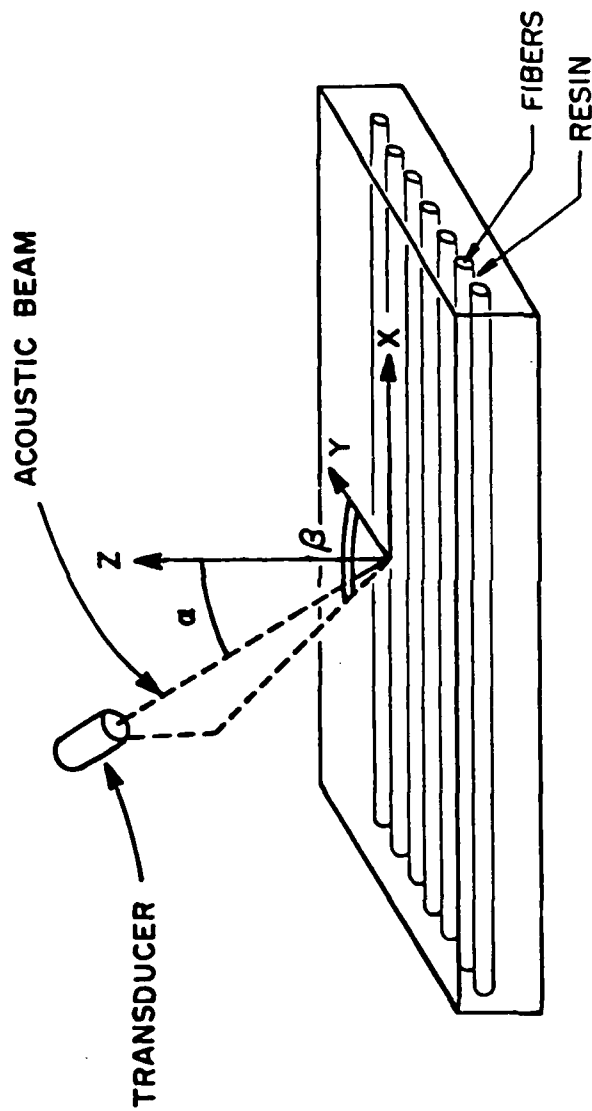
Figure 17. Ultrasonic attenuation record for FP/Mg specimen without intentional flaws (Specimen 1-1).

A second method of determining the ultrasonic attenuation required the use of a 10 MHz, shear wave, contact transducer operated in the pulse-echo mode. Ultrasonic attenuation records similar to that shown in Figure 17 were generated and reduced using the equations presented above. When the contact transducer was used, propylene glycol ($Z = 2.5 \times 10^6 \text{ kg/m}^2\text{s}$) was used as an acoustic couplant. The specimens were inspected in air so there was no reason to use the specimen holder shown in Figure 15.

2.2.3 Ultrasonic Backscattering

Ultrasonic backscattering is a technique which utilizes the inhomogeneous, layered nature of the composite to detect and image dominant microstructural features, such as cracks, fibers, etc. The basic concept¹⁰ is that a defect can be identified and possibly characterized from the magnitude and angular distribution of the scattered energy. This can be accomplished by using a device, shown schematically in Figure 18, which allows a transducer to be rotated at various surface incident angles. Since the maximum backscattered energy is received by the transmitting/receiving transducer when the transducer is normal to the defect, the shape, location, and orientation of the defect can be determined approximately by angularly indexing the transducer until a maximum reflected signal is generated.

The fixture built for the backscattering inspection is shown in Figure 19. The unit was edge mounted on a 61 cm (24 in.) cubic tank. A specimen was mounted in the special specimen holder which rests on the lower horizontal platform. The transducer was mounted in a holder which, like the support rods, had provision for vertical height adjustment. This was required because focused transducers are used and the focal length must be maintained throughout the full 360° rotation. The incident angle of the transducer was adjustable through 0° and 60° from the normal to the specimen surface. A potentiometer, mounted at the rotational pivot point, supplied a linearly variable voltage to an X-Y plotter to directly generate a reflected amplitude versus angular displacement curve.



WHERE:

α - ANGLE OF INCIDENCE

β - ANGLE BETWEEN Y-AXIS AND THE TRANSMITTER
BEAM TRAJECTORY ON THE LAYER PLANE

Figure 18. Detection of fiber orientation by ultrasonic backscattering measurements.

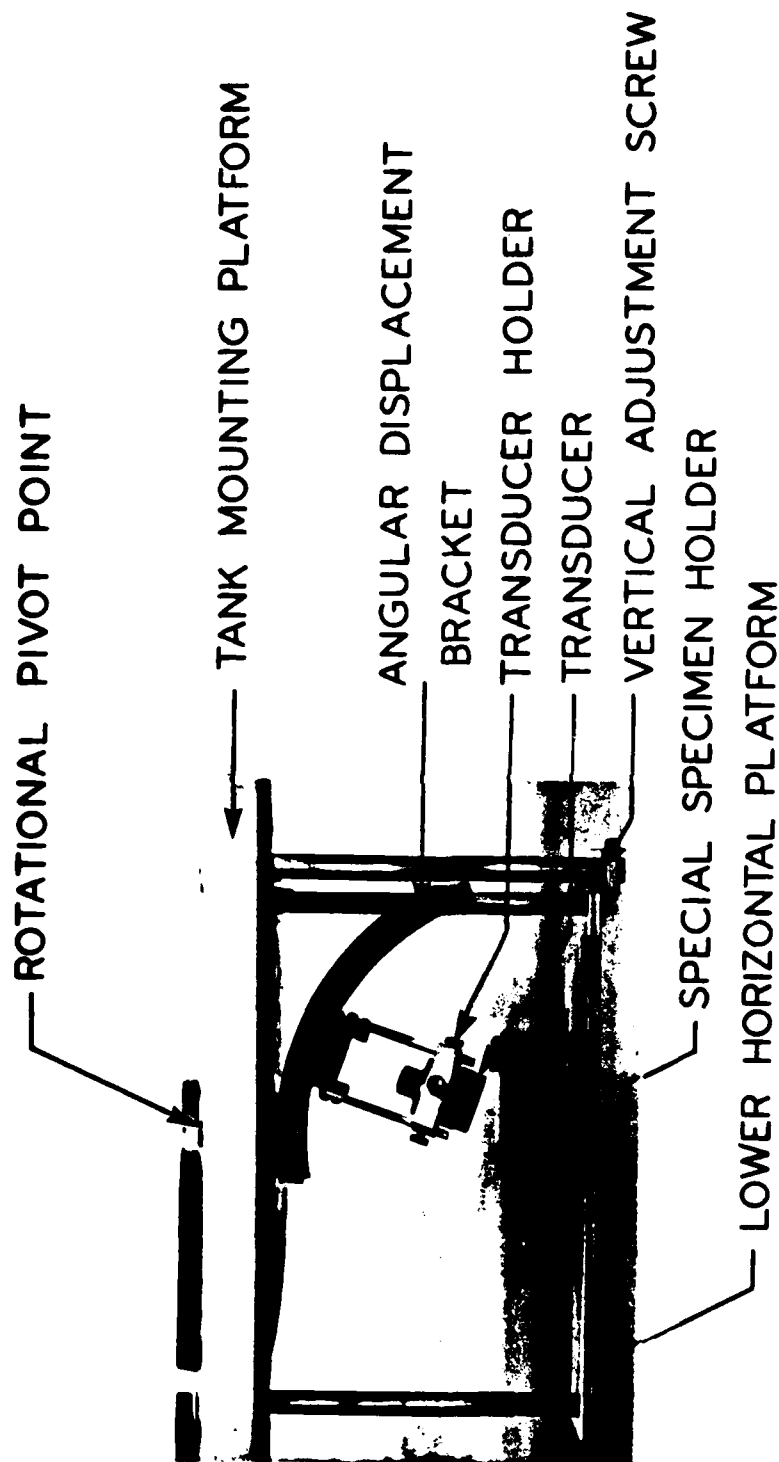


Figure 19. Backscattering measurement fixture.

2.2.4 Wave Propagation Velocity

The wave propagation velocities were determined using a Panametrics Model 5221 ultrasonic thickness gage. This is equivalent to measuring the wave propagation velocity, since the velocity or travel time must be known to measure the thickness. Any deviation between the thickness measured ultrasonically and that measured directly with a micrometer is related to the difference between the assumed and actual wave propagation velocity.

The longitudinal wave propagation velocities along the three principal material axes of an anisotropic material are given by:

$$c_{11} = \sqrt{\frac{Q_{11}}{\rho}}$$

$$c_{22} = \sqrt{\frac{Q_{22}}{\rho}}$$

$$c_{33} = \sqrt{\frac{Q_{33}}{\rho}}$$

where Q_{ij} are stiffnesses and ρ the material density. Any change in propagation velocity is related to changes in modulus and/or density. In the case of thin composite plates two of the equations above are simplified to:

$$c_{11} = \sqrt{\frac{Q_{11}}{\rho}} = \sqrt{\frac{E_{11}}{\rho (1 - \nu_{12} \nu_{21})}}$$

$$c_{22} = \sqrt{\frac{Q_{22}}{\rho}} = \sqrt{\frac{E_{22}}{\rho (1 - \nu_{12} \nu_{21})}}$$

Subscripts 1 and 2 denote fiber and transverse to the fiber directions. Subscript 3 denotes the normal to the plate direction. In the case of the FP/Mg specimens in question, with a 0.50 fiber volume ratio, the following properties¹¹

$$E_{11} = 207 \text{ GPa } (30 \times 10^6 \text{ psi})$$

$$E_{22} = 103 \text{ GPa } (15 \times 10^6 \text{ psi})$$

$$\nu_{12} = 0.28$$

$$v_{21} = 0.14$$

$$\rho = 2.850 \text{ kg/m}^3$$

were used to compute

$$C_{11} = 8,690 \text{ ms}^{-1} \text{ (342,125 in./sec)}$$

$$C_{22} = 6,145 \text{ ms}^{-1} \text{ (241,930 in./sec)}.$$

An approximate value for the velocity across the thickness is:

$$C_{33} = 6,400 \text{ ms}^{-1} \text{ (251,840 in./sec)}.$$

This then implies that any major deviation of the wave propagation velocity, as indicated by the ultrasonic thickness gage and the C_{33} value shown above, can be assumed to be due to a change in modulus and/or density. A change in modulus could be due to fiber-matrix debonding (Type 2), fiber fracture (Type 5), or matrix fracture (Type 7). A change in density could be due to porosity (Type 3) or a nonuniform fiber distribution (Type 6).

2.2.5 X-Ray Radiography

X-ray radiography was done with fine-grained, single emulsion X-ray films. The radiographs were generated using a 62 kV/10 mA excitation energy throughout a 25 sec exposure time. Initially, it was thought that a zinc iodide based penetrant would enhance the radiographic detailing of internal defects; but, the difficulties associated with the preparation and use of the penetrant solution, along with time restrictions, precluded its use. Additionally, the types of defects (adjacent to a free surface or edge) which could be enhanced by the penetrant solution were readily definable by ultrasonic inspection techniques.

2.3 TEST PROGRAM

The objective of the program was to apply nondestructive evaluation methods to assess the integrity of FP/Mg composite specimens with various flaw/defect types. Previous program experience¹²⁻¹⁴ indicated that of the five NDE methods described in the preceding section, ultrasonic inspection would be the foundation evaluation procedure to which the other procedures would provide supplemental/complementary information.

IIT RESEARCH INSTITUTE

Again, based on previous program experience, and the inherent acoustic propagation properties of composite laminate specimens, it was assumed that the lower frequency (1 and 2.25 MHz) transducers could be expected to supply very little information on material integrity. After a cursory inspection of several FP/Mg specimens with the 1 and 2.25 MHz transducers operated in the pulse-echo mode, the above assumption was borne out and full surface scanning of the specimens was initiated using a 5 MHz transducer operated in the pulse-echo mode. Results from the 5 MHz inspections indicated that a higher frequency transducer should generate a more detailed C-scan. It was then decided to conduct all subsequent ultrasonic inspections with the 15 MHz transducer, the highest frequency in IITRI's inventory of transducers.

Because of difficulties associated with using the X-Y plotter in the pen-lift mode during some of the preliminary ultrasonic inspections, many analog C-scans were generated. With the repair of the plotter, we were able to generate both pen-lift and analog C-scans of a single specimen in consecutive surface scans. Because of the sensitivity of the high frequency ultrasound to the surface smoothness of the specimens, and because of the triggering voltages required to operate the pen-lift mechanism on the plotter, it was determined that the analog C-scan was a more representative assessment of material integrity than the traditionally accepted pen-lift C-scan. A-scan oscilloscope photographs were made at selected points of interest as indicated by the analog or pen-lift C-scans.

In order not to bias the results of the wave attenuation or wave propagation velocity inspections, preliminary data were taken in a random "blind" procedure. That is, the ultrasonic C-scans were not available to the equipment operator at the time the attenuation or propagation velocity measurements were taken. Only after reduction of the raw data, and a general correlation between C-scan and propagation velocity/attenuation coefficient could be drawn, were measurements taken at locations of "apparent material flaw/damage" as indicated by the C-scans. The term "apparent material flaw/damage" refers to the fact that the true material integrity could not be determined until sectioning and micrographic inspections were completed.

The X-ray radiography and backscattering measurements were taken without regard to the other inspection procedures since they would not affect the results of those procedures.

Each of the NDE procedures was applied to all of the specimens sequentially to completion before a different or variation of a procedure was initiated. For example, all the 5 MHz ultrasonic inspections were completed before the wave propagation velocity measurements were started.

3. RESULTS

Results of the assessment of material integrity as determined by nondestructive evaluation are presented here for a representative specimen of each of the specimen types investigated. Ultrasonic C-scans of the remaining specimens of each group are presented in the Appendix.

3.1 TYPE 1 SPECIMEN

The representative specimen for the Type 1 group, with no intentional flaws, is Specimen 1-1.

3.1.1 Physical Properties

Prior to nondestructive inspection, all specimens were weighed and measured. This was done so that experimentally determined values of wave propagation velocity could be compared with the corresponding theoretical values.

$$L_{1-1} = 12.87 \text{ cm (5.068 in.)}$$

$$W_{1-1} = 3.82 \text{ cm (1.504 in.)}$$

$$T_{1-1} = 0.59 \text{ cm (0.231 in.)}$$

$$M_{1-1} = 81.2016 \text{ g (0.179 lb)}$$

where L = "average" length

W = "average" width

T = "average" thickness

M = "average" mass of the specimen indicated by subscript.

The "average" value is based on a minimum of four independent measurements.

Since $\rho = M/L \times W \times T$, where ρ = density, substituting value results in $\rho_{1-1} = 2.80 \text{ g/cm}^3 \text{ (0.101 lb/in}^3\text{)}$.

Replacing ρ_{1-1} in the wave propagation velocity equation presented in Subsection 2.2.4 yields

$$C_{33,1-1} = 6209 \text{ ms}^{-1} \text{ (244,400 in/sec)}.$$

As a baseline, a similar evaluation was done on a coupon of ZE41A magnesium alloy without FP fibers with the following results:

$$\rho_{\text{Mg}} = 1.81 \text{ g/cm}^3, \text{ and } C_{33\text{Mg}} = 5645 \text{ ms}^{-1} (222,190 \text{ in/sec}).$$

3.1.2 Ultrasonic Inspection

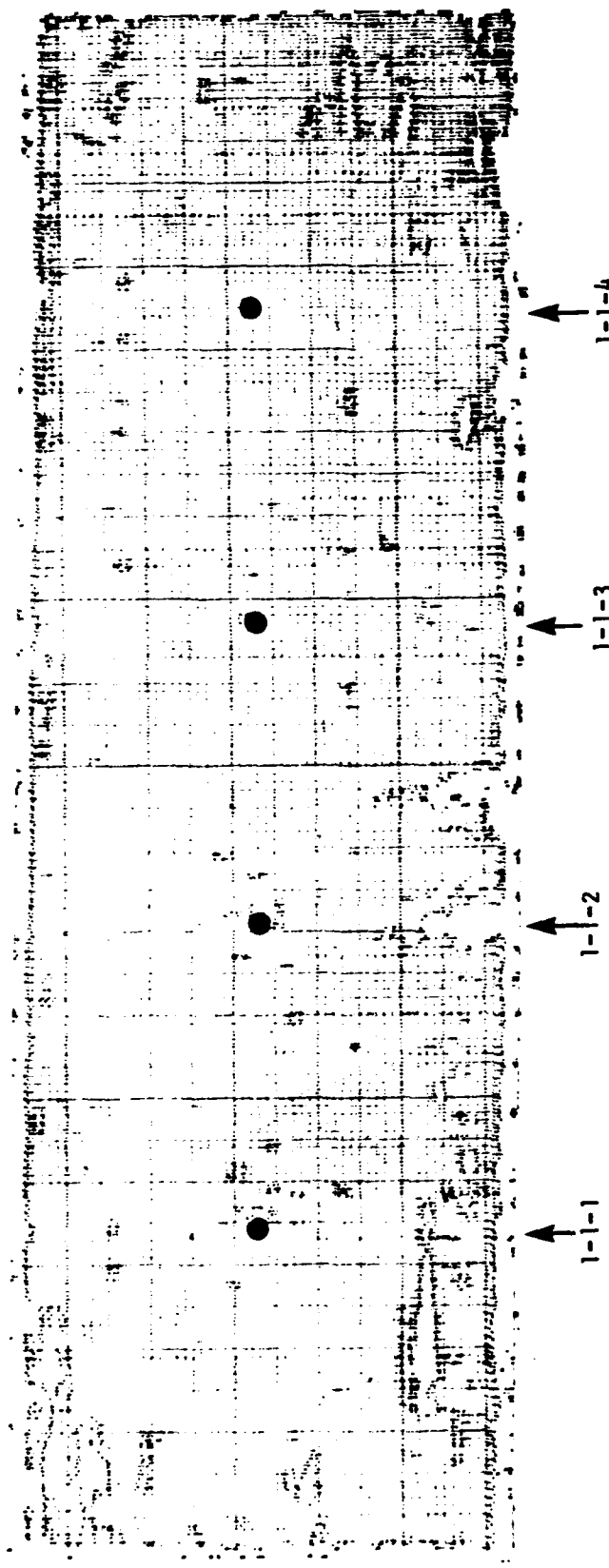
Figures 20 and 21 are pen-lift and analog C-scans, respectively, of Specimen 1-1. Both C-scans were generated using a 15 MHz, immersion, compression wave transducer operated in the pulse-echo mode with the specimen held in the special fixture (Figure 15).

The areas of "apparent flaws" were determined to be either surface irregularities or excess amounts of sealant which extruded onto the front face of the specimen. This determination was made by visual inspection and by interpretation of A-scan photographs taken at the areas of "apparent flaws." Figure 22 shows characteristic A-scans at an "apparently unflawed and flawed" location on Specimen 1-1.

The key to interpreting the two A-scans in Figure 22 is the relative shape and size of the front and back-face reflections. The difference between the A-scan at the "unflawed location (Figure 22a) and at the "flawed" location (Figure 22b) is a decrease in the amplitude of the front-face reflection of the waveform. This is an indication of a minor irregularity at the front-face of the specimen. In this instance an air bubble was attached to the front-face of Specimen 1-1. Similar A-scans were generated where surface irregularities (such as scratches) or excess sealant were present. Figure 23, a pen-lift C-scan of Specimen 1-1, which was generated using a 5 MHz, immersion, compression wave transducer operated in the pulse-echo mode, gives a better overall representation of the material integrity for this particular specimen, but is less sensitive to the presence of defects than the C-scans shown in Figures 20 and 21. This exemplifies the fact that the C-scan only indicates the presence of a defect, and provides limited information about the type or severity of a defect.

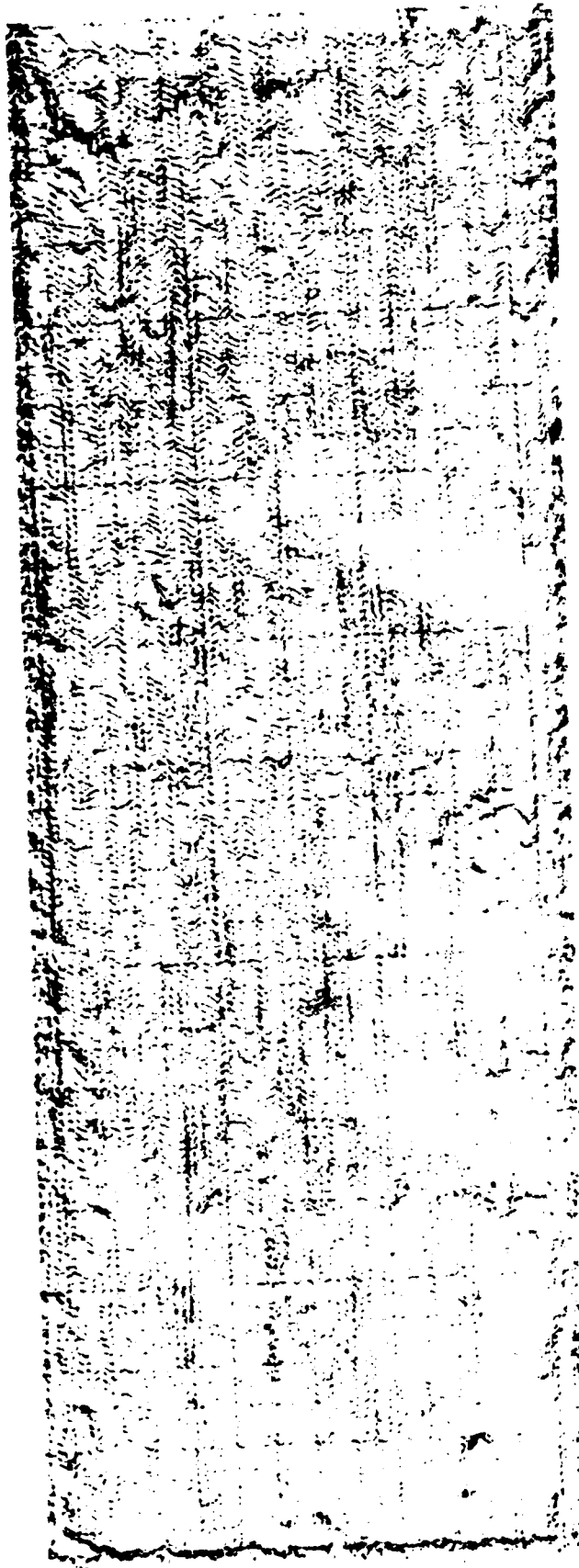
3.1.3 Wave Propagation Velocity

Figure 24 is a schematic drawing showing the locations where wave propagation velocity measurements were taken on Specimen 1-1 and the specimens



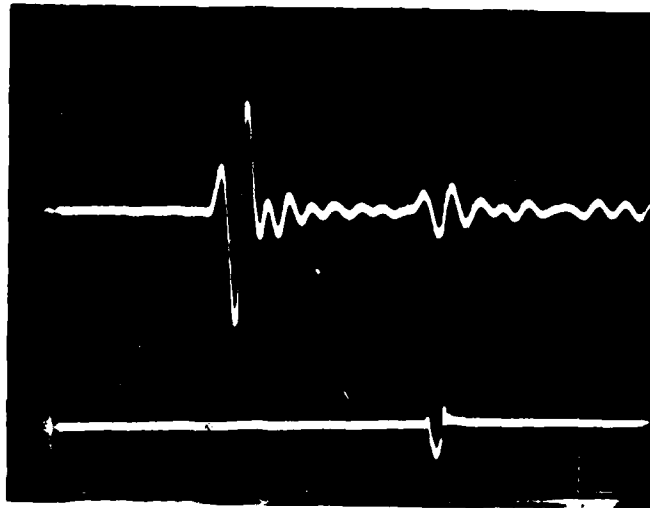
Repetition Rate	2K	Hz	Gated RF	Medium / Low
Damping	Variable/Maximum	Ohms	Frequency	Greater Than 8 MHz
Energy	2		Peak Polarity	Negative
Receiver Attenuation	4	dB	Gain	x10
High Pass Filter	1.0	MHz	Gain	40
Marked RF	Interface			dB

Figure 20. Pen-lift C-scan of FP/Mg Specimen 1-1 (no intentional flaws),
15 MHz transducer in pulse-echo mode.

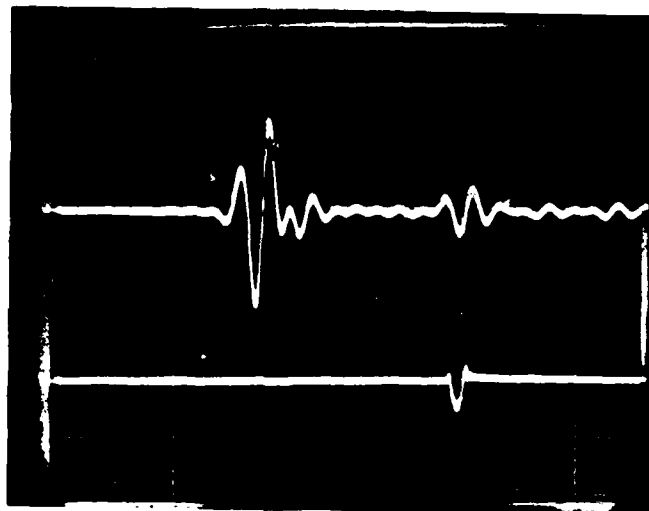


Repetition Rate	2K	Hz	Gated RF	Medium / Low
Damping	Variable/Maximum	Ohms	Frequency	Greater Than 8 MHz
Energy	1		Peak Polarity	Negative
Receiver Attenuation	6	dB	Gain	x10
High Pass Filter	1.0	MHz	Gain	40
Marked RF	Interface			

Figure 21. Analog C-scan of FP/Mg Specimen 1-1 (no intentional flaws),
15 MHz transducer in pulse-echo mode.

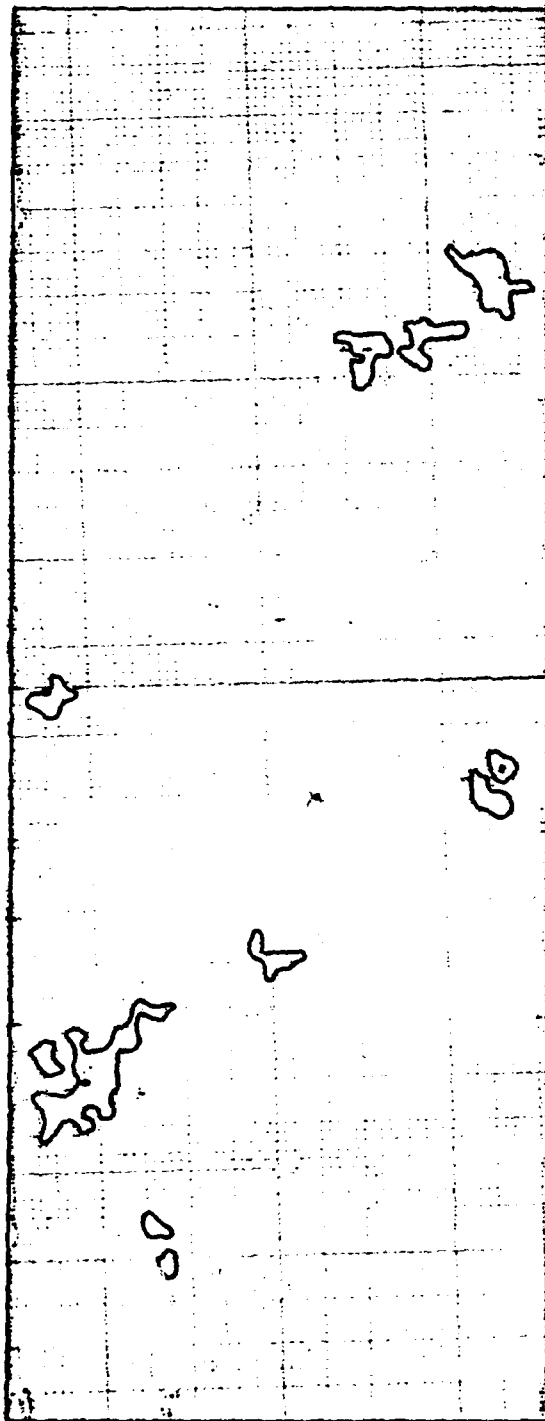


(a)



(b)

Figure 22. Amplitude-time records (A-scans) of ultrasonic pulse at two locations of Specimen 1-1. (a) Unflawed location, (b) flawed location. (0.5 V/div, 0.5 μ sec/div) 15 MHz transducer in pulse-echo mode.



Repetition Rate	2K	Hz	Gated RF	Medium	/ Low
Damping	Variable/Maximum	Ohms	Frequency	Less Than	8 MHz
Energy	4		Peak Polarity	Negative	
Receiver Attenuation	0	dB	Gain	x10	
High Pass Filter	1.0	MHz	Gain	20	dB
Marked RF	Interface				

Figure 23. Pen-lift C-scan of FP/Mg Specimen 1-1 (no intentional flaws),
15 MHz transducer in pulse-echo mode.

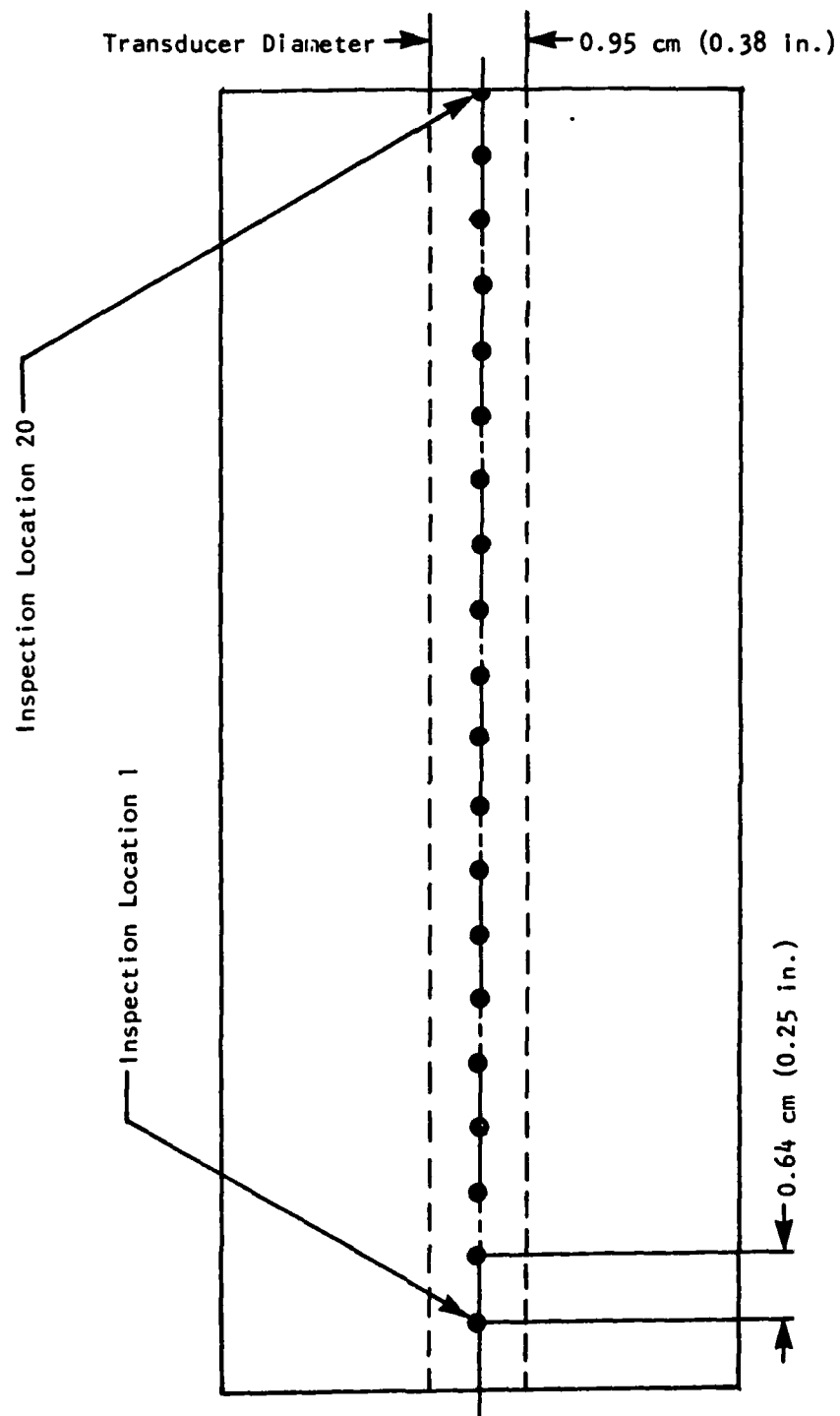


Figure 24. Locations of measurements of wave propagation velocity.

shown in the subsections to follow. This procedure was used to generate a data base large enough that an average velocity and gross deviations from the average velocity could be readily determined.

Table 1 shows the wave propagation velocities for the 20 inspection locations shown in Figure 24 and the average wave propagation velocity of the 20 measurements. There is good agreement (less than 5% deviation) between the empirical average of 6466 ms^{-1} and the theoretical value of 6209 ms^{-1} . This was expected since the Type 1 specimens had no intentional flaws. The continuity of the velocity measurements (the deviation was less than $\pm 3\%$ from the average) indicates that the specimen material was "uniform" in integrity. "Uniform" means within a reasonably acceptable variation range of $\pm 5\%$ from both the empirical average and the calculated, theoretical value of wave propagation velocity. The wave propagation velocity technique indicated uniform material integrity in keeping with theory for a specimen with no intentional flaws.

3.1.4 Wave Attenuation

Figure 20 shows the four locations where ultrasonic wave attenuation measurements were recorded. The material attenuation coefficients shown in Table 2 were determined by using the water delay line and contact transducer techniques.

The attenuation coefficients are in "good agreement" with the ultrasonic C-scans and wave propagation velocity results for Specimen 1-1. For the purpose of this report, "good agreement" means that the calculated attenuation coefficients were consistent at the various inspection locations for both the water delay line and contact transducer technique, and with one another within each of the two techniques. As was indicated by the wave propagation data, the continuity of the material attenuation data indicates the material was "uniform" in integrity.

The consistency of the measured wave propagation velocities and material attenuation coefficients indicated that the average values shown in Tables 1 and 2, respectively, could be used as the baseline to which subsequent data are compared.

TABLE 1. WAVE PROPAGATION VELOCITY ACROSS
THE THICKNESS AT VARIOUS LOCATIONS
ALONG SPECIMEN CENTERLINE (SPECIMEN 1-1)

<u>Inspection Location</u>	<u>Velocity, ms⁻¹ (10⁵ in/sec)</u>
1	6461 (2.543)
2	6479 (2.550)
3	6486 (2.553)
4	6512 (2.563)
5	6527 (2.569)
6	6507 (2.561)
7	6486 (2.553)
8	6512 (2.563)
9	6494 (2.556)
10	6499 (2.558)
11	6479 (2.550)
12	6502 (2.559)
13	6433 (2.532)
14	6423 (2.528)
15	6453 (2.540)
16	6461 (2.543)
17	6471 (2.547)
18	6453 (2.540)
19	6339 (2.495)
20	6344 (2.497)
Average:	6466 (2.545)

TABLE 2. ULTRASONIC WAVE ATTENUATION COEFFICIENTS (SPECIMEN 1-1)

Inspection Location	Attenuation (α), dB		Specimen Thickness d , cm (in.)	Material Attenuation (α), dB/cm (dB/in.)	
	Water Delay Line	Contact Transducer		Water Delay Line	Contact Transducer
1-1-1	0.189	0.202	0.585 (0.230)	0.32 (0.82)	0.35 (0.88)
1-1-2	0.193	0.204	0.585 (0.230)	0.33 (0.83)	0.35 (0.88)
1-1-3	0.195	0.204	0.585 (0.230)	0.33 (0.83)	0.35 (0.88)
1-1-4	0.191	0.202	0.585 (0.230)	0.33 (0.83)	0.35 (0.88)
Average	0.192	0.203	0.585 (0.230)	0.33 (0.83)	0.35 (0.88)

3.1.5 X-Ray Radiography

Figure 25 shows the X-ray radiography for Specimen 1-1. As was expected for a specimen with no intentional flaws, the radiograph shows no indication of the presence of any material damage.



Figure 25. X-ray radiograph of FP/Mg specimen with no intentional flaws (Specimen 1-1).

3.1.6 Ultrasonic Backscattering

Figure 26 is a characteristic backscatter curve of Specimen 1-1. The incident angle (α) of the 5 MHz immersion transducer operated in the pulse-echo mode was 20° with respect to a line normal to the front-face surface plane of the specimen. The curve shows activity only as the focal axis of the transducer sweeps near and through the plane normal to the fiber orientation. Any activity shown away from $\theta = 90^\circ \pm 5^\circ$ would be due to a material defect, since all the specimens, with the exception of Type 4, had a uniaxial fiber orientation. The curve in Figure 26 indicates no material defects in the area of inspection of Specimen 1-1.

3.1.7 Micrographic Inspection

Figures 27 and 28 show four micrographs each of sections cut and polished from Specimen 1-1. The sections indicated on Figures 27 and 28 correspond to the inspection locations shown on Figure 20. These micrographs indicate the specimen had uniform material integrity, as expected for a specimen with no intentional flaws. There are no indications of gross defects in the material at any of the inspection locations. At the 200X magnification, individual fiber bundles can be seen as dark circles, but no gross material defects are

IIT RESEARCH INSTITUTE

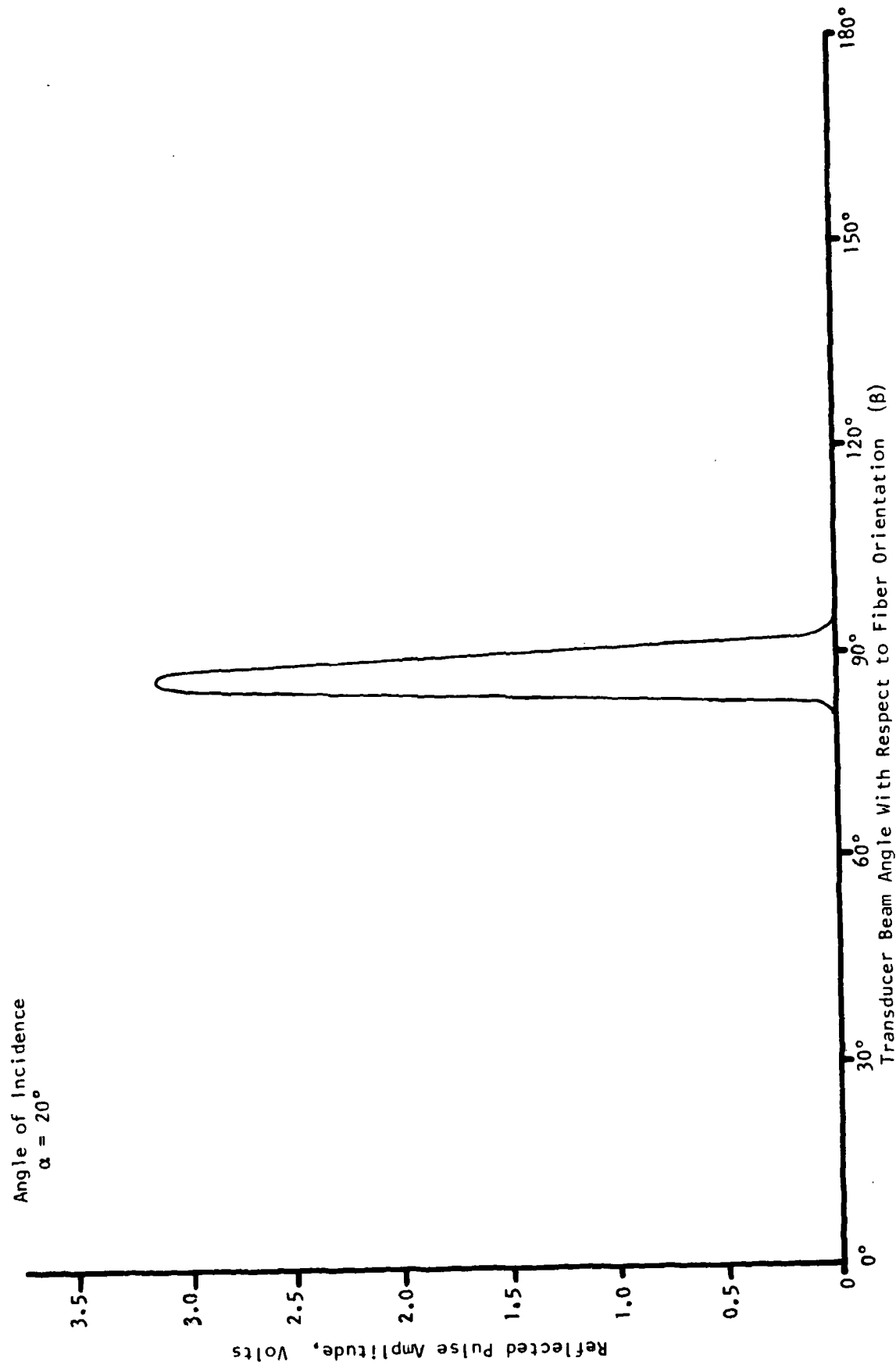
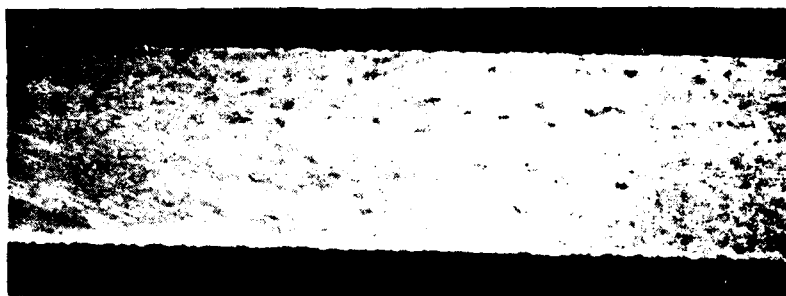


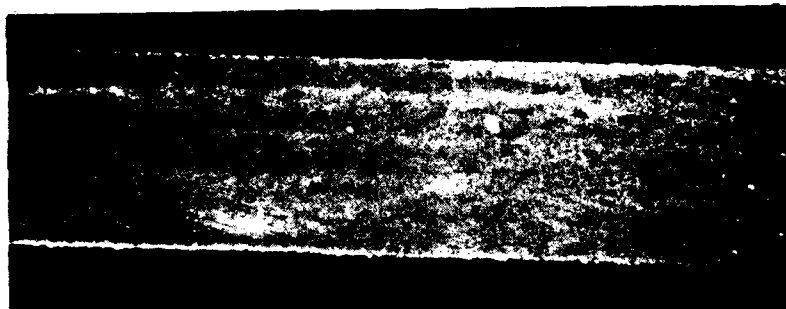
Figure 26. Ultrasonic backscattering curve of FP/Mg specimen with no intentional flaws (Specimen 1-1).



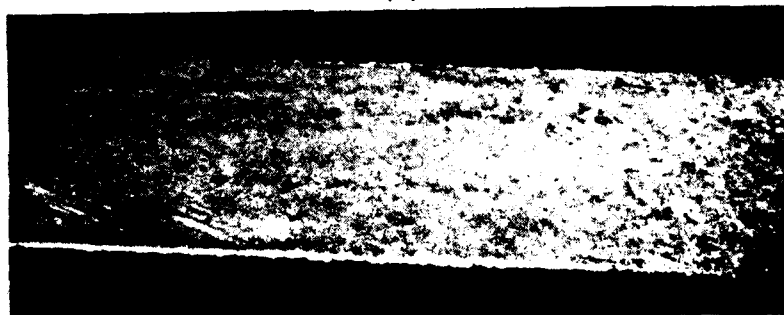
(a)



(b)



(c)



(d)

Figure 27. Micrographs (5X) of FP/Mg Specimen 1-1 (no intentional flaws) at four locations: (a) Location 1-1-1, (b) Location 1-1-2, (c) Location 1-1-3, and (d) Location 1-1-4.

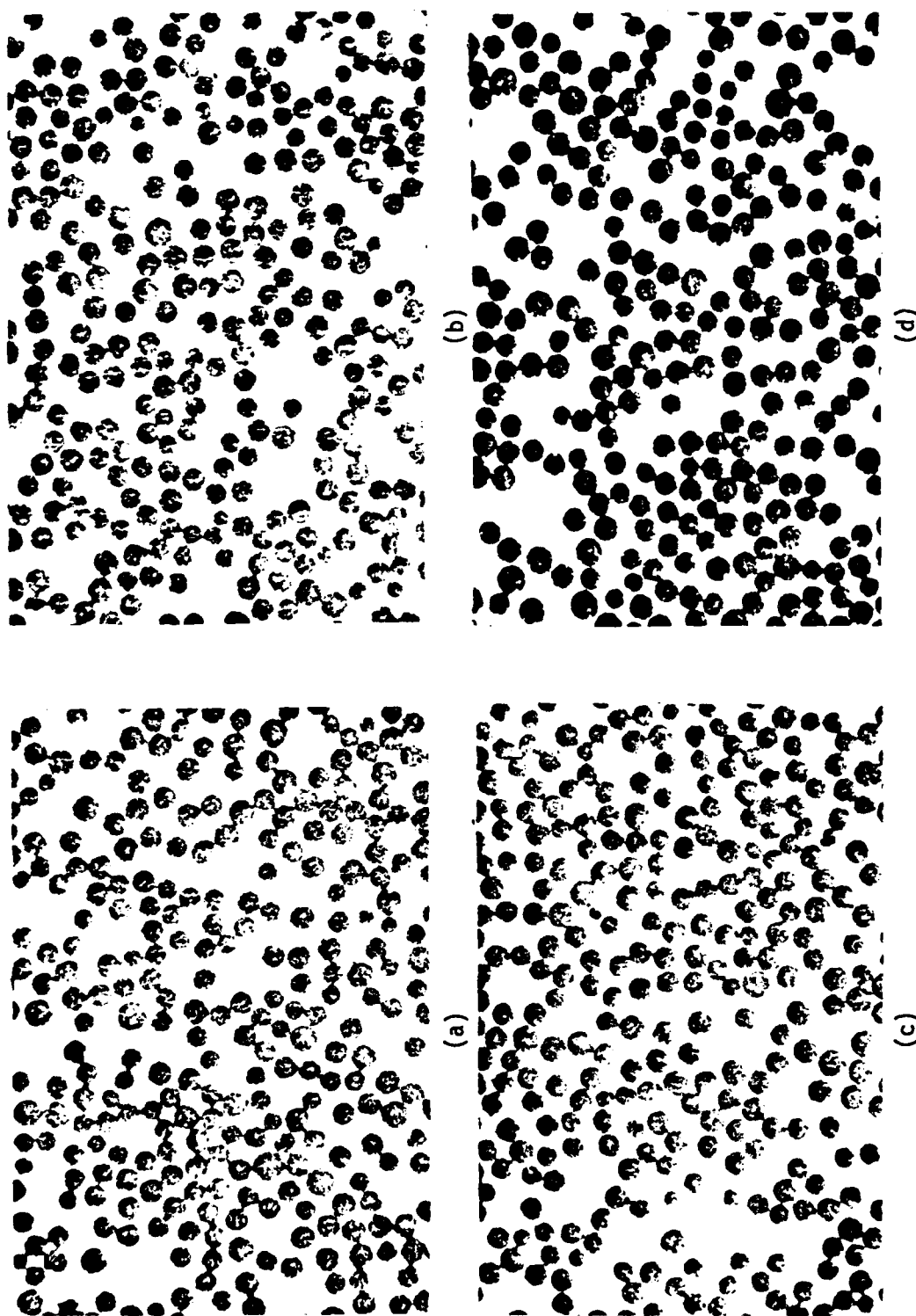


Figure 28. Micrographs (200X) of FP/Mg Specimen 1-1 (no intentional flaws) at four section locations: (a) Location 1-1-1, (b) Location 1-1-2, (c) Location 1-1-3, and (d) Location 1-1-4.

evident. The fiber bundles appear to be uniformly distributed throughout the area of inspection of the micrograph.

3.1.8 Comparison of Inspection Procedures

All of the NDE procedures used to evaluate Specimen 1-1 indicated that the specimen had uniform material integrity within acceptable experimental tolerances in keeping with its "no intentional flaws" description. The NDE procedures indicated that there would be no difficulties in using all the procedures on all the specimens with reproducible results. It was determined that the ultrasonic C-scan would be the primary imaging NDE technique, while the other techniques would be required to provide support data to accurately define the defect type.

3.2 TYPE 2 SPECIMEN

The representative specimen for the Type 2 group, with fiber-matrix debonding, is Specimen 2-1.

3.2.1 Physical Properties

The pertinent physical properties for Specimen 2-1 are as follows:

$$L_{2-1} = 12.87 \text{ cm (5.066 in.)}$$

$$W_{2-1} = 3.82 \text{ cm (1.505 in.)}$$

$$T_{2-1} = 0.64 \text{ cm (0.252 in.)}$$

$$M_{2-1} = 91.4231 \text{ g (0.201 lb)}$$

$$\rho_{2-1} = 2.91 \text{ g/cm}^3 \text{ (0.105 lb/in}^3\text{)}$$

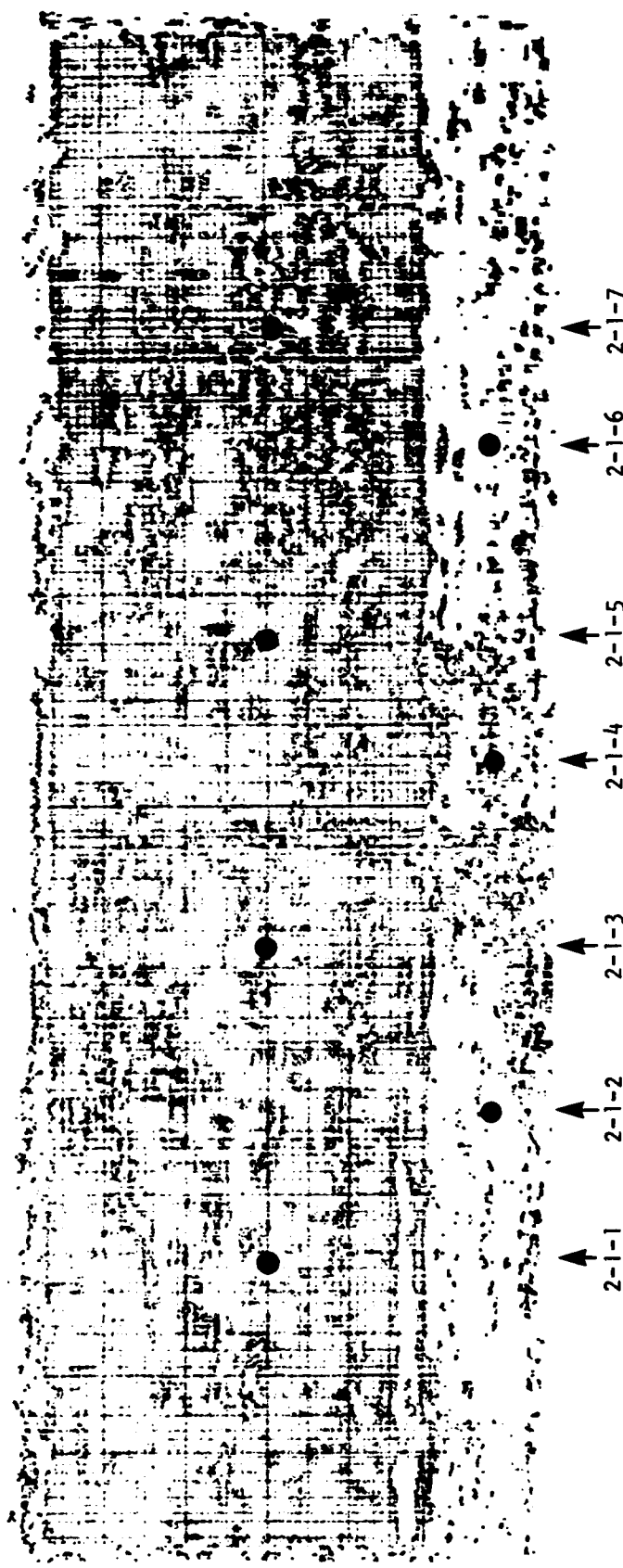
$$C_{33_{2-1}} = 6090 \text{ ms}^{-1} \text{ (239,700 in/sec).}$$

These values indicate a 4% higher density, and 2% lower theoretical wave propagation velocity than the baseline of Specimen 1-1. These values are within an acceptable tolerance of $\pm 5\%$ from the baseline values.

3.2.2 Ultrasonic Inspection

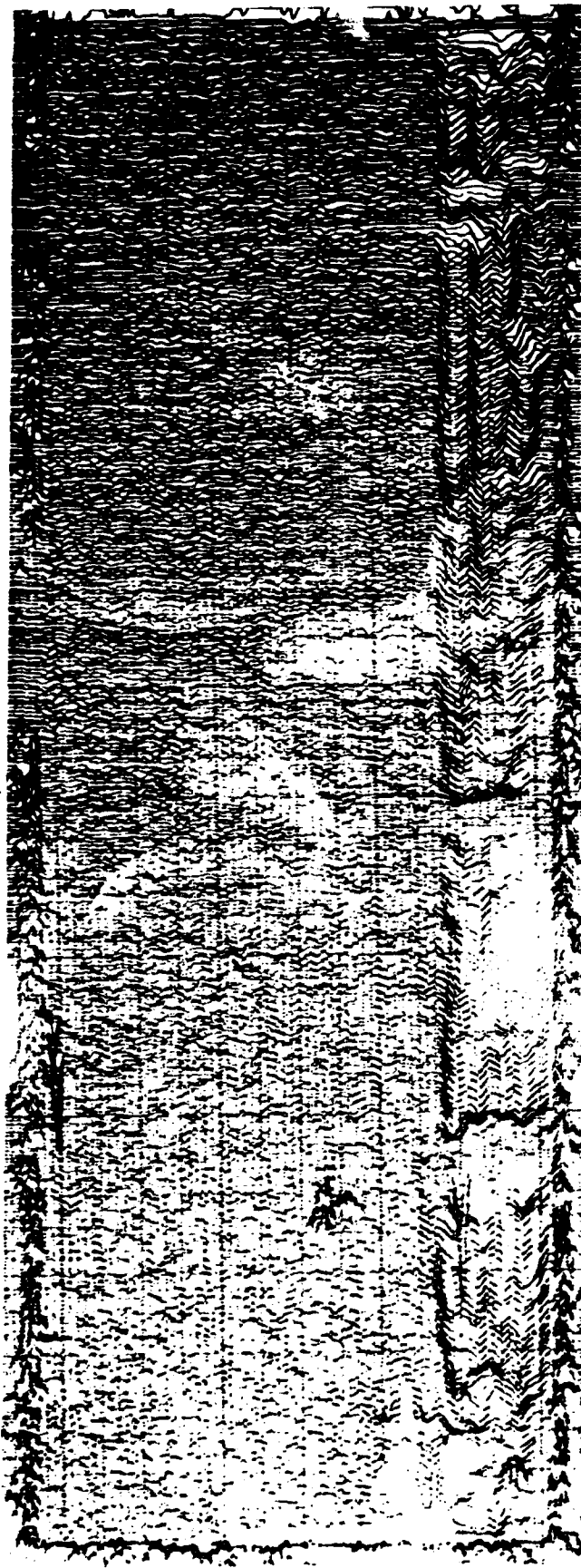
Figures 29 and 30 are pen-lift and analog C-scans, respectively, of Specimen 2-1. Both C-scans were generated using a 15 MHz immersion, compression wave transducer operated in the pulse-echo mode with the specimen held in the special fixture.

Both C-scans show a strip of apparently flawed material running the length of the specimen adjacent to the lower edge. The strip was 1.47 cm



Repetition Rate	2K	Hz	Gated RF	Medium / Low
Damping	Variable/Maximum	Ohms	Frequency	Greater Than 8 MHz
Energy	4		Peak Polarity	Negative
Receiver Attenuation	0	dB	Gain	x10
High Pass Filter	1.0	MHz	Gain	40
Marked RF	Interface			

Figure 29. Pen-lift C-scan of FP/Mg Specimen 2-1 (fiber-matrix debonding), 15 MHz transducer in pulse-echo mode.



Repetition Rate	2K	Hz	Gated RF	Medium / Low
Damping Variable/Maximum	1	Ohms	Frequency	Greater Than 8 MHz
Energy	1		Peak Polarity	Negative
Receiver Attenuation	6	dB	Gain	x10
High Pass Filter	1.0	MHz	Gain	40
Marked RF	Interface			dB

Figure 30. Analog C-scan of FP/Mg Specimen 2-1 (fiber-matrix debonding),
15 MHz transducer in pulse-echo mode.

(0.58 in.) wide. The remaining areas of apparent flaws were determined to be surface irregularities by A-scan interpretation.

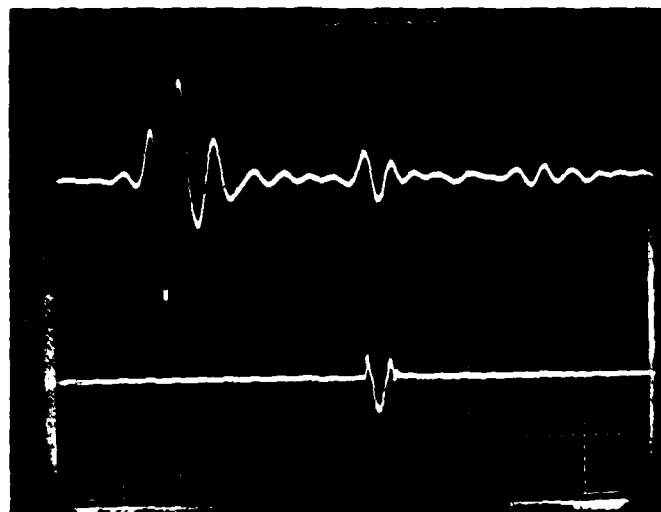
A-scan photographs were taken in the strip of apparently flawed material as indicated by the C-scans (Figures 29 and 30). Figure 31 shows an A-scan at an unflawed location (Figure 31a) and an apparently flawed location within the strip (Figure 31b). The A-scan of the unflawed location of Specimen 2-1 is in good agreement with a similar A-scan of an unflawed location of Specimen 1-1 (Figure 22a). Figure 31b is a classic representation of a specimen with a delamination. The delamination is indicated by the large "M" shape in the waveform between the front and back-face reflections.

The delamination acts like a free surface, in that it reflects a majority of the ultrasound back to the transducer instead of allowing the ultrasound to pass across the delamination to be reflected by the back-face of the specimen. The amplitude of the delamination reflection is determined by the relative positions of the transmitting/receiving transducer and the delamination within the specimen. The closer the transducer is to the delamination, the higher the reflection amplitude because the material attenuation is less. Because a small portion of the ultrasound crossed the delamination, the amplitude of the back-face reflection decreased to where the location of the back-face was almost unidentifiable. The position of the delamination reflection indicates the delamination could be expected to be found near the mid-thickness of the specimen, most probably between the third and fourth plies or fourth and fifth plies.

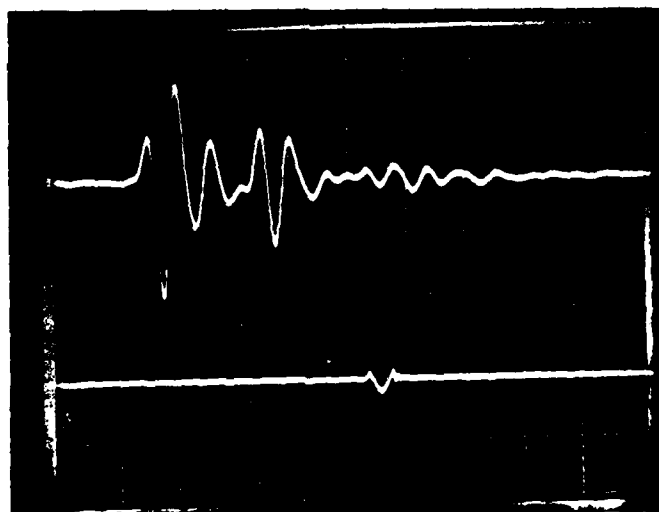
For Specimen 2-1, ultrasonic inspection, pen-lift/analog C-scan, and A-scan photographs gave a representative indication of the presence of a delamination near the mid-thickness of the specimen. Visual inspection of Specimen 2-1 confirmed the presence of the delamination since the defect was open to the free surface on the lower edge. Subsequent discussions with DuPont personnel, reported in the ninth monthly progress report (IITRI-M06084-9), indicated that the Type 2 specimens were fabricated with delaminations instead of fiber-matrix debonding.

3.2.3 Wave Propagation Velocity

Table 3 shows the wave propagation velocities for the 20 inspection locations shown in Figure 24 and the average wave propagation velocity of the 20



(a)



(b)

Figure 31. Amplitude-time records (A-scans) of ultrasonic pulse at two locations of Specimen 2-1 (fiber-matrix debonding). (a) Unflawed location, (b) flawed location. (0.5 V/div, 0.5 μ s/div.) 15 MHz transducer in pulse-echo mode.

TABLE 3. WAVE PROPAGATION VELOCITY ACROSS
THE THICKNESS AT VARIOUS LOCATIONS
ALONG SPECIMEN CENTERLINE (SPECIMEN 2-1)

<u>Inspection Location</u>	<u>Velocity, ms⁻¹ (10⁵ in/sec)</u>
1	12513 (4.925)
2	13305 (5.237)
3	13366 (5.261)
4	13727 (5.403)
5	13709 (5.396)
6	13034 (5.130)
7	13697 (5.391)
8	13079 (5.148)
9	13646 (5.371)
10	13196 (5.194)
11	14009 (5.514)
12	13183 (5.189)
13	13745 (5.410)
14	13567 (5.340)
15	13506 (5.316)
16	12348 (4.860)
17	12899 (5.077)
18	12924 (5.086)
19	12449 (4.900)
20	12833 (5.051)
Average:	13237 (5.210)

measurements. There is little correlation between the average wave propagation velocity shown in Table 3 and the theoretical value of 6900 ms^{-1} and the empirical value of 6466 ms^{-1} from Specimen 1-1. This is directly traceable to the presence of the delamination shown in the ultrasonic C-scan.

The average wave propagation velocity of $13,237 \text{ ms}^{-1}$ ($521,000 \text{ in/sec}$) for Specimen 2-1 is approximately twice the theoretical and empirical values shown above. This occurred because the delamination was at mid-thickness and because the thickness gage is an ultrasonic device. Once again the ultrasound was reflected by the delamination instead of the back-face of the specimen. Since the wave propagation velocity setting on the thickness gage was set such that the ultrasonically indicated thickness corresponded to that determined by micrometer, the wave propagation velocity appeared to be twice as fast as expected. By approximately correcting for the presence of the delamination by dividing by 2 (since the delamination was near mid-thickness), the "corrected" average wave propagation velocity is 6619 ms^{-1} ($260,500 \text{ in/sec}$) which is within 9% of the theoretical value and within 3% of the empirical value for Specimen 1-1.

The large variation in the individual measurements of wave propagation velocity was also caused by the delamination. The irregular nature (variable material thicknesses and delamination separation distances) of interlaminar separations tends to dissipate ultrasonic wave energy at various rates at various locations on the specimen resulting in a scattering of the measured wave propagation velocities.

For Specimen 2-1, wave propagation velocity measurements supported the ultrasonic C-scans and agreed very well with the A-scans as to the position of the delamination through the thickness.

3.2.4 Wave Attenuation

Figure 29 shows the seven locations where ultrasonic wave attenuation measurements were recorded. Because of the dissipative nature of the delamination and its mid-thickness location, it was impossible to get a sufficient number of measurable reflected pulse amplitudes to reduce the attenuation coefficient equations. Neither the water delay line nor the contact transducer technique was able to generate reproducible values for Specimen 2-1. Either

of the two techniques could be expected to work on Specimen 2-1 if a higher transducer excitation energy was available.

3.2.5 X-Ray Radiography

Figure 32 shows the X-ray radiograph for Specimen 2-1 where a contrast change indicates the presence of the delamination shown in the ultrasonic C-scans. No enhancement media was used to generate Figure 31. Both the extent and width of the delamination agree well with the C-scan.



Figure 32. X-ray radiograph of FP/Mg specimen with fiber-matrix debonding/delamination (Specimen 2-1).

This indicates that X-ray radiography works well in showing a gross planar defect parallel to the fiber plies. The contrast difference between the unflawed and flawed areas of material could be enhanced with the use of a dye or penetrant since the delamination is open to a free surface.

For Specimen 2-1, X-ray radiography supported the ultrasonic C-scans as to the extent of the delamination, but did not provide any through-the-thickness information as did the A-scans.

3.2.6 Ultrasonic Backscattering

Figure 33 is a backscatter curve of Specimen 2-1. The incident angle (α) of the 5 MHz immersion transducer operated in the pulse-echo mode was 20° with respect to a line normal to the front-face surface plane of the specimen. As before, the curve shows activity only as the focal axis of the transducer sweeps near and through the plane normal to the fiber orientation.

The only apparent effect of the defect area is the reduction of the reflected pulse amplitude from that of Specimen 1-1 (Figure 26). This is because of the attenuative nature of the delamination in that multiple internal reflections occur between the delamination and free surfaces causing a reduction of reflected pulse amplitude.

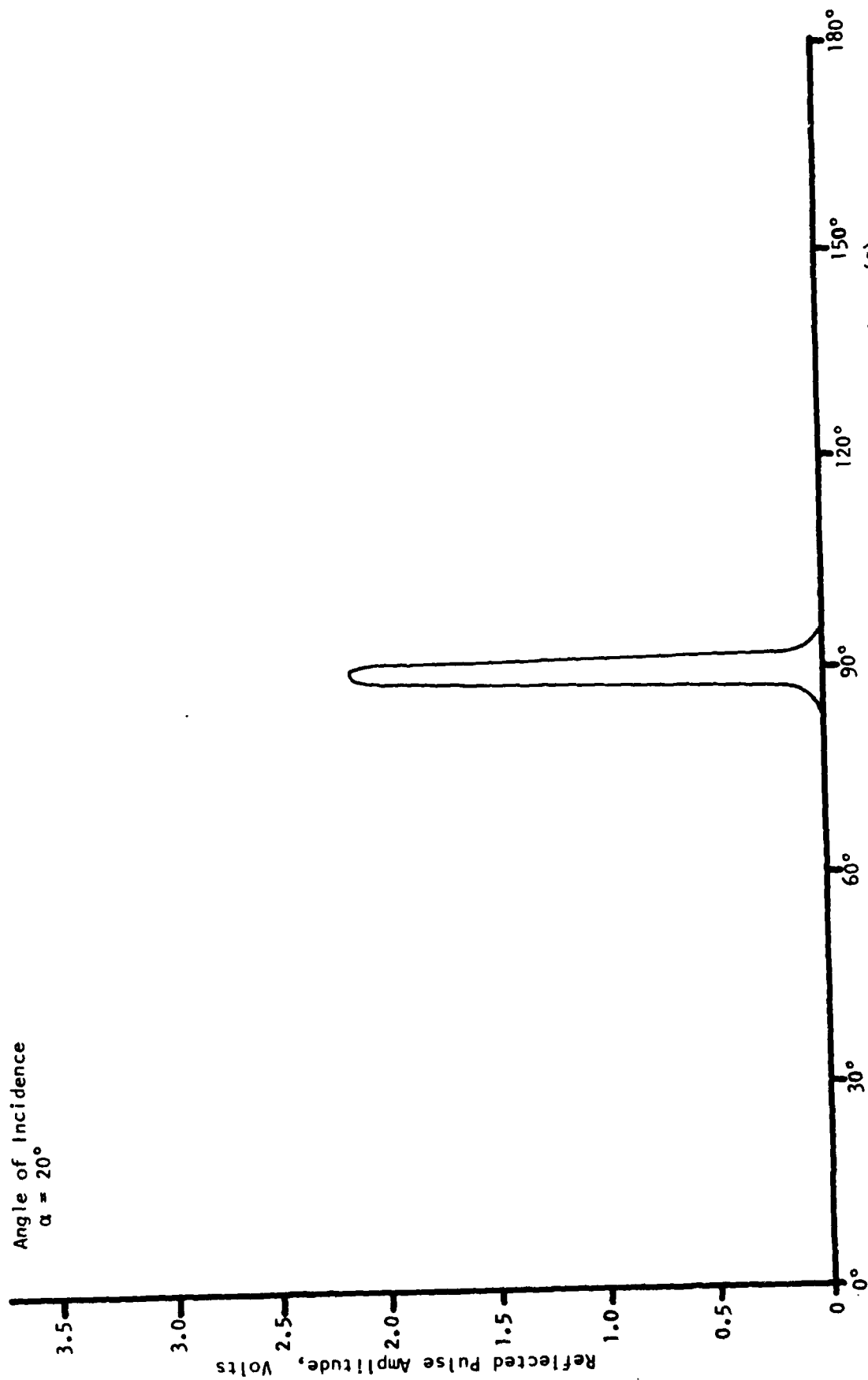


Figure 33. Ultrasonic backscattering curve of FP/Mg specimen with fiber-matrix debonding (Specimen 2-1).

3.2.7 Micrographic Inspection

Figures 34 and 35 show four micrographs each of sections cut and polished from Specimen 2-1. Section locations 2-1-1, 2-1-2, 2-1-3, and 2-1-4 on Figures 34 and 35 correspond to inspection locations 2-1-1, 2-1-3, 2-1-5, and 2-1-7 on Figure 29, respectively.

The micrographs clearly show the debonding/delamination indicated by the ultrasonic C-scans. The extent of the delamination across the width of the specimen is far greater than that shown by the C-scan. This indicates that the delamination was "tight" or filled beyond the point indicated by the ultrasonic C-scans. A "tight" delamination is one where the material has two distinct surfaces, but they are compressed together by internal or external forces to such an extent that ultrasound passes across the delamination as if it were not present. A tight delamination can be shown by ultrasonic inspection by using lower frequency (longer wavelength) ultrasound or raising the attenuation level of the ultrasonic pulser-receiver if the presence of a tight delamination is expected. Care must be taken if either of the two changes mentioned above is to be implemented because these could result in distortion, misinterpretation, or overlooking critical defects within the material. It is normally assumed that an area of tight delamination accompanies a gross delamination since the stress distribution within a specimen precludes the possibility of a delamination being present without a material transition accompanying it.

The 200X micrographs in Figure 35 tend to support the filled delamination assumption. This comes from the fact that the originals of the figures shown illustrate grey tones at the delamination instead of the dark black normally associated with cracks/delaminations viewed under high magnification. The material in the delamination could be either an oxide form of the matrix (from prolonged immersion during scanning) or a mineral deposit trapped in the delamination supplied by the water immersion medium.

3.2.8 Comparison of Inspection Procedures

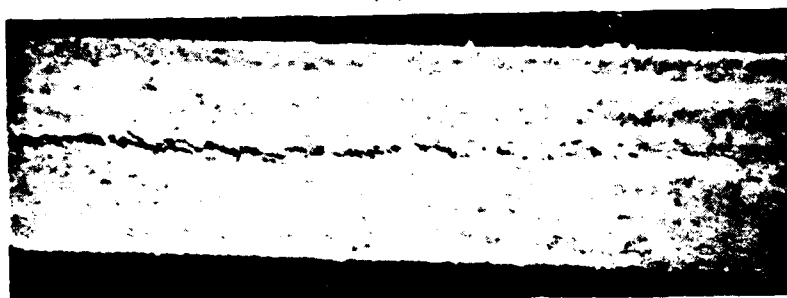
Of the NDE procedures used to evaluate Specimen 2-1, ultrasonic inspection, wave propagation velocity, and X-ray radiography indicated the presence of the mid-thickness delamination. Ultrasonic inspection (C-scans with supporting A-scans) gave the most information in that it determined the extent of



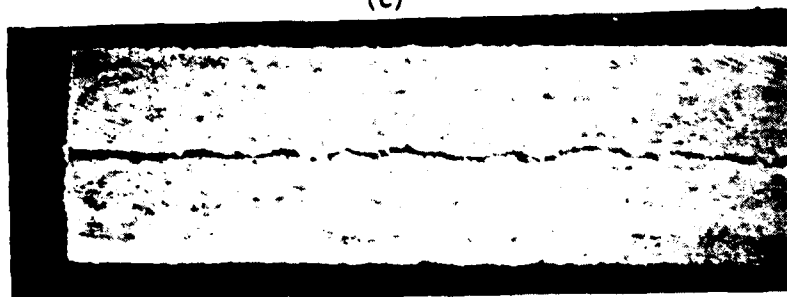
(a)



(b)



(c)



(d)

Figure 34. Micrographs (5X) of FP/Mg Specimen 2-1 (fiber-matrix debonding) at four section locations: (a) Location 2-1-1, (b) Location 2-1-2, (c) Location 2-1-3, and (d) Location 2-1-4.

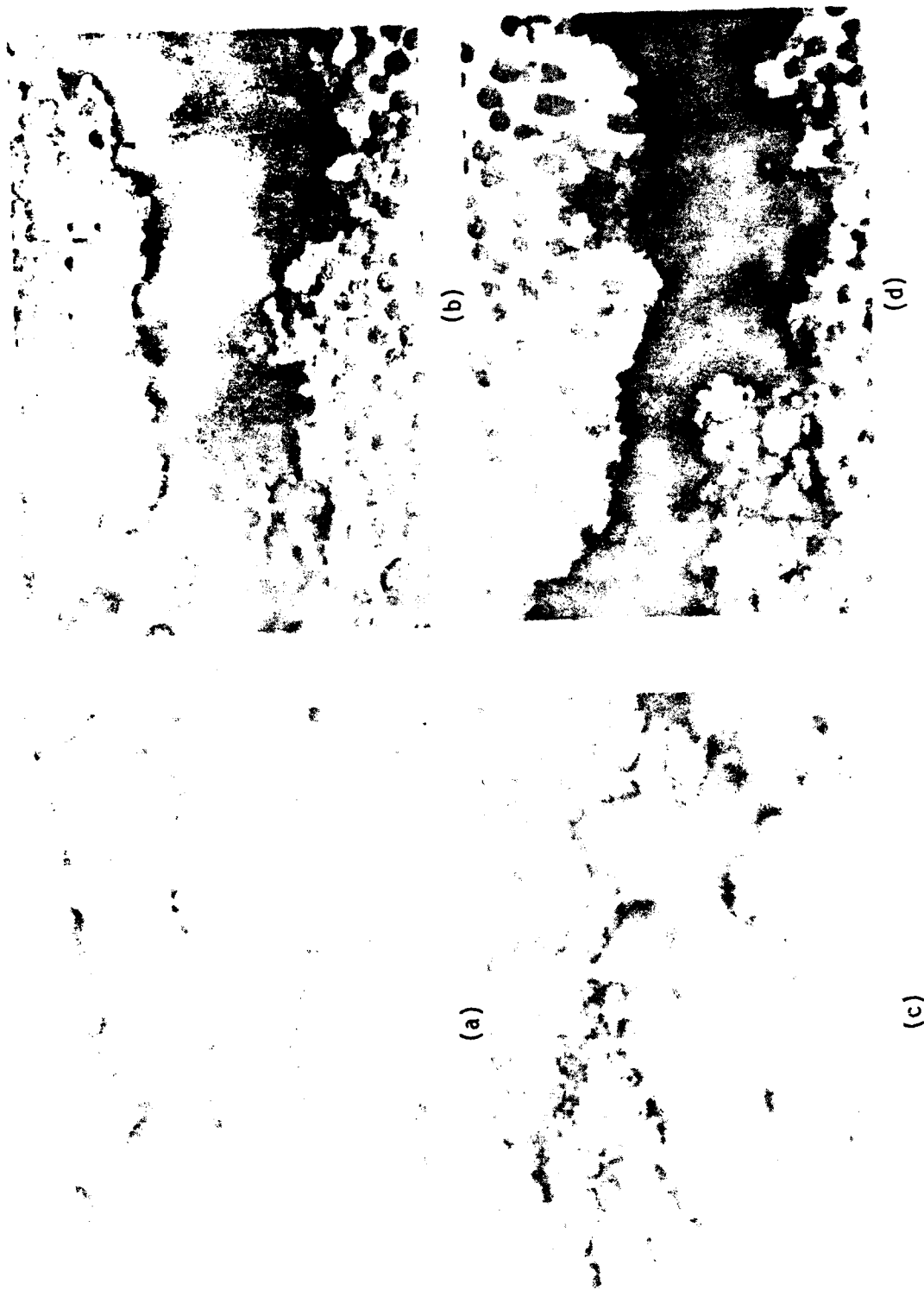


Figure 35. Micrographs (200X) of FP/Mg Specimen 2-1 (fiber-matrix debonding) at four section locations: (a) Location 2-1-1, (b) Location 2-1-2, (c) Location 2-1-3, and (d) Location 2-1-4.

the delamination strip (by C-scan) and its through-the-thickness location (by A-scan). Wave propagation velocity measurements indicated the presence of a gross planar defect, but could not supply any through-the-thickness information.

Wave attenuation and backscattering provided virtually no information as to the state of material integrity of Specimen 2-1.

3.3 TYPE 3 SPECIMEN

The representative specimen for the Type 3 group, with porosity, is Specimen 3-1.

3.3.1 Physical Properties

The pertinent physical properties for Specimen 3-1 are as follows:

$$\begin{aligned}L_{3-1} &= 12.91 \text{ cm (5.083 in.)} \\W_{3-1} &= 3.84 \text{ cm (1.510 in.)} \\T_{3-1} &= 0.44 \text{ cm (0.174 in.)} \\M_{3-1} &= 63.4985 \text{ g (0.140 lb)} \\\rho_{3-1} &= 2.91 \text{ g/cm (0.105 lb/in)} \\C_{33-1} &= 6090 \text{ ms}^{-1} (239,700 \text{ in/sec})\end{aligned}$$

The physical properties of ρ_{3-1} and C_{33-1} are identical to those values for Specimen 2-1 and are within an acceptable tolerance of $\pm 5\%$ from the baseline values.

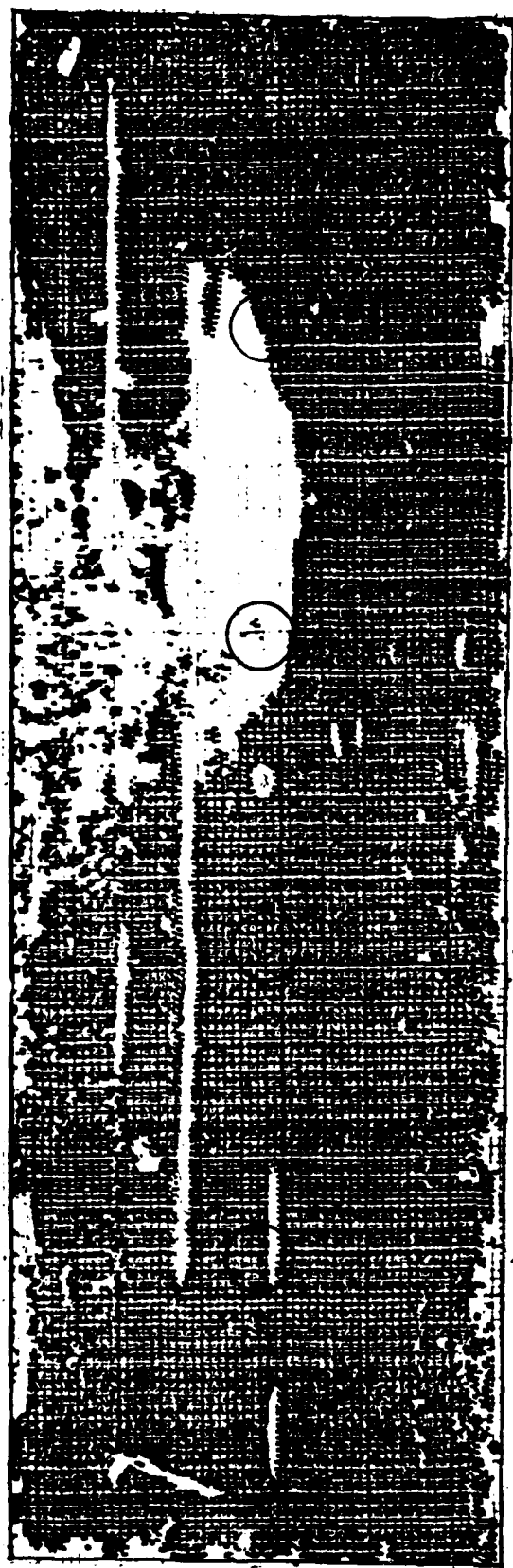
3.3.2 Ultrasonic Inspection

Figures 36 and 37 are pen-lift and analog C-scans, respectively, of Specimen 3-1. Both C-scans were generated using a 15 MHz immersion, compression wave transducer operated in the pulse-echo mode with the specimen held in the special fixture.

Both C-scans show a well-defined area of apparently flawed material involving approximately 20% of the specimen. The narrow bands of apparent damage running parallel to the fiber direction were identified as surface scratches by A-scan interpretation and visual inspection.

Figure 38 shows an A-scan photograph of Specimen 3-1 at an unflawed, and a flawed location, respectively. The A-scan photograph of the flawed location (Figure 38b) was taken at inspection location 3-1-3 as indicated on Figure 36.

IIT RESEARCH INSTITUTE



3-1-4

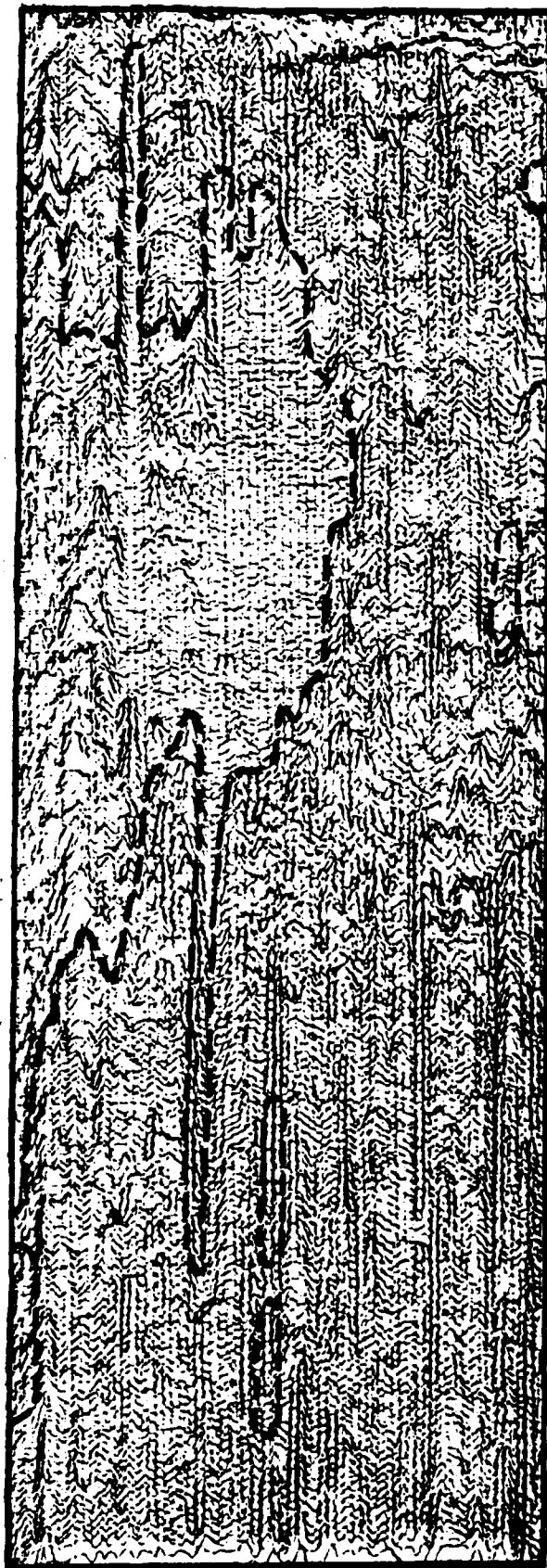
3-1-3

3-1-2

3-1-1

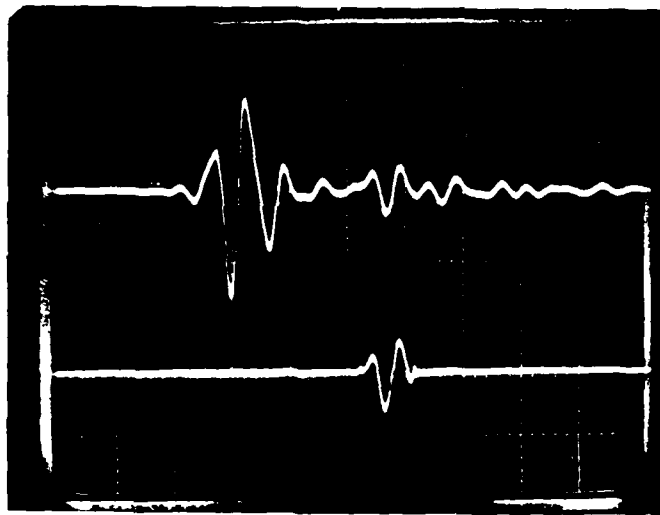
Repetition Rate	2K	Hz	Gated RF	Medium / Low
Damping	Variable/Maximum	Ohms	Frequency	Less Than 8 MHz
Energy	1		Peak Polarity	Negative
Receiver Attenuation	0	dB	Gain	x10
High Pass Filter	1.0	MHz	Gain	40 dB
Marked RF	Interface			

Figure 36. Pen-lift C-scan of FP/Mg Specimen 3-1 (porosity),
15 MHz transducer in pulse-echo mode.

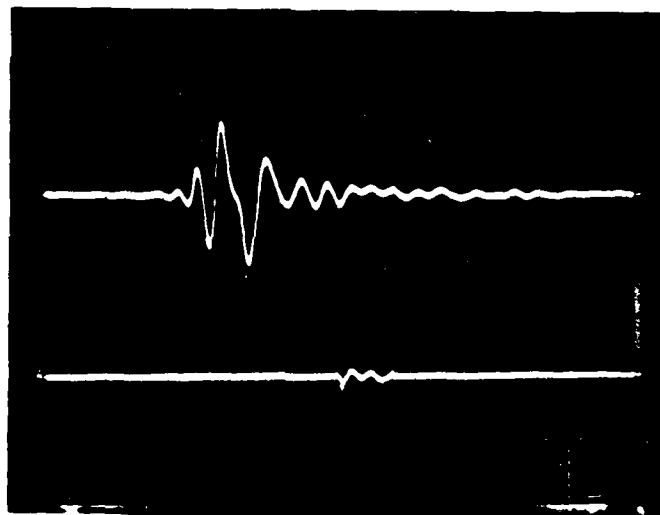


Repetition Rate	2K	Hz	Gated RF	Medium / Low
Damping	Variable/Maximum	Ohms	Frequency	Less Than 8 MHz
Energy	1		Peak Polarity	Negative
Receiver Attenuation	6	dB	Gain	x10
High Pass Filter	1.0	MHz	Gain	40 dB
Marked RF	Interface			

Figure 37. Analog C-scan of FP/Mg Specimen 3-1 (porosity),
15 MHz transducer in pulse-echo mode.



(a)



(b)

Figure 38. Amplitude-time records (A-scans) of ultrasonic pulse at two locations of Specimen 3-1 (porosity). (a) Unflawed location, (b) flawed location. (0.5 V/div, 0.5 μ s/div.) 15 MHz transducer in pulse-echo mode.

IIT RESEARCH INSTITUTE

the transmitting/receiving transducer. The fact that the specimen leached air from the front-face at the apparently flawed area when immersed in water indicates the front-face surface did have porosity. The small "M" at mid-thickness indicates that the porosity was not through-the-thickness. The "M" indicates a reflective surface since the waveform is inverted. This implies that the porosity existed through the first fifth and sixth plies and the last 2 or 3 plies were left intact. The back-face reflection disappears because of the combined effect of the porosity and the reflective surface. The porosity causes rapid and severe dissipation of the ultrasonic wave energy because of impedance difference between the fiber/matrix material and the entrapped air pores. The porosity forms an energy sink which allows the wave intensity to decrease radially as opposed to remaining more coherent in the axis normal to the front-face. The reflective surface adds to the dissipation in that a portion of the minimal wave energy remaining after transmission through the porous medium is lost in reflection from the surface. Therefore, the net result is that the porosity and reflective surface dissipated enough of the ultrasonic wave energy that the wave could not "reach" the back-face of the specimen so the back-face effectively "disappeared" from the A-scan.

For Specimen 3-1, ultrasonic inspection, pen-lift/analog C-scan, and A-scan photographs gave an indication of the presence of an area of porosity involving up to 6 of the 8 plies of the specimen.

3.3.3 Wave Propagation Velocity

Table 4 shows the wave propagation velocities for the 20 inspection locations shown in Figure 24 and the average wave propagation velocity of the 20 measurements. The average wave propagation velocity for Specimen 3-1 is within 11% of the theoretical value of 6090 ms^{-1} for Specimen 3-1 and within 5% of the empirical average of 6466 ms^{-1} for Specimen 1-1.

Of particular interest for this specimen are the wave velocities at the four inspection locations shown on Figure 36 (3-1-1 through 3-1-4) and inspection location 15 from Table 4. Inspection locations 3-1-1, 3-1-2, 3-1-3, and 3-1-4 correspond to locations 4, 8, 12, and 16 of Table 4, respectively. The selected data for these locations are compiled in Table 5.

The data in Table 5 correlates very well with the ultrasonic C-scans shown in the preceding subsection. At location 3-1-2 there is no apparent

TABLE 4. WAVE PROPAGATION VELOCITY ACROSS
THE THICKNESS AT VARIOUS LOCATIONS
ALONG SPECIMEN CENTERLINE (SPECIMEN 3-1)

<u>Inspection Location</u>	<u>Velocity, ms⁻¹ (10⁵ in/sec)</u>
1	6610 (2.602)
2	6687 (2.632)
3	6738 (2.652)
4	6679 (2.629)
5	6710 (2.641)
6	6751 (2.657)
7	6761 (2.661)
8	6771 (2.665)
9	6674 (2.627)
10	6522 (2.567)
11	6428 (2.530)
12	6120 (2.409)
13	5943 (2.339)
14	5864 (2.308)
15	10279 (4.046)
16	6723 (2.646)
17	6659 (2.621)
18	6690 (2.633)
19	6702 (2.638)
20	6778 (2.668)
Average:	6756 (2.659)

material damage which is shown as the highest "near average" wave velocity. Conversely, at location 3-1-3 there is apparent material damage where the lowest "near average" wave velocity appears. Locations 3-1-1 and 3-1-4 show varying amounts of apparent damage with wave velocities within the velocity extremes of locations 3-1-2 and 3-1-3, respectively.

Location 15 (from Table 4) shows a disproportionately high wave velocity. This supports the existence of the reflective surface indicated in the A-scan (Figure 38b) in the preceding subsection. As was seen for Specimen 2-1, the presence of a reflective surface (the delamination in Specimen 2-1) causes an apparent increase in the wave propagation velocity because the ultrasonic thickness gage was set to correspond to a finite micrometer measurement, not the through-the-thickness location of a reflective surface. The magnitude of the apparent wave velocity also supports the conclusion that the reflective surface was near the fifth or sixth ply away from the transducer. Based on the average wave propagation velocity of 6570 ms^{-1} (calculated using the 19 values from Table 4 excluding inspection location 1), if the reflective surface was at mid-thickness the apparent wave velocity would be approximately $13,140 \text{ ms}^{-1}$. Correcting for the wave velocity decrease due to the porosity in the travel path before the reflective surface indicates that an apparent wave propagation velocity of $10,279 \text{ ms}^{-1}$ would be seen if the reflective surface was 72% into the thickness of the specimen from the front-face. For an 8-ply specimen, this corresponds to between the fifth and sixth plies.

For Specimen 3-1, wave propagation velocity measurements supported the ultrasonic C-scans and agreed very well with the A-scans as to the extent of the porosity through-the-thickness.

3.3.4 Wave Attenuation

Table 6 shows the wave attenuation coefficients calculated from wave amplitude measurements generated by the water delay line and the contact transducer techniques. The inspection locations shown in Table 6 correspond to those shown in Figure 36.

The material attenuation coefficients in Table 6 show good correlation with one another and correspond very well with the C-scans (Figures 36 and 37). Inversely to the wave propagation velocities of the preceding subsection, the maximum attenuation values are seen at inspection location 3-1-3

TABLE 5. SELECTED VALUES OF WAVE PROPAGATION VELOCITY
FOR FP/Mg SPECIMEN WITH POROSITY (SPECIMEN 3-1)

Inspection Location Fig. 34 (Table 4)		Velocity,
		ms^{-1} (10^5 in/sec)
3-1-1	(4)	6679 (2.629)
3-1-2	(8)	6771 (2.665)
3-1-3	(12)	6120 (2.409)
	(15)	10279 (4.046)
3-1-4	(16)	6723 (2.646)

TABLE 6. ULTRASONIC WAVE ATTENUATION FOR FP/Mg
SPECIMEN WITH POROSITY (SPECIMEN 3-1)

Inspection Location	Material Attenuation (α), dB/cm (dB/in.)	
	Water Delay Line	Contact Transducer
3-1-1	0.52 (1.32)	0.45 (1.14)
3-1-2	0.44 (1.12)	0.45 (1.14)
3-1-3	0.81 (2.05)	0.76 (1.93)
3-1-4	0.55 (1.39)	0.50 (1.27)

(inspection area totally apparently flawed), and the minimum attenuation values at inspection location 3-1-2 (inspection area totally apparently un-flawed). Again, inspection locations 3-1-1 and 3-1-4 have attenuation values between the extremes of locations 3-1-2 and 3-1-3, which indicated relative percentages of apparent damage.

The material attenuation coefficients calculated for Specimen 3-1 at inspection location 3-1-3 are indicative of the presence of an attenuative defect such as porosity. The nature of the attenuation is due to the impedance mismatch between the FP/Mg material and air pores. This results in a lower ultrasonic wave energy transmission across each succeeding interface; hence, the wave energy rapidly decreases as the wave passes through the specimen.

For Specimen 3-1, the ultrasonic wave attenuation coefficients give an accurate indication as to the presence of a defect such as porosity. The attenuation coefficients correspond very well with the ultrasonic inspection and wave propagation velocity data.

3.3.5 X-Ray Radiography

Figure 39 shows the X-ray radiograph for Specimen 3-1. This radiograph has no contrast variations which give any indication of the presence of the porosity indicated by the preceding NDE techniques.

The radiograph could possibly show the area of porosity if an enhancement medium were used since the porous area is in contact with two free surfaces.

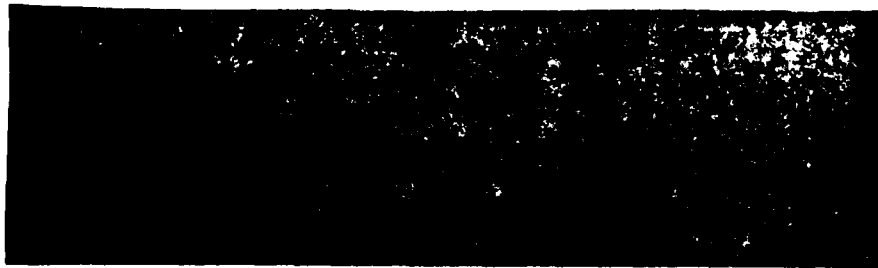


Figure 39. X-ray radiograph of FP/Mg specimen with porosity (Specimen 3-1).

3.3.6 Ultrasonic Backscattering

Figure 40 is a backscatter curve of Specimen 3-1. The incident angle (α) of the 5 MHz immersion transducer operated in the pulse-echo mode was 20° with respect to a line normal to the front-face surface plane of the specimen. As before, the curve shows activity only as the focal axis of the transducer sweeps near and through the plane normal to the fiber orientation.

Similar to Specimen 2-1, the only apparent effect of the defect area is the reduction of the reflected pulse amplitude. This is because of the attenuative nature of the porosity which causes a reduction of the reflected pulse amplitude.

Ultrasonic backscattering does not appear to be applicable for determination of defects such as porosity. This technique gave no appreciable information as to the state of the material integrity of Specimen 3-1.

3.3.7 Micrographic Inspection

Figure 41 shows six, and Figure 42 shows four micrographs of sections cut and polished from Specimen 3-1, respectively. The section locations indicated on Figures 41 and 42 correspond to the inspection locations shown on Figure 36.

The lower power micrographs, Figure 41, proved to be very disappointing in that the area of apparent porosity indicated in the C-scans did not appear as a gross material defect. At the 200X magnification level, apparent pores can be seen, especially in Figures 42a and 42b, as highlighted by the arrows. The pores appear as dark regions void of matrix material, but where fiber ends can be seen. The large dark areas on Figures 42a, 42c, and 42d are fracture or free edge surfaces of the respective sections. The viewing area of the 200X micrograph is very limited and does not show the distribution of the porosity. In general, there was no pattern to the pore distribution. The pores were essentially uniformly distributed throughout the cross-sections.

3.3.8 Comparison of Inspection Procedures

Of the NDE procedures used to evaluate Specimen 3-1, ultrasonic inspection, wave propagation velocity, and material attenuation coefficients indicated the presence of porosity. Ultrasonic inspection (C-scans with supporting A-scans) gave the most information in that it determined the extent of the

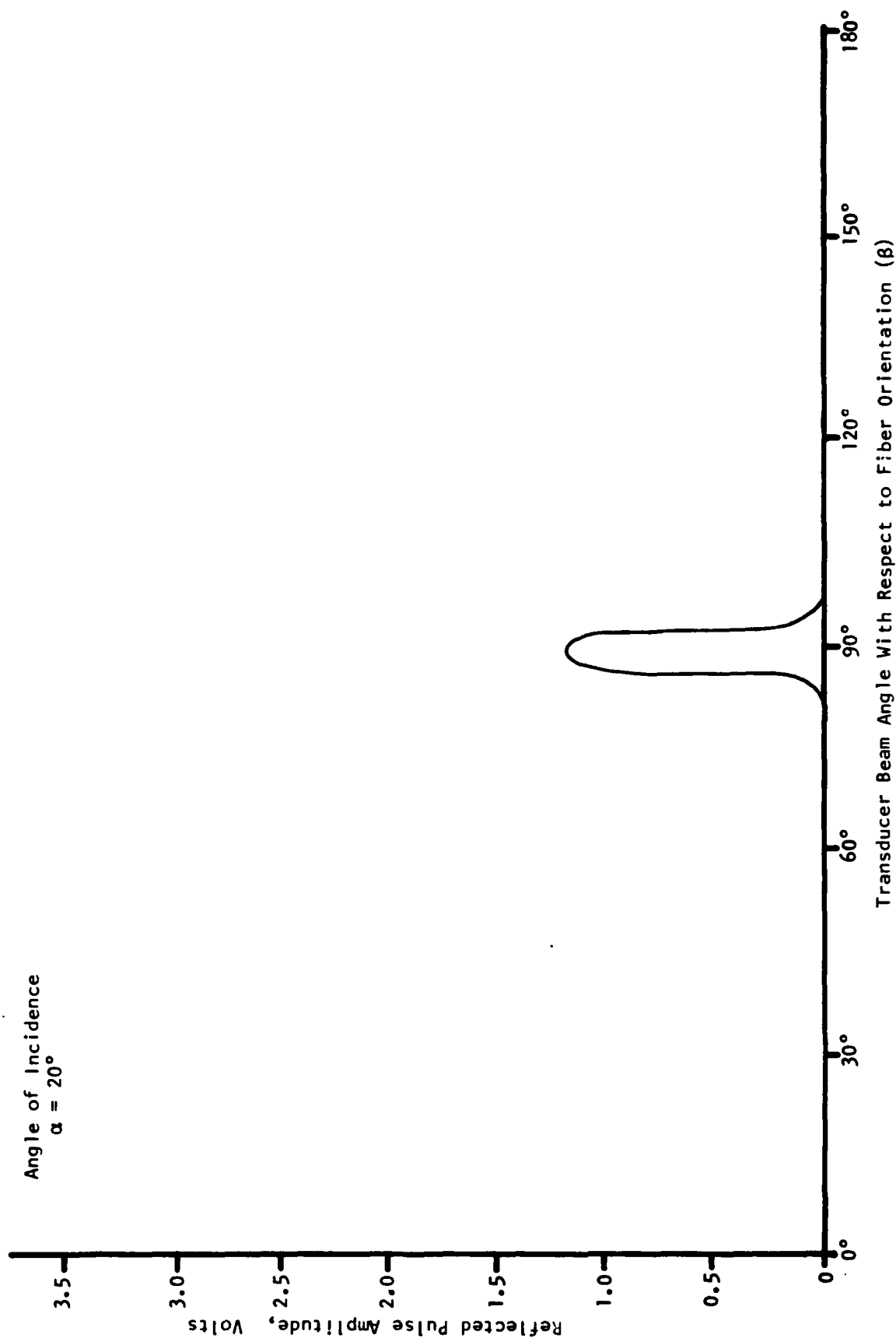


Figure 40. Ultrasonic backscattering curve of FP/Mg specimen with porosity (Specimen 3-1).

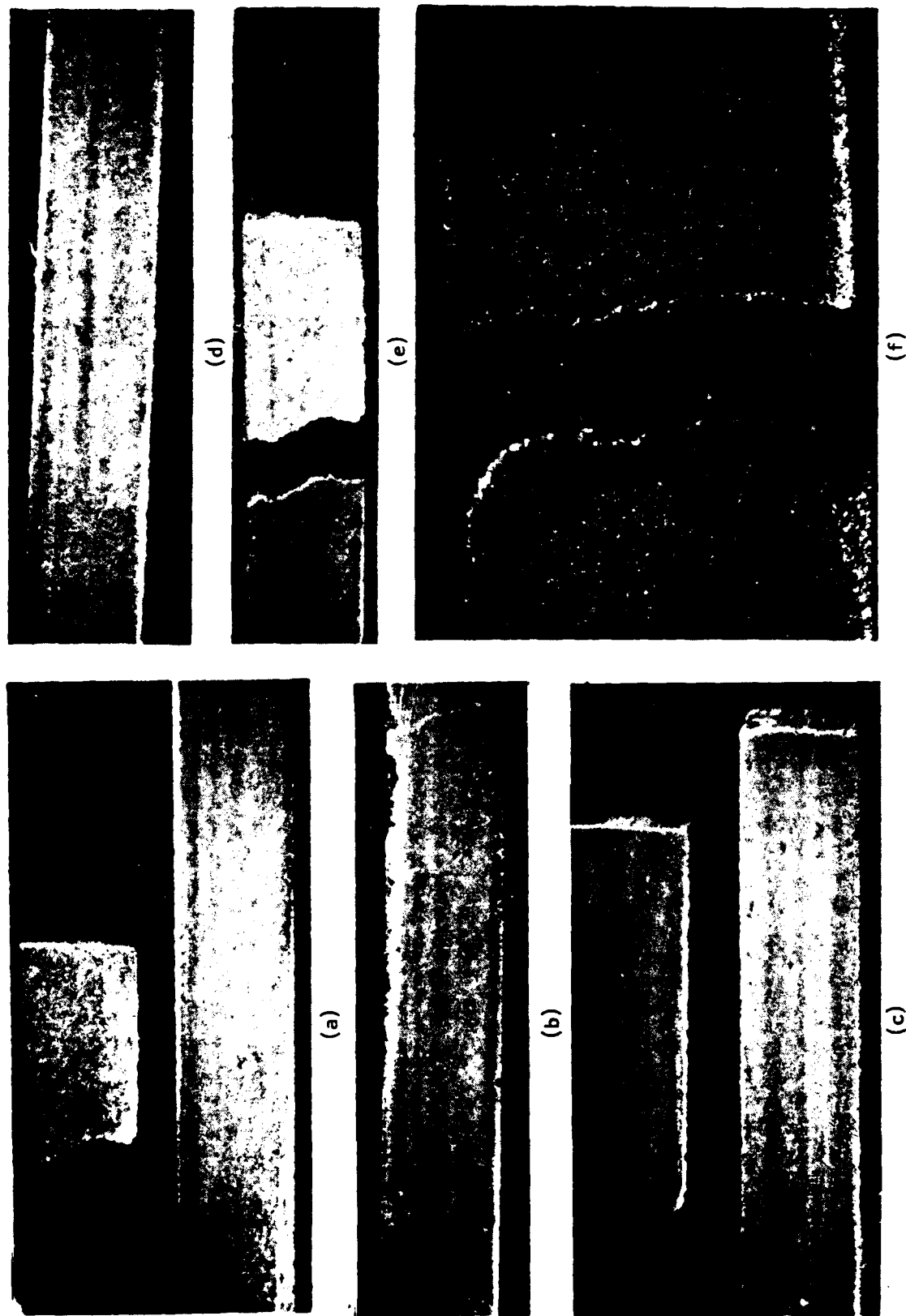


Figure 41. Micrographs of FP/Mg Specimen 3-1 (porosity) at four section locations: At 5X, (a) Location 3-1-1, (b) Location 3-1-2, (c) Location 3-1-3, (d) Location 3-1-1, (e) Location 3-1-4, (f) Location 3-1-3.

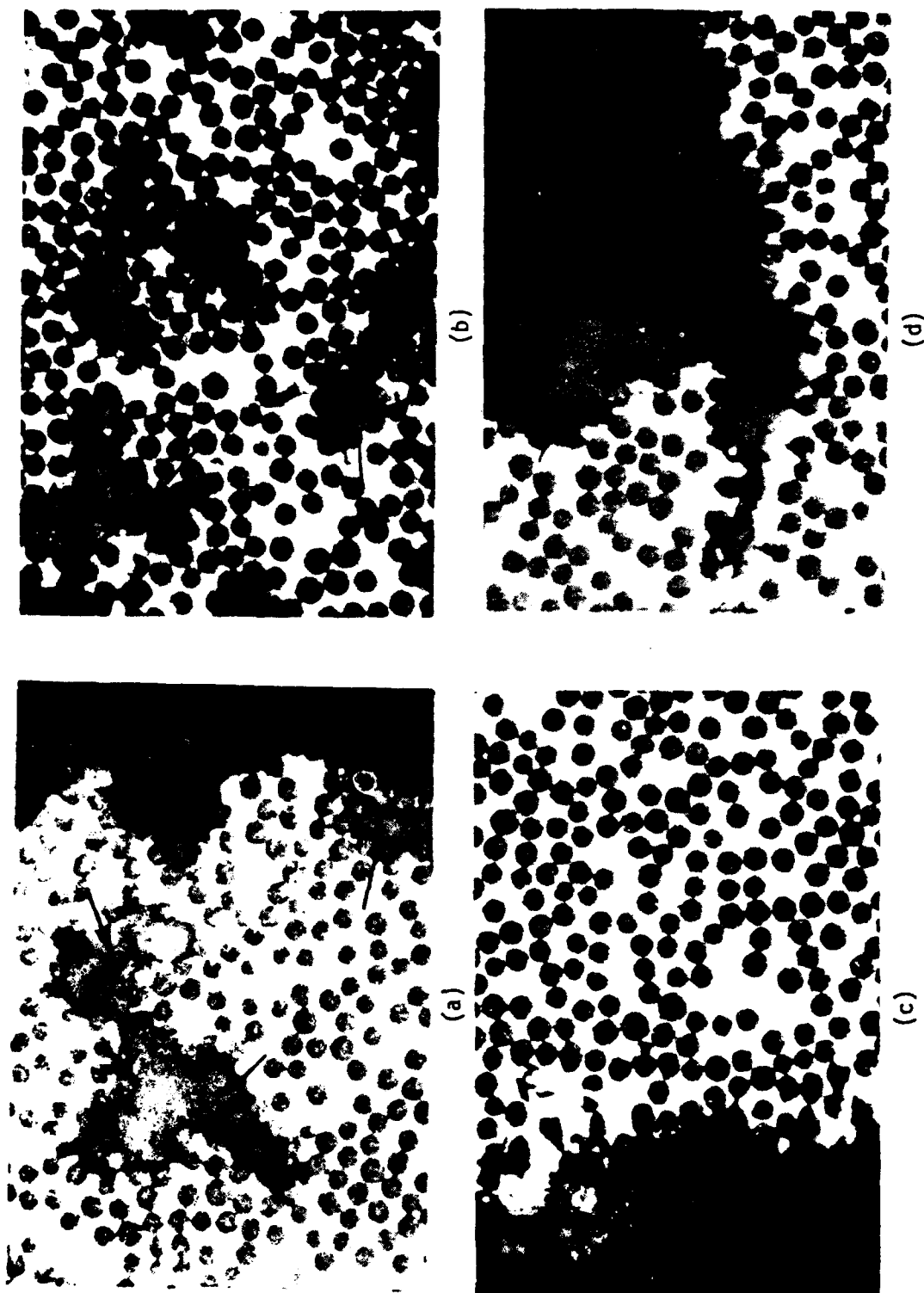


Figure 42. Micrographs (200X) of FP/Mg Specimen 3-1 (porosity) at four section locations:
 (a) Location 3-1-1, (b) Location 3-1-2, (c) Location 3-1-3, and (d) Location 3-1-4.

area of porosity (by C-scan) and its depth through-the-thickness (by A-scan). Wave propagation measurements corresponded with A-scan information as to the apparent depth through-the-thickness of the porous area and with wave attenuation coefficients as to the dissipative nature of the defect indicating the presence of a porous defect.

X-ray radiography and ultrasonic backscattering provided virtually no information as to the state of material integrity of Specimen 3-1.

3.4 TYPE 4

The representative specimen for the Type 4 group, with fiber misalignment, is Specimen 4-1.

3.4.1 Physical Properties

The pertinent physical properties for Specimen 4-1 are as follows:

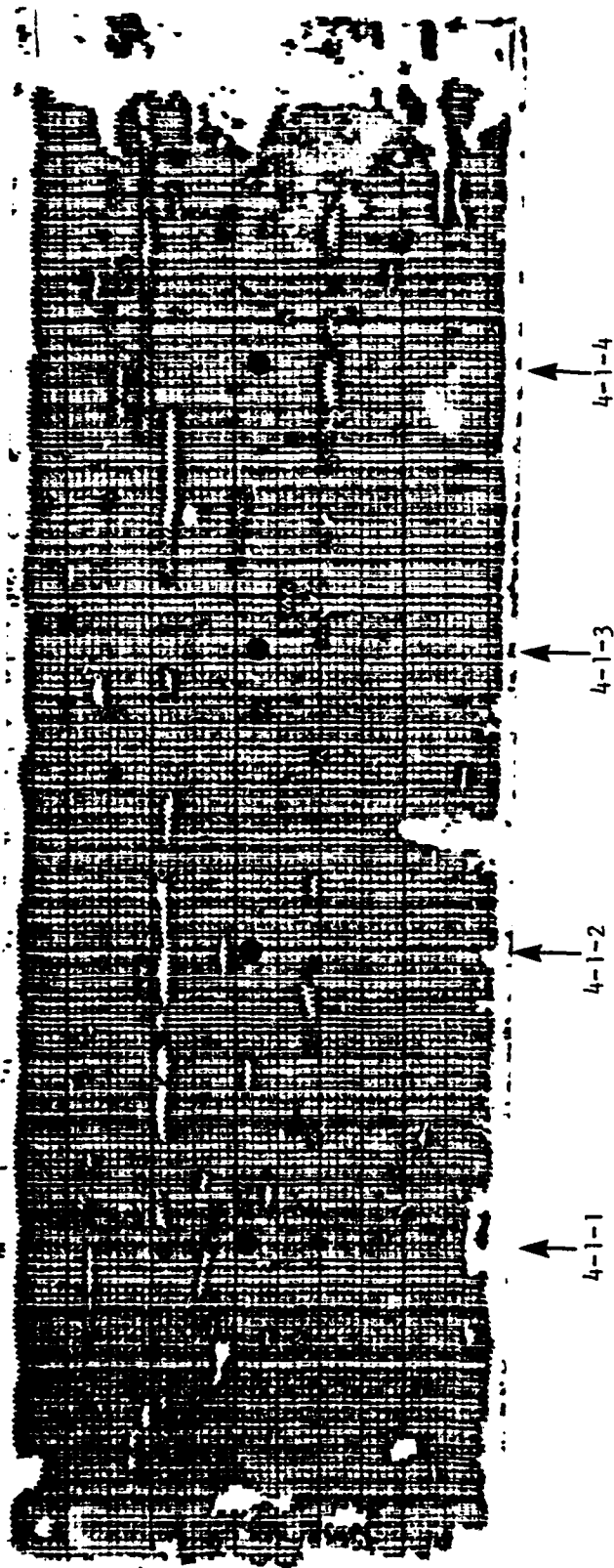
L_{4-1}	= 12.87 cm (5.066 in.)
W_{4-1}	= 3.82 cm (1.505 in.)
T_{4-1}	= 0.64 cm (0.252 in.)
M_{4-1}	= 89.4511 g (0.197 lb)
ρ_{4-1}	= 2.84 g/cm ³ (0.102 lb/in)
$C33_{4-1}$	= 6166 ms ⁻¹ (242,700 in/sec).

The physical properties of ρ_{4-1} and $C33_{4-1}$ are within an acceptable tolerance of $\pm 5\%$ from the baseline values.

3.4.2 Ultrasonic Inspection

Figures 43 and 44 are pen-lift and analog C-scans, respectively of Specimen 4-1. Both C-scans were generated using a 15 MHz immersion, compression wave transducer operated in the pulse-echo mode with the specimen held in the special fixture.

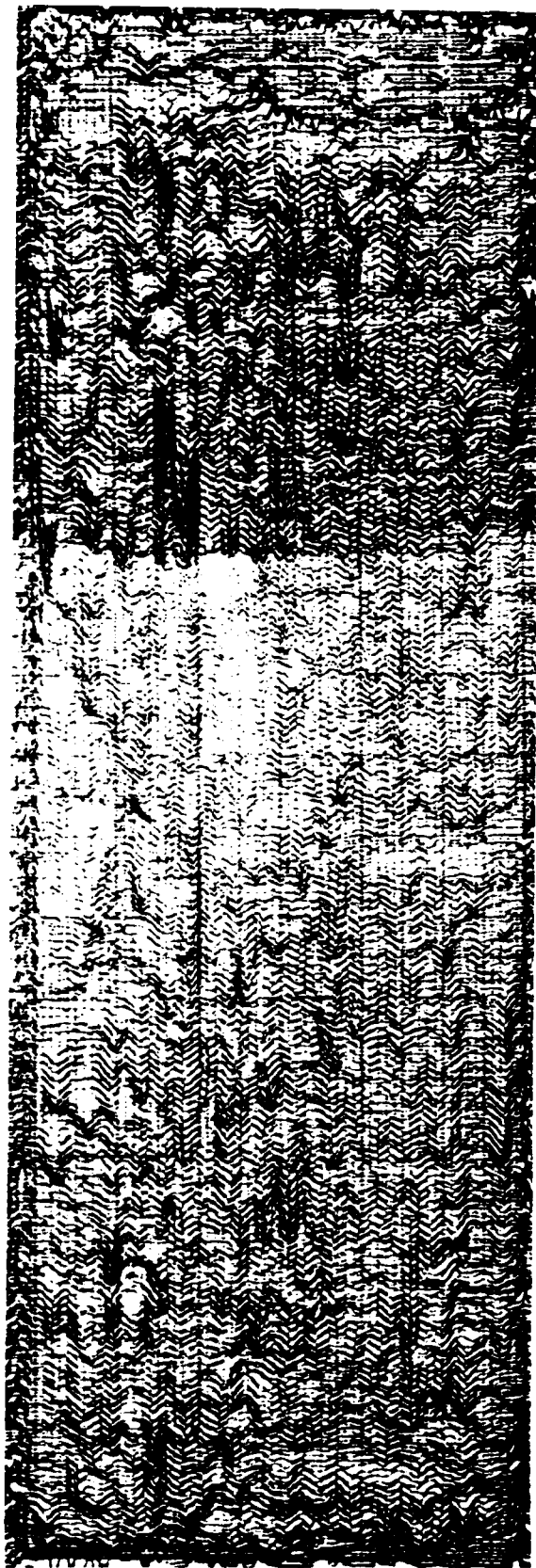
Neither C-scans show any material defect areas which could be interpreted as being misaligned fibers. The strips of defect areas parallel to the principal fiber direction were identified as surface scratches by visual inspection. The apparent defect area near the mid-length of the specimen perpendicular to the fiber direction and in contact with the lower edge was an area of excess sealant which bled onto the specimen after it was inserted in the specimen holder.



Repetition Rate	2K	Hz
Damping	Variable/Maximum	Ohms
Energy	2	
Receiver Attenuation	2	dB
High Pass Filter	1.0	MHz
Marked RF	Interface	

Gated RF	Medium / Low
Frequency	Greater Than 8 MHz
Peak Polarity	Negative
Gain	x10
Gain	40
	dB

Figure 43. Pen-lift C-scan of FP/Mg Specimen 4-1 (fiber misalignment), 15 MHz transducer in pulse-echo mode.



Repetition Rate	2K	Hz	Gated RF	Medium / Low
Damping Variable/Maximum	1	Ohms	Frequency	Greater Than 8 MHz
Energy	1		Peak Polarity	Negative
Receiver Attenuation	6	dB	Gain	x10
High Pass Filter	1.0	MHz	Gain	40
Marked RF	Interface			dB

Figure 4a. Analog C-scan of FP/Mg Specimen 4-1 (fiber misalignment),
15 MHz transducer in pulse-echo mode.

Figure 45 is a typical A-scan photograph of Specimen 4-1 at an unflawed location. This A-scan is representative of any unflawed location on Specimen 4-1. The fact that both the front and back-face reflections are very well defined in the A-scan indicates that the presence of fiber misalignment does not affect the transmission of the ultrasound. This was expected since a slight fiber misalignment (as in this case where it was 10°) does not affect the material density and barely changes the modulus of the specimen. Because ultrasonic inspection relies upon a change in reflected wave amplitude as the mechanism to indicate the presence of a defect, and because the wave amplitude is a function of wave attenuation which is a function of specimen density and modulus, a minimum number of apparent defect areas were generated. All of the apparent defect areas were caused by surface irregularities.

For Specimen 4-1, ultrasonic inspection, pen-lift/analog C-scans and A-scan photographs gave no indication as to the presence of fiber misalignment. Ultrasonic inspection could become an applicable technique if a higher frequency (greater than 15 MHz) were used or if the current transducers could be operated with a higher excitation energy.

3.4.3 Wave Propagation Velocity

Table 7 shows the wave propagation velocities for the 20 inspection locations shown in Figure 24 and the average wave propagation velocity of the 20 measurements. The average wave propagation velocity for Specimen 4-1 is within 6% of the theoretical value of 6166 ms^{-1} for Specimen 4-1 and within 2% of the empirical average of 6466 ms^{-1} for Specimen 1-1.

The wave propagation values in Table 7 are very consistent from inspection location 1 to inspection location 20 (the variation is less than $\pm 3\%$ from the average). This fact, along with the closeness of the average wave propagation velocities of Specimens 1-1 and 4-1, indicates that the presence of fiber misalignment cannot be shown by the wave propagation velocity technique for Specimen 4-1.

3.4.4 Wave Attenuation

Table 8 shows the material attenuation coefficients calculated for Specimen 4-1 from measurements taken using both the water delay line and contact transducer technique. The inspection locations indicated in Table 8 correspond to those shown on Figure 43.

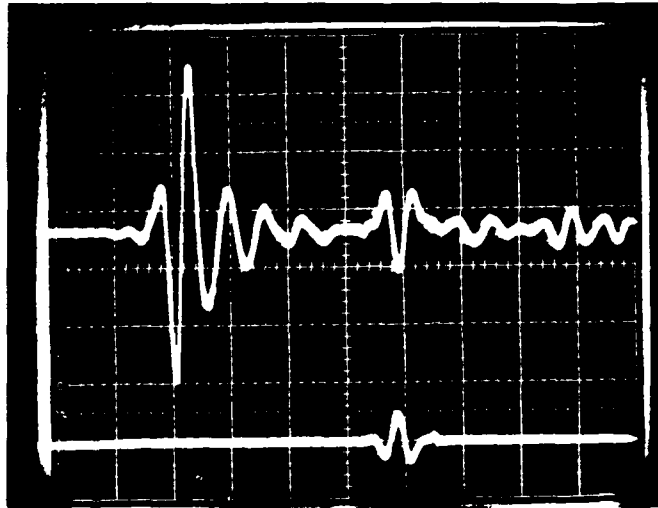


Figure 45. Amplitude-time record (A-scan) of ultrasonic pulse at an unflawed location of Specimen 4-1 (fiber misalignment). (0.2 V/div, 10 μ s/div.) 15 MHz transducer in pulse-echo mode.

TABLE 7. WAVE PROPAGATION VELOCITY ACROSS
THE THICKNESS AT VARIOUS LOCATIONS
ALONG SPECIMEN CENTERLINE (SPECIMEN 4-1)

Inspection Location	Velocity, ms ⁻¹ (10 ⁵ in/sec)
1	6522 (2.567)
2	6466 (2.545)
3	6509 (2.562)
4	6514 (2.564)
5	6491 (2.555)
6	6486 (2.553)
7	6514 (2.564)
8	6507 (2.561)
9	6540 (2.574)
10	6550 (2.578)
11	6550 (2.578)
12	6545 (2.576)
13	6557 (2.581)
14	6585 (2.592)
15	6578 (2.589)
16	6578 (2.589)
17	6527 (2.569)
18	6517 (2.565)
19	6542 (2.575)
20	6618 (2.605)
Average:	6535 (2.572)

TABLE 8. ULTRASONIC WAVE ATTENUATION COEFFICIENTS (SPECIMEN 4-1)

Inspection Location	Attenuation (α), dB		Specimen Thickness d , cm (in.)	Material Attenuation (α), dB/cm (dB/in.)	
	Water Delay Line	Contact Transducer		Water Delay Line	Contact Transducer
4-1-1	0.169	0.164	0.638 (0.251)	0.26 (0.67)	0.26 (0.67)
4-1-2	0.170	0.165	0.638 (0.251)	0.27 (0.68)	0.26 (0.67)
4-1-3	0.169	0.162	0.638 (0.251)	0.26 (0.67)	0.25 (0.65)
4-1-4	0.168	0.161	0.638 (0.251)	0.26 (0.67)	0.26 (0.66)
Average	0.169	0.163	0.638 (0.251)	0.26 (0.67)	0.26 (0.66)

The average material attenuation coefficients in Table 8 agree very well with one another for the two techniques investigated. Additionally, the material attenuation coefficients calculated for each inspection location are very consistent with each other along the length of the specimen and are also consistent for a given inspection location when either evaluation technique was used.

The consistency mentioned above correlates very well with the results of ultrasonic inspection and wave propagation velocity analyses in that they all indicate uniform material integrity, but cannot distinguish the presence of the misaligned fiber plies. The reason the wave attenuation technique cannot discern the presence of the misaligned fibers in Specimen 4-1 is identical to that for ultrasonic inspection, i.e., the 10° of fiber misalignment is not drastic enough to affect the modulus of the specimen. Again, since ultrasound attenuation is primarily a function of specimen density or modulus, and for Specimen 4-1 neither density or modulus is drastically different from that of a specimen with no intentional flaws (Specimen 1-1), there is no mechanism within the specimen to cause noticeable wave attenuation.

For Specimen 4-1, ultrasonic wave attenuation does not give any indication of the presence of misaligned fibers; but, the technique is very consistent with the ultrasonic inspection and wave propagation techniques.

3.4.5 X-Ray Radiography

Figure 46 shows the X-ray radiograph for Specimen 4-1. This radiograph has no contrast variations which give any indication of the presence of fiber misalignment. It is doubtful that an enhancement medium would improve the results of Figure 46, since there are no flaw paths available to a penetrant from the free surfaces.



Figure 46. X-ray radiograph of FP/Mg specimen with fiber misalignment (Specimen 4-1).

IIT RESEARCH INSTITUTE

For Specimen 4-1, X-ray radiography does not give any indication of the presence of misaligned fibers.

3.4.6 Ultrasonic Backscattering

Figure 47 is a backscatter curve of Specimen 4-1. The incident angle (α) of the 5 MHz immersion transducer operated in the pulse-echo mode was 20° with respect to a line normal to the front-face surface plane of the specimen. This curve gives an indication as to the presence of the misaligned fibers. The misaligned fibers produce an offset in the curve at around $\beta = 80^\circ$, when the transducer focal axis is perpendicular to the misaligned fibers. The maximum reflected amplitude remains at $\beta = 90^\circ$ because a majority of the fiber plies are uniaxial. The dashed line segment indicates what the shape of the curve could have been expected to be without the presence of the misaligned fibers. The magnitude of the amplitude of the reflected pulse is closer to that shown for Specimen 1-1 (Figure 26) than either Specimen 2-1 (Figure 33) or Specimen 3-1 (Figure 40). This indicates that there are no attenuative defects (porosity, delamination, etc.) which would reduce the local material density or modulus and cause a drop in the amplitude of the reflected ultrasonic pulse.

For Specimen 4-1, ultrasonic backscattering does give an indication as to the presence of misaligned fibers. The backscatter curve could possibly be improved with a higher frequency transducer (greater than 5 MHz) and additional signal processing equipment between the pulser-receiver and X-Y plotter.

3.4.7 Micrographic Inspection

Figures 48 and 49 show four micrographs each of sections cut and polished from Specimen 4-1. The section locations indicated on Figures 48 and 49 correspond to the inspection locations on Figure 43.

The micrographs do not show, and were not expected to show, the two plies of misaligned fibers. This was because the degree angle of the misalignment is so slight that it barely affected the shape of the exposed fibers. Normally, off-axis fibers can be distinguished because they have an elliptical cross section when viewed along the fiber axis. This can be seen for one fiber bundle each in Figures 49a and 49d (highlighted by arrows), respectively. In

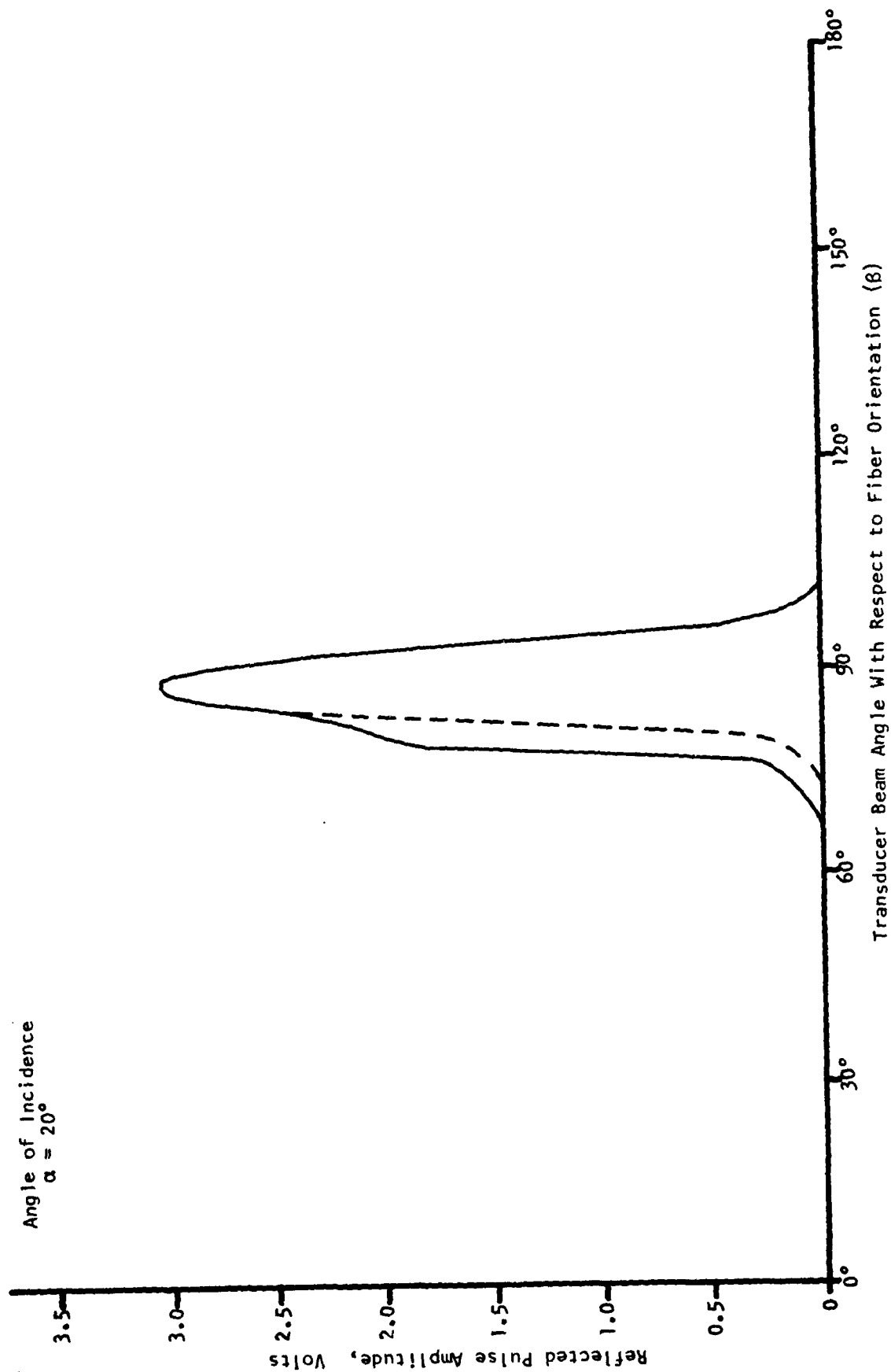
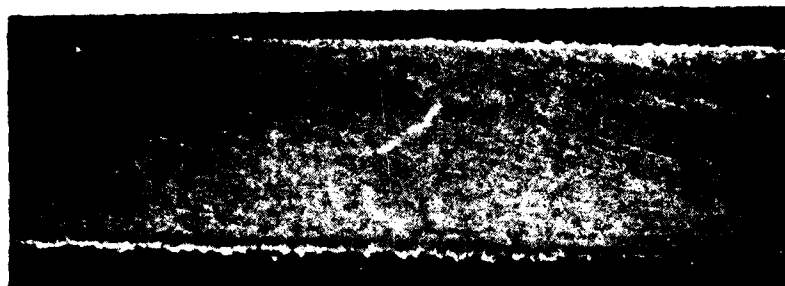


Figure 47. Ultrasonic backscattering curve of FP/Mg specimen with fiber misalignment (Specimen 4-1).



(a)



(b)



(c)



(d)

Figure 48. Micrographs (5X) of FP/Mg Specimen 4-1 (fiber misalignment) at four section locations: (a) Location 4-1-1, (b) Location 4-1-2, (c) Location 4-1-3, and (d) Location 4-1-4.

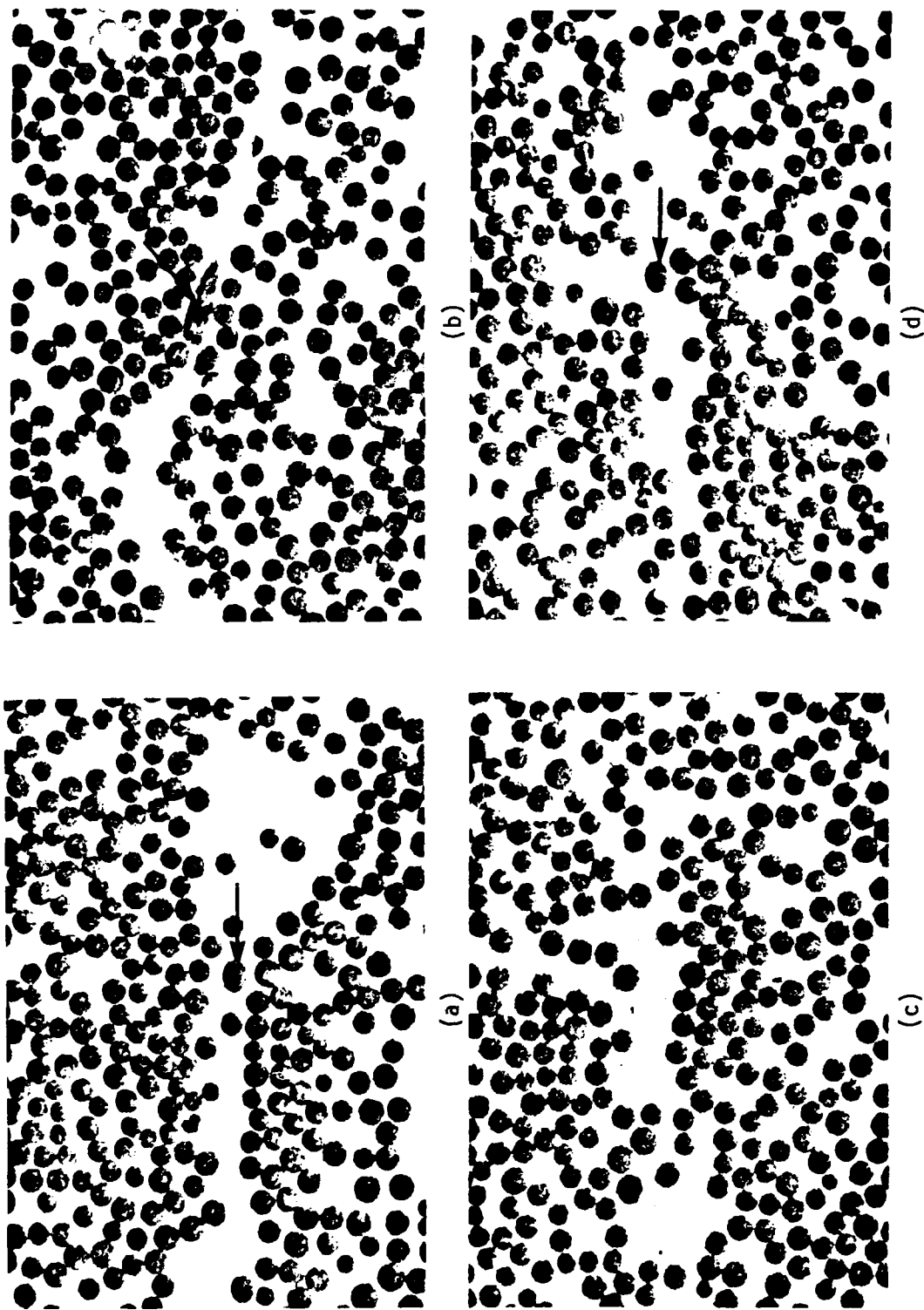


Figure 49. Micrographs (200X) of Fp/Mg Specimen 4-1 (fiber misalignment) at four section locations: (a) Location 4-1-1, (b) Location 4-1-2, (c) Location 4-1-3, and (d) Location 4-1-4.

most applications, composites are fabricated with the off-axis plies at an angle exceeding 20° to the fiber axis and the ellipse is well defined. This is only 10° and the ellipse is not well defined. Therefore, it is virtually impossible to distinguish the misaligned fibers from the aligned fibers. The long irregular shape in the center of Figure 49b is a fiber bundle segment which became embedded in the matrix, transverse to the fibers, during either the fabrication or sectioning/polishing process.

3.4.8 Comparison of Inspection Procedures

Of the NDE procedures used to evaluate Specimen 4-1, only ultrasonic backscattering indicated the presence of fiber misalignment. Because of the nature of the flaw, there was little or no abnormal material attenuation; and since the other ultrasonic techniques rely upon material attenuation as the defect indicating mechanism, they could not discern the presence of the fiber misalignment. All of the NDE procedures were consistent in that they all showed the specimen to have uniform material integrity.

3.5 TYPE 5 SPECIMENS

The representative specimen for the Type 5 group, with fiber fracture, is Specimen 5-1.

3.5.1 Physical Properties

The pertinent physical properties for Specimen 5-1 are as follows:

$$\begin{aligned}L_{5-1} &= 12.85 \text{ cm (5.060 in.)} \\W_{5-1} &= 3.82 \text{ cm (1.501 in.)} \\T_{5-1} &= 0.56 \text{ cm (0.219 in.)} \\M_{5-1} &= 79.5920 \text{ gm (0.175 lb)} \\\rho_{5-1} &= 2.90 \text{ gm/cm}^3 \text{ (0.104 lb/in}^3\text{)} \\C33_{5-1} &= 6,102 \text{ ms}^{-1} \text{ (240,200 in/sec).}\end{aligned}$$

The physical properties of ρ_{5-1} and $C33_{5-1}$ are within an acceptable tolerance of $\pm 5\%$ from the baseline values.

3.5.2 Ultrasonic Inspection

Figures 50 and 51 are pen-lift and analog C-scans, respectively, of Specimen 5-1. Both C-scans were generated using a 15 MHz immersion, compression

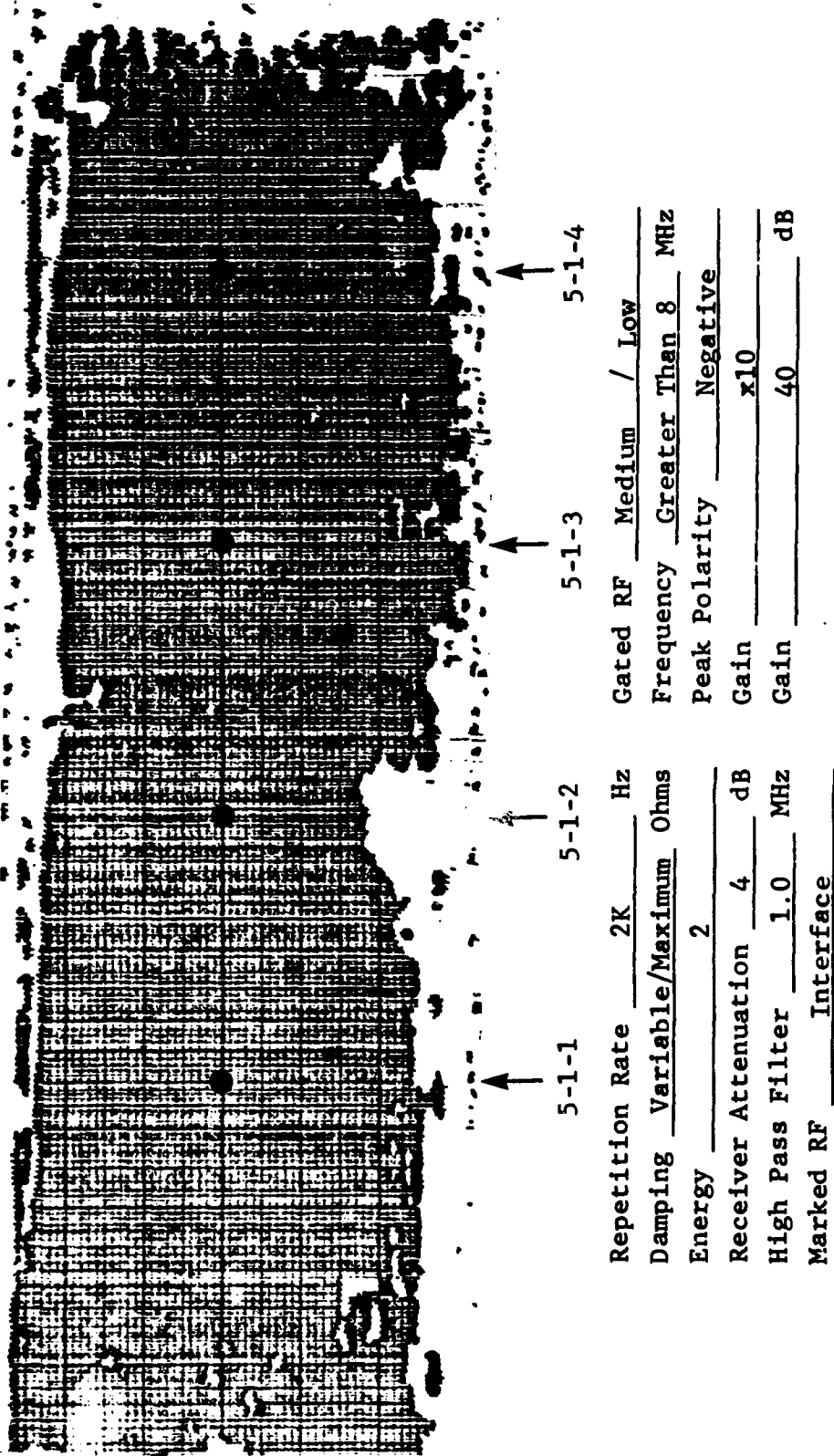


Figure 50. Pen-lift C-scan of FP/Mg Specimen 5-1 (fiber fracture),
15 MHz transducer in pulse-echo mode.

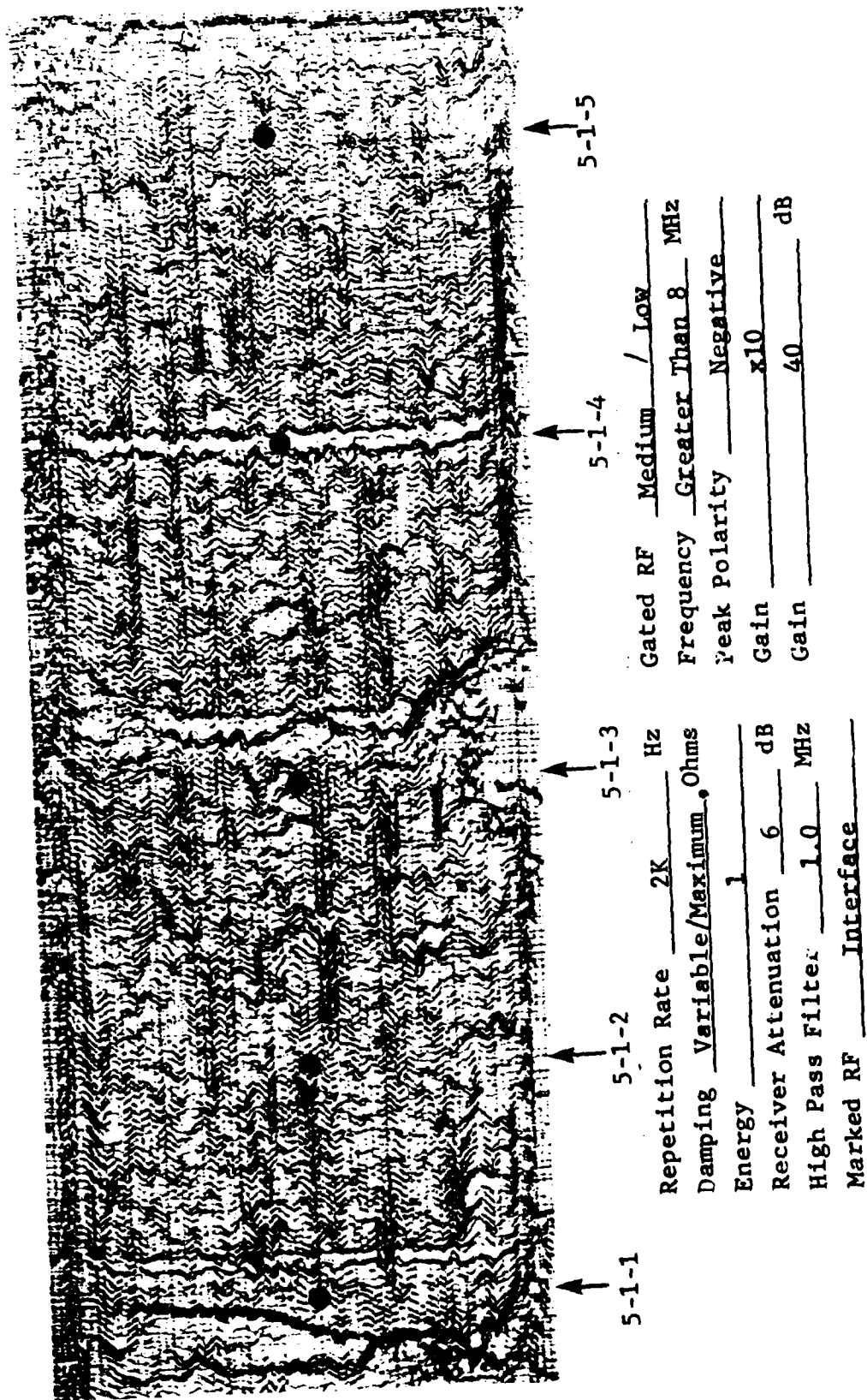


Figure 51. Analog C-scan of FP/Mg Specimen 5-1 (fiber fracture),
 15 MHz transducer in pulse-echo mode.

F/G 11/4

MAY 82 S W SCHRAMM: I M DANIEL

DAAG46-80-C-0070

IITRI-M06084-14

AMMRC-TR-82-35

NL

2 of 2
4/21/2023

END
DATE
FILMED
F 1 82
DTIC

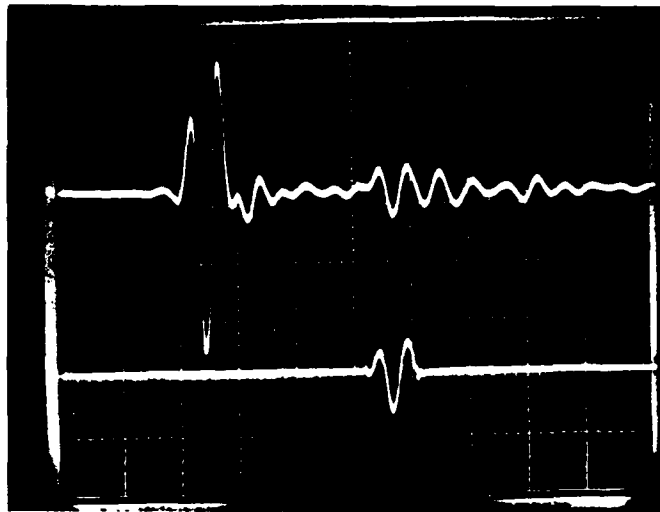
wave transducer operated in the pulse-echo mode with the specimen held in the special fixture.

The pen-lift C-scan gives virtually no indication of the presence of the three fiber fractures, whereas the analog C-scan clearly indicates the presence of three distinct bands of apparent fiber fracture. A-scan photograph interpretation indicated that the edge damage was of a delaminative nature partially involving the center band of apparent fiber fracture. The delaminations may have been caused during the fiber fracture creation or when the specimen was cut to its final size.

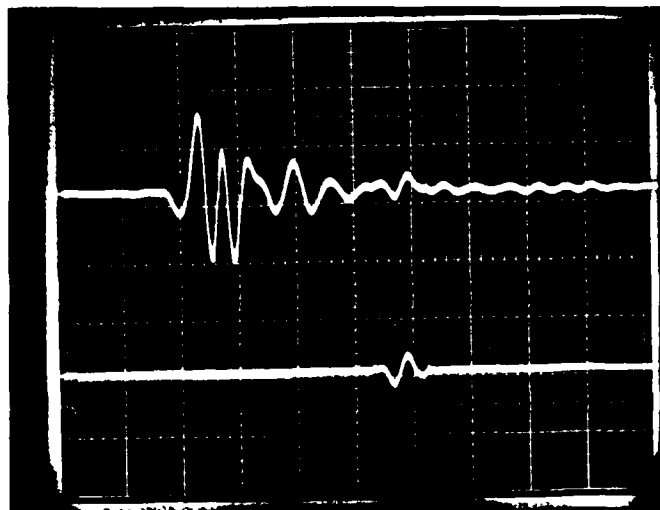
Figure 52 shows a typical A-scan photograph of Specimen 5-1 at an unflawed (Figure 52a) and a flawed (Figure 52b) location, respectively. Figure 52a corresponds to inspection location 5-1-2 of Figure 51, and Figure 52b corresponds to inspection location 5-1-4 of Figure 51. Figure 52a is a characteristic waveform for apparently undamaged material in that it has a well-defined front and back-face reflection similar to that shown in Figure 22a for Specimen 1-1 (no intentional flaws). Figure 52b clearly indicates an area of apparent damage by the misshaping of the front-face reflection, the formation of a mid-thickness pulse similar to that shown in Figure 31b for Specimen 2-1 (fiber-matrix debonding/delamination), and the near total disappearance of the back-face reflection. Figure 52b indicates the presence of a highly attenuative defect which has a reflective surface associated with it. This is very similar to the waveform generated from Specimen 3-1 (porosity) shown in Figure 38b. The reduction of the amplitude of the front-face reflection indicates that the apparent fiber fracture involved the material plies adjacent to the front surface of the specimen as seen by the transmitting/receiving transducer. The mid-thickness pulse indicates the presence of a reflective surface. This could be expected since the fiber fracture was manufactured and the number of plies which had the fractures were closely controlled. This means that there would be an obvious demarcation between the plies with or without fiber fracture. The fact that the back-face reflection can be clearly identified, albeit at a lower amplitude than for the unflawed location, indicates that the attenuative effect of the apparent fiber fracture was not as great as that of porosity where the back-face reflection virtually disappeared.

For Specimen 5-1, analog C-scan and A-scan photographs give a clear indication of the presence of fiber fracture. It is a distinct possibility that

IIT RESEARCH INSTITUTE



(a)



(b)

Figure 52. Amplitude-time records (A-scans) of ultrasonic pulses at two locations of Specimen 5-1 (fiber fracture). (a) Unflawed location, (b) flawed location. (0.5 V/div, 0.5 μ s/div.) 15 MHz transducer in pulse-echo mode.

pen-lift C-scans could indicate the presence of fiber fracture if higher frequency (greater than 15 MHz) transducers were used, or if the voltage gating was changed from its nominal values for triggering of the plotter pen-lift mechanism.

3.5.3 Wave Propagation Velocity

Table 9 shows the wave propagation velocities for the 20 inspection locations shown in Figure 24 and the average wave propagation velocity of the 20 measurements. The average wave propagation velocity for Specimen 5-1 is within 10% of the theoretical value of 6102 ms^{-1} for Specimen 5-1 and within 4% of the empirical average of 6466 ms^{-1} for Specimen 1-1.

Of particular interest are inspection locations 2, 6, 10, 15, and 19 of Table 10 which correspond to locations 5-1-1, 5-1-2, 5-1-3, 5-1-4, and 5-1-5, respectively, of Figure 51. These locations are highlighted in Table 10.

Inspection locations 5-1-1, 5-1-2, 5-1-3, and 5-1-4 correspond to areas of apparently unflawed material on Figure 51. The wave propagation velocities for the four locations have a variation of less than $\pm 5\%$ from the specimen empirical average of 6684 ms^{-1} . These values are also within 4% of the average wave propagation velocity of Specimen 1-1 (with no intentional flaws) which indicates that material at those locations is of a uniform integrity, similar to that of Specimen 1-1.

Conversely, inspection location 5-1-4, which corresponds to a band of apparent fiber fracture on Figure 50, shows a definite decrease in the wave propagation velocity when compared to the other values shown in Table 10. The decrease in wave velocity for Specimen 5-1 is not as drastic as that for Specimen 3-1 (porosity), but is significant enough to be considered a clear indication of fiber fracture.

For Specimen 5-1, wave propagation velocities give an indication of the presence of fiber fractures.

3.5.4 Wave Attenuation

Table 11 shows the material attenuation coefficients calculated for Specimen 5-1 from measurements taken using the water delay line and contact transducer techniques. The inspection locations indicated in Table 11 correspond to those shown on Figure 51.

TABLE 9. WAVE PROPAGATION VELOCITY ACROSS
THE THICKNESS AT VARIOUS LOCATIONS
ALONG SPECIMEN CENTERLINE (SPECIMEN 5-1)

<u>Inspection Location</u>	<u>Velocity, ms⁻¹ (10⁵ in/sec)</u>
1	6684 (2.631)
2	6646 (2.616)
3	6677 (2.628)
4	6636 (2.612)
5	6695 (2.635)
6	6679 (2.629)
7	6758 (2.660)
8	6748 (2.656)
9	6758 (2.660)
10	6717 (2.644)
11	6669 (2.625)
12	6725 (2.647)
13	6641 (2.614)
14	6728 (2.648)
15	6527 (2.569)
16	6565 (2.584)
17	6651 (2.618)
18	6773 (2.666)
19	6720 (2.645)
20	6684 (2.631)
Average:	6684 (2.631)

TABLE 10. SELECTED VALUES OF WAVE PROPAGATION VELOCITY
(SPECIMEN 5-1)

Inspection Location Fig. 47 (Table 9)	Velocity, ms^{-1} (10^5 in/sec)
5-1-1 (2)	6646 (2.616)
5-1-2 (6)	6679 (2.629)
5-1-3 (10)	6717 (2.644)
5-1-4 (15)	6527 (2.569)
5-1-5 (19)	6720 (2.645)

TABLE 11. ULTRASONIC WAVE ATTENUATION COEFFICIENTS (SPECIMEN 5-1)

Inspection Location	Attenuation (α), dB		Specimen Thickness d_1 , cm (in.)	Material Attenuation (α), dB/cm (dB/in.)	
	Water Delay Line	Contact Transducer		Water Delay Line	Contact Transducer
5-1-1	0.172	0.168	0.538 (0.213)	0.32 (0.80)	0.31 (0.79)
5-1-2	0.173	0.170	0.541 (0.213)	0.32 (0.80)	0.32 (0.80)
5-1-3	0.134	0.145	0.536 (0.211)	0.25 (0.62)	0.27 (0.69)
5-1-4	0.225	0.216	0.538 (0.212)	0.42 (1.06)	0.40 (1.02)
5-1-5	0.188	0.173	0.538 (0.212)	0.35 (0.89)	0.32 (0.82)
Average	0.178	0.174	0.538 (0.212)	0.33 (0.83)	0.32 (0.82)

The material attenuation coefficients at inspection locations 5-1-1, 5-1-2, 5-1-3, and 5-1-5 are consistent with one another for the water delay line and contact transducer techniques. The average values of 0.33 dB/cm and 0.32 dB/cm, respectively, for Specimen 5-1 also agree very well with the values of 0.33 dB/cm and 0.35 dB/cm, respectively, for Specimen 1-1 (with no intentional flaws). The material attenuation coefficients for inspection locations 5-1-1, 5-1-2, 5-1-3, and 5-1-5 correlate well with the analog C-scan (Figure 51) and indicate that there is no apparent material damage at those locations.

The material attenuation coefficient at location 5-1-4 is noticeably higher than that for the other four inspection locations. This indicates the presence of a material defect which is ultrasound attenuative. Fiber fracture is an attenuative defect since the modulus of the material decreases locally because of the decrease in stiffness associated with the broken fibers. The increase in the material attenuation coefficient due to apparent fiber fracture is lower than the increase in the material attenuation coefficient due to apparent fiber fracture. This implies that a defect which changes the density of a material locally has a greater attenuative effect on the ultra-sound passing through it than does a defect which changes the modulus of a material locally. This could become an important point in quantifying material attenuation coefficients to defect types.

3.5.5 X-ray Radiography

Figure 53 shows the X-ray radiograph for Specimen 5-1. This radiograph has no contrast variations which give any indication of the presence of fiber fractures. It is possible that an enhancement medium would improve the results of Figure 53, since the fiber fractures are open to the edges of the specimen. The lines of fiber fracture could possibly provide a flow path for the enhancement medium into the center of the specimen and be shown as a white band on a radiograph.

For Specimen 5-1, X-ray radiograph does not appear to give any indication of the presence of fiber fracture.



Figure 53. X-ray radiograph of FP/Mg specimen with fiber fracture (Specimen 5-1).

3.5.6 Ultrasonic Backscattering

Figure 54 is a backscatter curve of Specimen 5-1. The incident angle (α) of the 5 MHz immersion transducer operated in the pulse-echo mode was 20° with respect to a line normal to the front-face surface plane of the specimen.

This curve gives no indication of the presence of fiber fracture beyond the decrease of the amplitude of the reflected pulse. The only activity on the curve occurs when the transducer focal axis sweeps near and through the plane normal to the fiber orientation.

For Specimen 5-1, ultrasonic backscattering does not appear to give any appreciable indication of the presence of fiber fracture.

3.5.7 Micrographic Inspection

Figure 55 shows six, and Figure 56 shows four micrographs of sections cut and polished from Specimen 5-1. The section locations on Figures 55 and 56 correspond to the inspection locations on Figure 50.

With the exception of section 5-1-2, Figures 55b and 55e, these micrographs show no indications of the presence of any gross material defects. A possible explanation for this is that the defect (i.e., the broken fibers) is in the same plane as the section inspection surface. This means there is no perspective angle available where the defect can be compared against a uniform material background. The defect could be exposed if the section were cut in a plane parallel to the fibers. This is very difficult to execute since the section cut has to be made slightly above the ply interface where the damaged fibers are located. Compounding the problem is that most separating blades

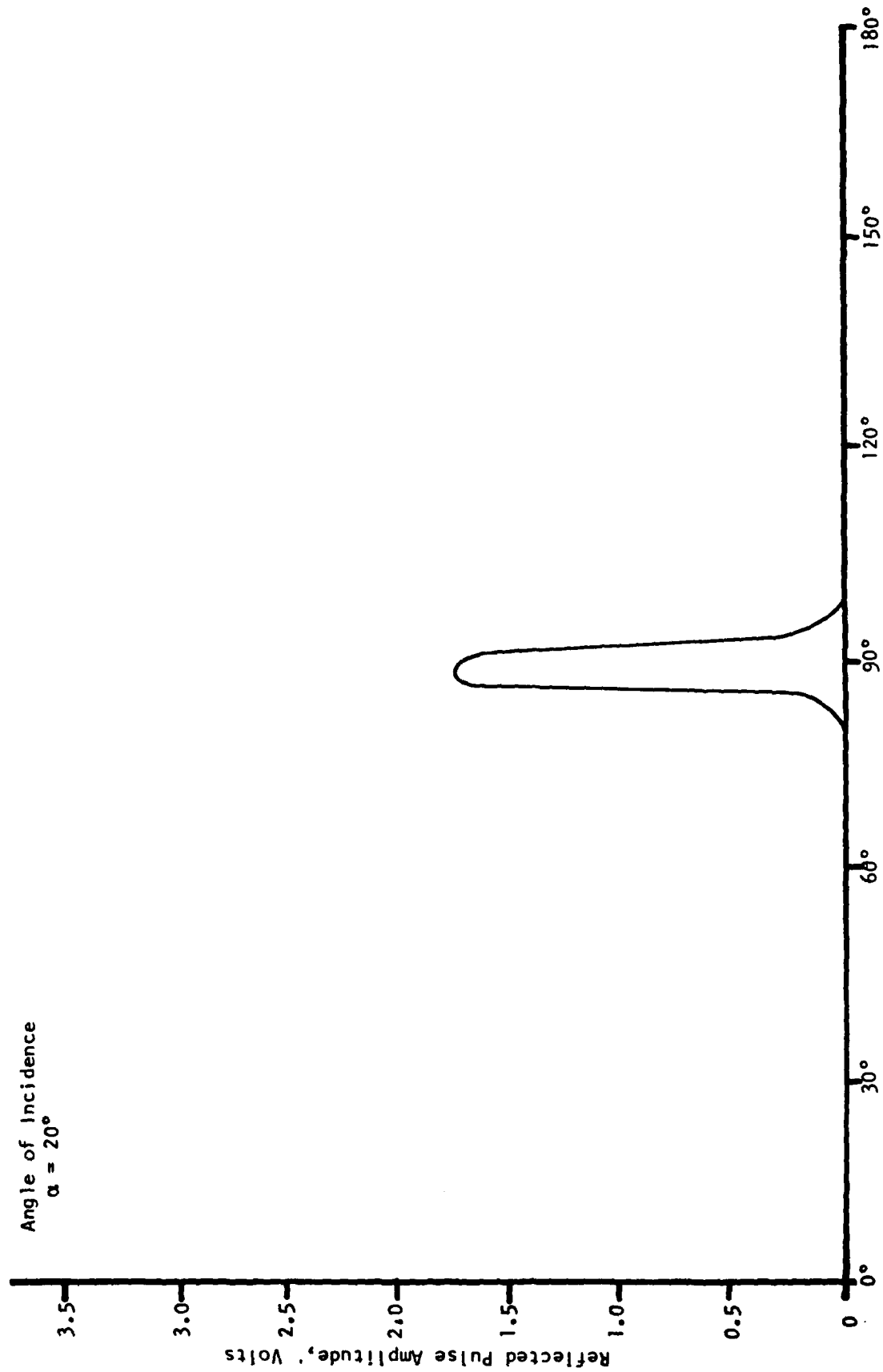


Figure 54. Ultrasonic backscattering curve of FP/Mg specimen with fiber fracture (Specimen 5-1).

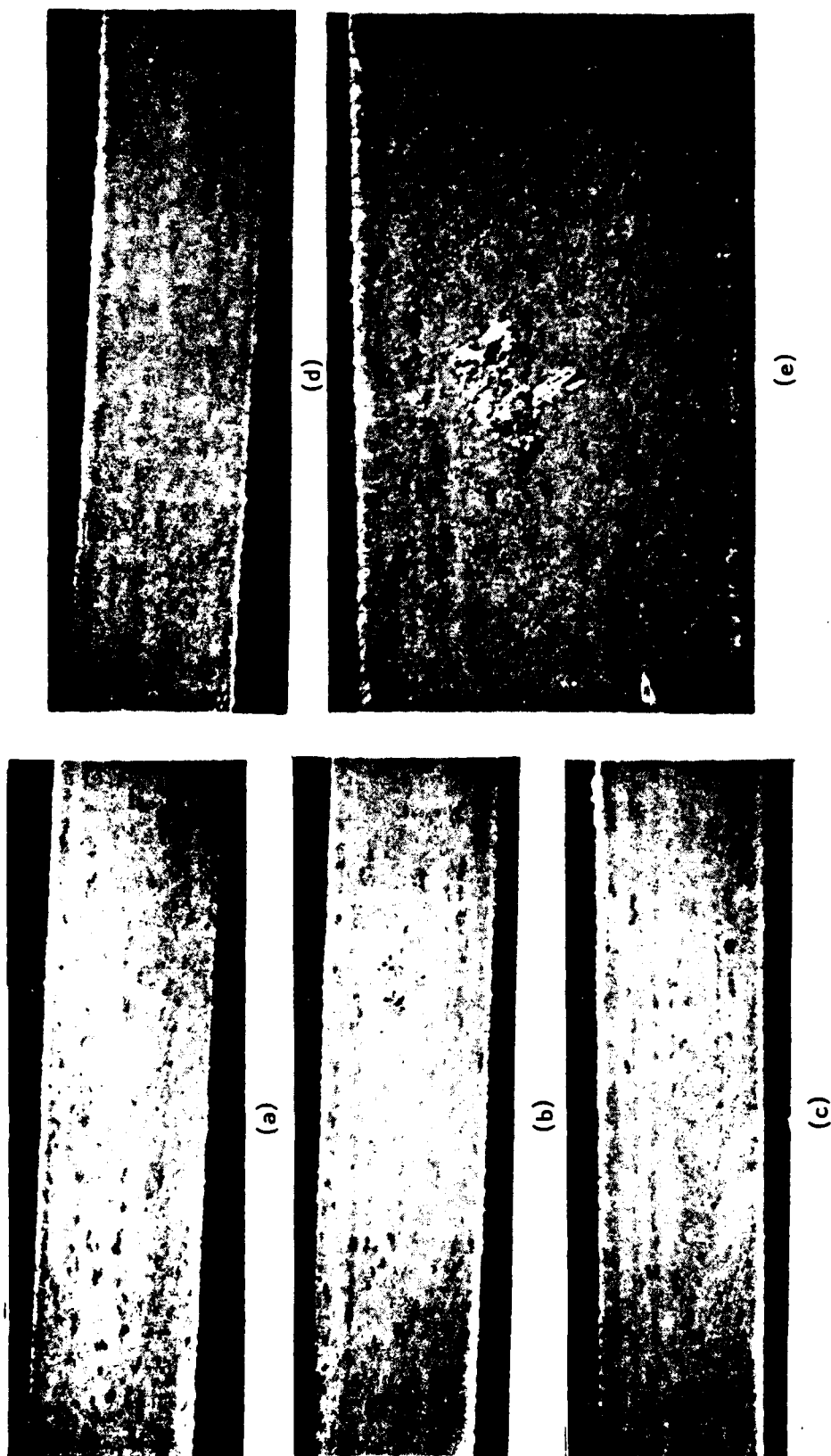


Figure 55. Micrographs of FP/Mg Specimen 5-1 (fiber fracture) at four section locations: At 5X, (a) Location 5-1-1, (b) Location 5-1-2, (c) Location 5-1-3, (d) Location 5-1-4; at 12X, (e) Location 5-1-2.

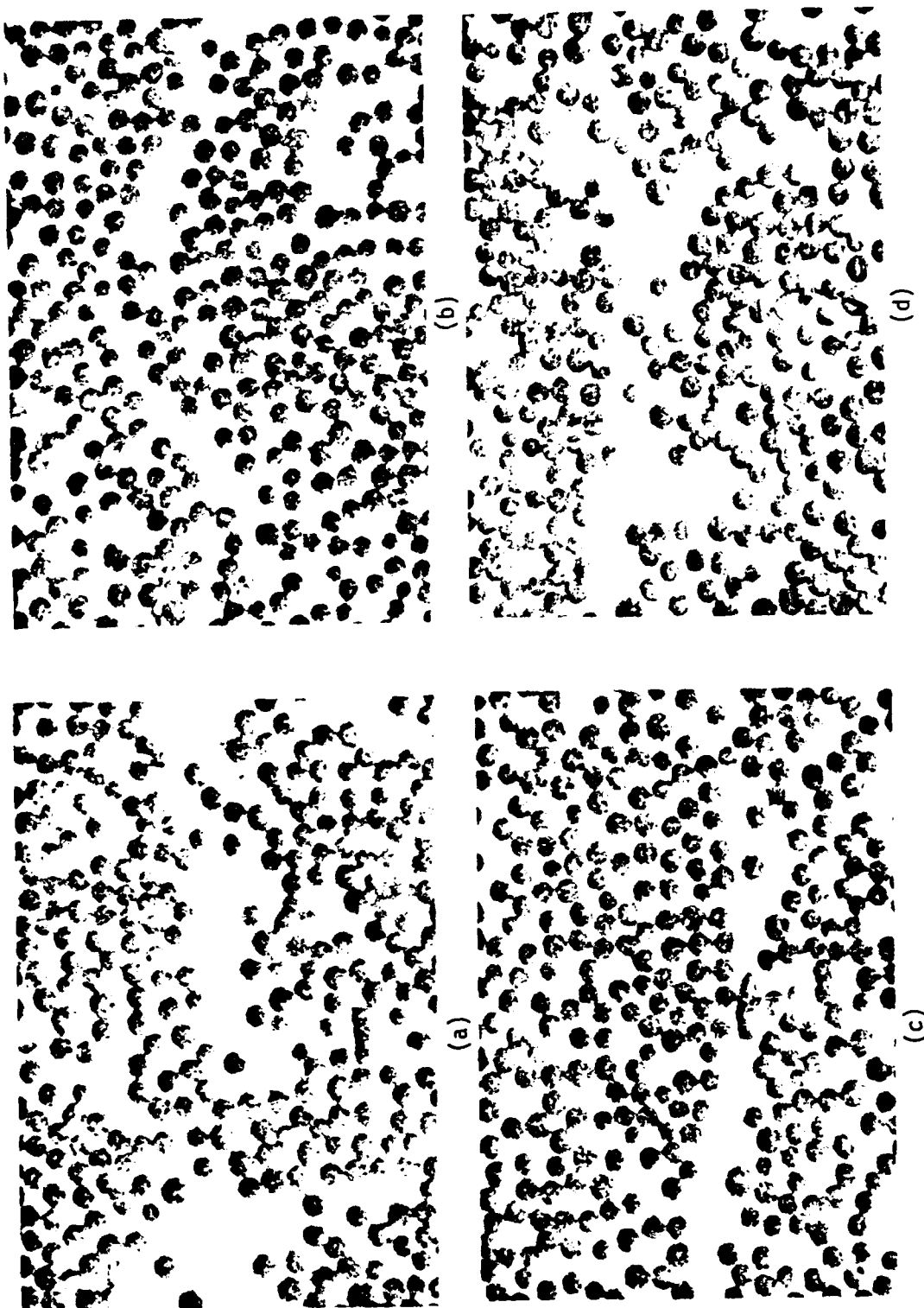


Figure 56. Micrographs (200X) of FP/Mg Specimen 5-1 (fiber fracture) at four section locations: (a) Location 5-1-1, (b) Location 5-1-2, (c) Location 5-1-3, and (d) Location 5-1-4.

are on the order of half the thickness of the specimen which severely lessens the ability to hold close tolerances.

Figures 55b and 55e indicate the presence of a gross material defect approximately 0.85 cm (0.13 in.) square. The defect is in the plane normal to the fibers and was not distinguishable in either of the ultrasonic C-scans. Close inspection of Figure 55e indicates the defect appears to be porous, the type that should have been seen in the micrographs of the Type 3 specimen. The fact that neither ultrasonic C-scans indicated the presence of the defect, and since the section face opposite to that of section 5-1-2 shows no trace of the defect, it appears that the defect was very localized. Since the defect was parallel to the ultrasound path it may have been transparent to the ultrasound; hence, it would not appear on the C-scans.

3.5.8 Comparison of Inspection Procedures

Of the NDE procedures used to evaluate Specimen 5-1, ultrasonic inspection, wave propagation velocity, and wave attenuation indicated the presence of fiber fracture. Within ultrasonic inspection the analog C-scan and A-scan photographs indicated the presence of fiber fracture whereas the pen-lift C-scan gave no indication of the presence of fiber fracture. Interpretation of the A-scan photographs provided information about the through-the-thickness location and extent of the fiber fracture. The wave propagation velocity and material attenuation data were consistent with one another and with the analog C-scan in locating the fiber fractures and differentiating between the flawed and unflawed areas of the specimen. The calculated material attenuation coefficients indicated there may be a correlation between the change in material attenuation as a function of whether the defect affects the local density or local modulus of the target specimen.

X-ray radiography and ultrasonic backscattering provided virtually no information as to the state of material integrity of Specimen 5-1.

3.6 TYPE 6 SPECIMEN

The representative specimen for the Type 6 group, with nonuniform fiber distribution, is Specimen 6-2.

3.6.1 Physical Properties

The pertinent physical properties for Specimen 6-2 are as follows:

$$\begin{aligned}L_{6-2} &= 12.89 \text{ cm (5.076 in.)} \\W_{6-2} &= 3.82 \text{ cm (1.504 in.)} \\T_{6-2} &= 0.62 \text{ cm (0.243 in.)} \\M_{6-2} &= 88.0364 \text{ g (0.194 lb)} \\ \rho_{6-2} &= 2.88 \text{ g/cm}^3 \text{ (0.104 lb/in}^3\text{)} \\C33_{6-2} &= 6119 \text{ ms}^{-1} \text{ (240,840 in/sec).}\end{aligned}$$

The physical properties of ρ_{6-2} and $C33_{6-2}$ are within an acceptable tolerance of $\pm 5\%$ from the baseline values.

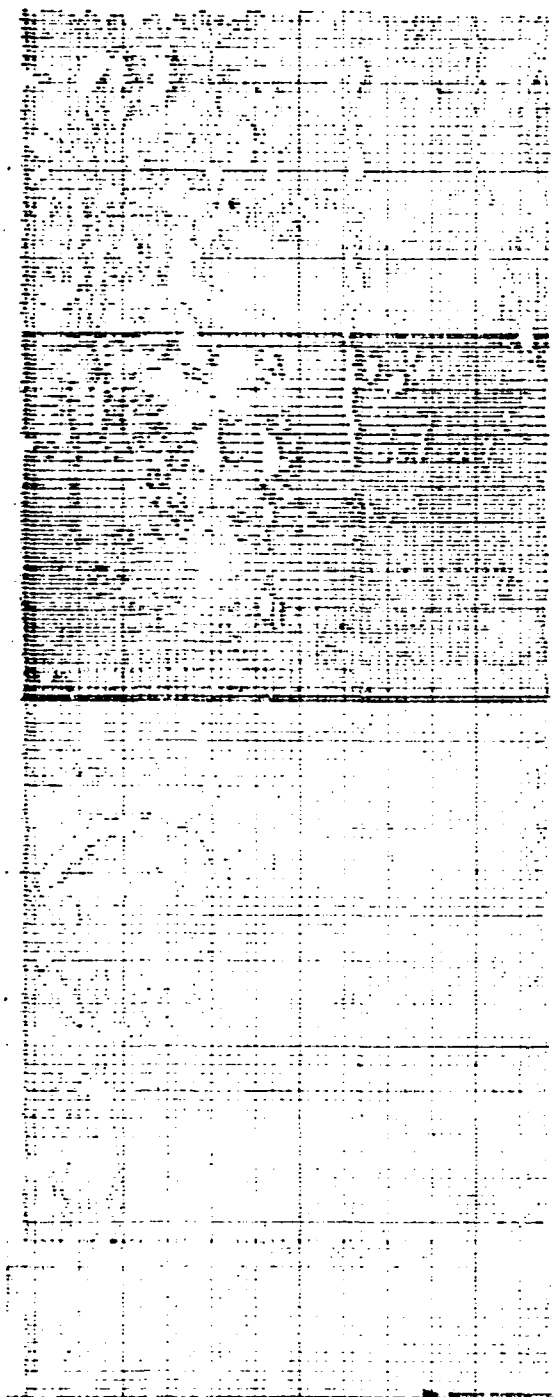
3.6.2 Ultrasonic Inspection

Figures 57 and 58 are pen-lift and analog C-scans, respectively, of Specimen 6-2. Both C-scans were generated using a 15 MHz immersion, compression wave transducer operated in the pulse-echo mode with the specimen held in the special fixture. Both the pen-lift and analog C-scan clearly shows the location and extent of the circular area of nonuniform fiber distribution. The circular area is at mid-length of the specimen. It is towards the left side of the specimen in Figure 57 because the left edge (approximately 20% of the scan length) was inadvertently cropped off before mounting. The additional areas of apparently flawed material on the two C-scans were determined to be surface irregularities by visual inspection and A-scan interpretation.

Figure 59 shows an A-scan photograph at an unflawed location (Figure 59a) and within the area of apparent nonuniform fiber distribution (Figure 59b). Figure 59a is a typical A-scan of a location of unflawed FP/Mg material. There is a well-defined front and back-face reflection with very little wave activity between the faces (once again, very similar to the A-scan of Specimen 1-1 with no intentional flaws, see Figure 22a).

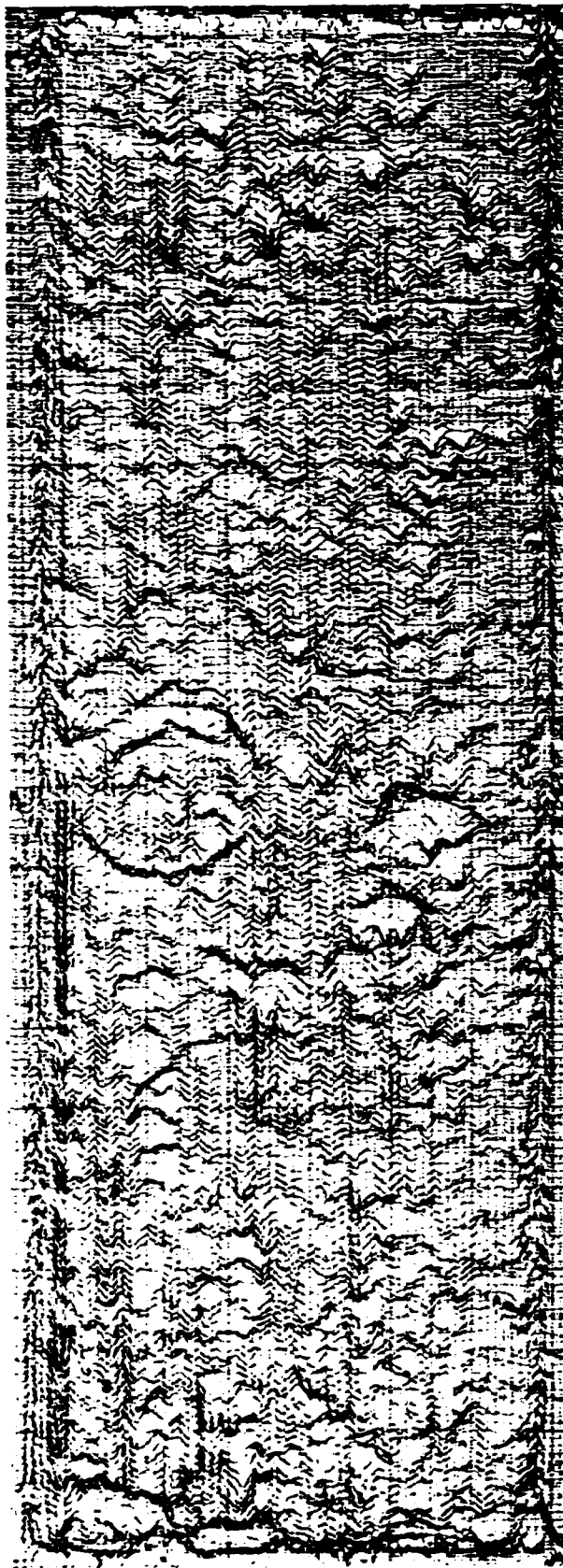
Figure 59b is an interesting version of an A-scan indicating a mid-thickness reflective surface, similar to the A-scans for Specimen 2-1 (fiber matrix debonding/delamination, see Figure 31b) and for Specimen 5-1 (fiber fracture, see Figure 52b). In Figure 59b, unlike Figures 31b and 52b, the presence of the mid-thickness pulse did not decrease the amplitude of either the front or back-face reflection from the specimen. The explanation for this phenomenon requires an understanding of how the area of nonuniform fiber distribution was

IIT RESEARCH INSTITUTE



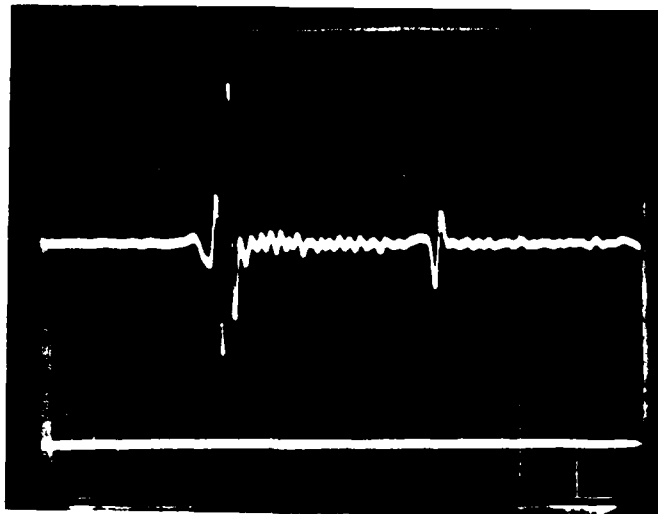
Repetition Rate	2K	Hz	Gated RF	Medium	/ Low
Damping	Variable/Maximum	Ohms	Frequency	Greater Than 8	MHz
Energy	3		Peak Polarity	Negative	
Receiver Attenuation	6	dB	Gain	x10	
High Pass Filter	1.0	MHz	Gain	40	dB
Marked RF	Interface				

Figure 57. Pen-lift C-scan of FP/Mg Specimen 6-2 (nonuniform fiber distribution), 15 MHz transducer in pulse-echo mode.

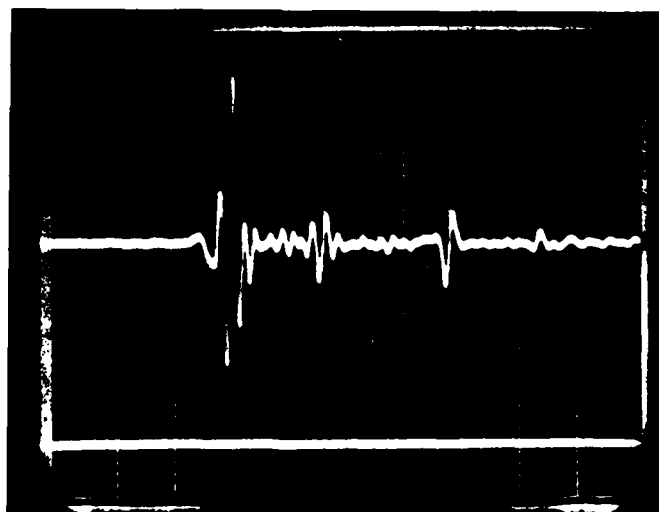


Repetition Rate	2K	Hz	Gated RF	Medium	/ Low
Damping Variable/Maximum	1	Ohms	Frequency	Greater Than 8	MHz
Energy	1		Peak Polarity	Negative	
Receiver Attenuation	6	dB	Gain	x10	
High Pass Filter	1.0	MHz	Gain	40	dB
Marked RF	Interface				

Figure 58. Analog C-scan of FP/Mg Specimen 6-2 (nonuniform fiber distribution), 15 MHz transducer in pulse-echo mode.



(a)



(b)

Figure 59. Amplitude-time records (A-scans) of ultrasonic pulse at two locations of Specimen 6-2 (nonuniform fiber distribution). (a) Unflawed location, (b) flawed location. (0.5 V/div, 0.5 μ s/div.) 15 MHz transducer in pulse-echo mode.

formed. The area was formed by removing a circular disk from the fibers forming the third and fourth plies of the specimen. When the molten magnesium matrix material was poured onto the stacked fiber laminate and migration along the fiber bundles occurred, the solid plies of fibers adjacent to the plies in which the disks were removed partially collapsed and "filled" the void area where the disks were removed. Once the magnesium solidified after cooling, there existed in the circular area a 6-ply FP/Mg composite with uneven ply spacing, surrounded by a ring of predominant pure magnesium transitioning into the evenly 8-ply FP/Mg composite. Therefore, the mid-thickness pulse in the A-scan was generated by the plies sagging into the circular area from which the fibers were removed and the fact that the fibers did not come into intimate contact with one another, but were separated by a small amount of pure matrix material giving the appearance of a delamination being present. The amplitudes of the front and back-face reflections did not apparently decrease because the change of the speed of the ultrasound through the area was not appreciable enough to appear on the oscilloscope.

The Type 6 specimens are unique in that the manufactured flaw is one where only the composition of the material changes as opposed to the material having a physical defect. This is an important distinction because this provides a basis for the determination of the difference between fabrication, quality control discontinuities, and service-related defects.

For Specimen 6-2, ultrasonic inspection gives a representative indication as to the presence and definition of areas of nonuniform fiber distribution.

3.6.3 Wave Propagation Velocity

Figure 60 shows the inspection locations on Specimen 6-2 where wave propagation velocity measurements were taken. Table 12 shows the wave propagation velocities for the 14 inspection locations shown in Figure 60, and the average wave propagation velocity of the first nine measurements. The average wave propagation velocity for Specimen 6-2 (for the unflawed locations) is within 6% of the theoretical value of 6119 ms^{-1} for Specimen 6-2 and within 1% of the empirical average of 6466 ms^{-1} for Specimen 1-1. As a comparison, the average wave propagation velocity for the 20 inspection locations shown in Figure 24 for Specimen 6-2 was 6466 ms^{-1} which is identical to the empirical average for Specimen 1-1.

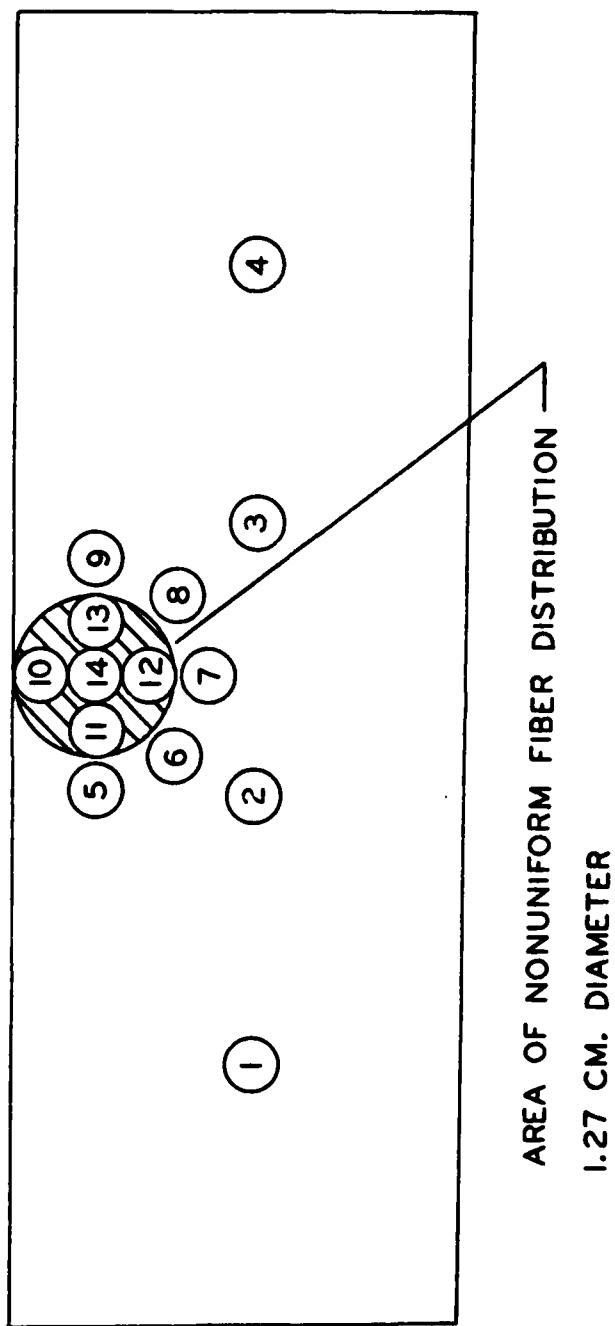


Figure 60. Wave propagation velocity inspection locations for FP/Mg Specimen 6-2 (nonuniform fiber distribution).

TABLE 12. WAVE PROPAGATION VELOCITY ACROSS
THE THICKNESS AT VARIOUS LOCATIONS
ALONG SPECIMEN CENTERLINE (SPECIMEN 6-2)

<u>Inspection Location</u>	<u>Velocity, ms⁻¹ (10⁵ in/sec)</u>
6-2-1	6499 (2.558)
6-2-2	6443 (2.536)
6-2-3	6469 (2.546)
6-2-4	6410 (2.523)
6-2-5	6433 (2.532)
6-2-6	6468 (2.546)
6-2-7	6443 (2.536)
6-2-8	6471 (2.547)
6-2-9	6484 (2.552)
6-2-10	6250 (2.460)
6-2-11	6263 (2.465)
6-2-12	6293 (2.477)
6-2-13	6260 (2.464)
6-2-14	6275 (2.470)
Average 6-2-1 to 6-2-9	6458 (2.542)
Average 6-2-10 to 6-2-14	6268 (2.467)

The wave propagation velocities for the five inspection locations (6-2-10 through 6-2-14) within the area of nonuniform fiber distribution as indicated by the C-scans (Figures 57 and 58) show a moderate decrease from that within the areas of no apparent material defect. The decrease of the wave propagation is a direct function of the change in composition of the material in that area. This is shown by the following equation:

$$C33_{6-2a} = (PCT \ C33_{1-1E})(C33_{1-1E}) + (PCT \ C33_{Mg})(C33_{Mg})$$

where $C33_{6-2a}$ = theoretical average wave propagation velocity within the area of nonuniform fiber distribution

$PCT \ C33_{1-1E}$ = percentage of the specimen thickness having the wave propagation velocity equal to the empirical average of Specimen 1-1 (= 0.75, since 6 of the 8-ply thickness is composite)

$C33_{1-1E}$ = empirical average wave propagation velocity of Specimen 1-1 (= 6466 ms^{-1})

$PCT \ C33_{Mg}$ = empirical average wave propagation velocity of the ZE41A magnesium coupon (= 5645 ms^{-1})

Replacing values,

$$C33_{6-2a} = (0.75)(6466) + (0.25)(5645) = 6261 \text{ ms}^{-1}$$

The theoretical value of the average wave propagation velocity is nearly identical to the measured average wave propagation velocity for the area of nonuniform fiber distribution for Specimen 6-2.

For Specimen 6-2, wave propagation velocity values give a clear indication of the presence of an area of nonuniform fiber distribution.

3.6.4 Wave Attenuation

Table 13 shows the material attenuation coefficients calculated for Specimen 6-2 from measurements taken using the water delay line and contact transducer techniques. The inspection locations indicated in Table 13 correspond to those shown on Figure 60.

The material attenuation coefficients for inspection locations 6-2-1 through 6-2-4 show good agreement with one another for the water delay line technique, but not so for the contact transducer technique. This is explained

TABLE 13. ULTRASONIC WAVE ATTENUATION COEFFICIENTS (SPECIMEN 6-2)

Inspection Location	Attenuation (α), dB		Specimen Thickness d_1 , cm (in.)	Material Attenuation (α), dB/cm (dB/in.)	
	Water Delay Line	Contact Transducer		Water Delay Line	Contact Transducer
6-2-1	0.291	0.242	0.62 (0.243)	0.47 (1.19)	0.39 (0.99)
6-2-2	0.273	0.291	0.62 (0.243)	0.44 (1.11)	0.47 (1.20)
6-2-3	0.273	0.329	0.62 (0.243)	0.44 (1.11)	0.53 (1.35)
6-2-4	0.293	0.256	0.61 (0.240)	0.48 (1.21)	0.42 (1.06)
6-2-14	0.477	0.335	0.62 (0.243)	0.77 (1.97)	0.54 (1.37)

by the fact that the surface of the specimen was very irregular (as shown in the C-scans, see Figures 57 and 58); hence, the measurements taken with the contact transducer were not as reproducible for Specimen 6-2 as the preceding specimens.

The material attenuation coefficient at inspection location 6-2-14 (within the area of nonuniform fiber distribution) is appreciably higher than those indicated for the other locations. This would be expected at an area of nonuniform fiber distribution because that type of defect causes a decrease in both local density and local modulus which increases the material wave attenuation coefficient.

For Specimen 6-2, wave attenuation coefficients give an indication of the presence of nonuniform fiber distribution.

3.6.5 X-Ray Radiography

Figure 61 shows the X-ray radiograph for Specimen 6-2. Although it cannot be seen in Figure 61, the circular area of nonuniform fiber distribution can be faintly seen in the original radiograph. An enhancement medium would not improve the quality of a radiograph of Specimen 6-2 since the defect is neither free surface attached (which provides a flow path for the medium), or the type of defect into which the medium could flow if it were free surface attached.

For Specimen 6-2, X-ray radiography gives a faint indication of the presence of an area of nonuniform fiber distribution.



Figure 61. X-ray radiograph of FP/Mg specimen with nonuniform fiber distribution (Specimen 6-2).

3.6.6 Ultrasonic Backscattering

Figure 62 is a backscatter curve of Specimen 6-2. The incident angle (α) of the 5 MHz immersion transducer operated in the pulse-echo mode was 20° with respect to a line normal to the front-face surface plane of the specimen.

This curve gives no indication of the presence of an area of nonuniform fiber distribution beyond the decrease of the amplitude of the reflected pulse. The only activity on the curve occurs when the transducer focal axis sweeps near and through the plane normal to the fiber orientation.

For Specimen 6-2, ultrasonic backscattering does not appear to give any appreciable indication of the presence of an area of nonuniform fiber distribution.

3.6.7 Micrographic Inspection

Figures 63 and 64 show three micrographs each of sections cut and polished from Specimen 6-2.

The micrographs in Figure 63 show the area (highlighted with arrows) of nonuniform fiber distribution. There is a line of demarcation on either side of the "defect." The bright white spots on the micrographs are calcium deposits left on the specimen after immersion. Figure 63a shows the poor surface condition of the specimen when the section was cut and photographed. A disturbing fact about the surface degradation is that this specimen was polished on the front and back-face surfaces before the NDE assessment was started. This degradation effect was seen on several specimens (both polished and unpolished) even though special handling considerations were taken after the specimens were immersed for ultrasonic inspection. The specimens seemed to hold water, which probably accelerated the degradation mechanism. It does not appear that this material, unless treated with a moisture barrier, is particularly suited for use in a humid environment.

At 200X, the area of nonuniform fiber distribution is apparent in Figure 64b when compared with Figures 64a and 64c. The micrographs shown as Figures 64a and 64c were taken at sections cut through inspection locations 1 and 4 as shown in Figure 60. These two locations have no intentional flaws or defects. Figures 64a and 64c are very similar to the micrographs shown in Figure 28 for Specimen 1-1 (no intentional flaws) as would be expected. The major difference between the micrograph of the area of nonuniform fiber distribution

IIT RESEARCH INSTITUTE

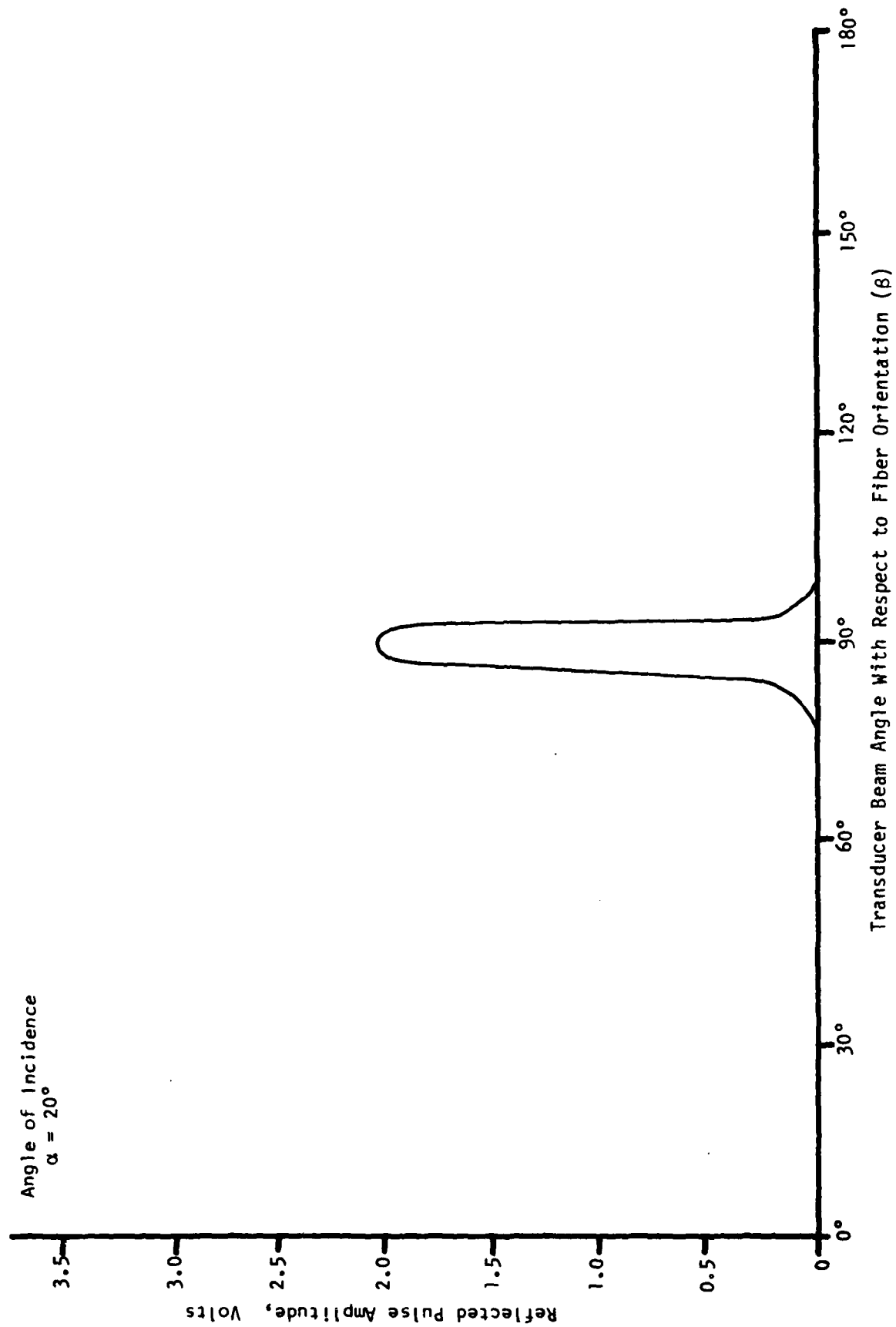


Figure 62. Ultrasonic backscattering curve of FP/Mg specimen with nonuniform fiber distribution (Specimen 6-2).

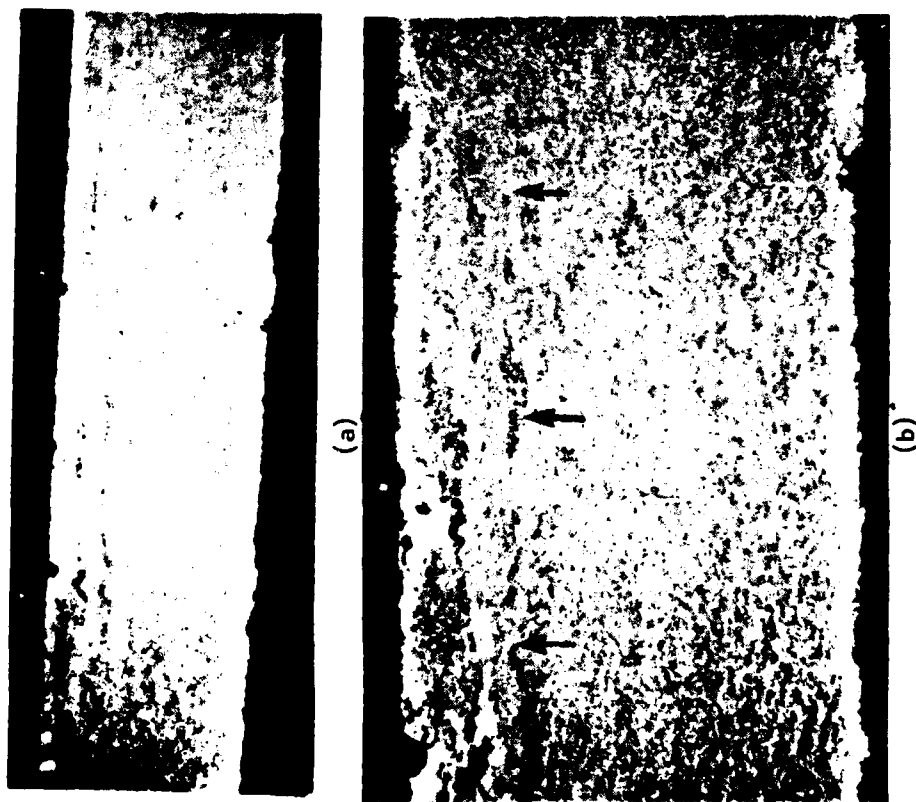
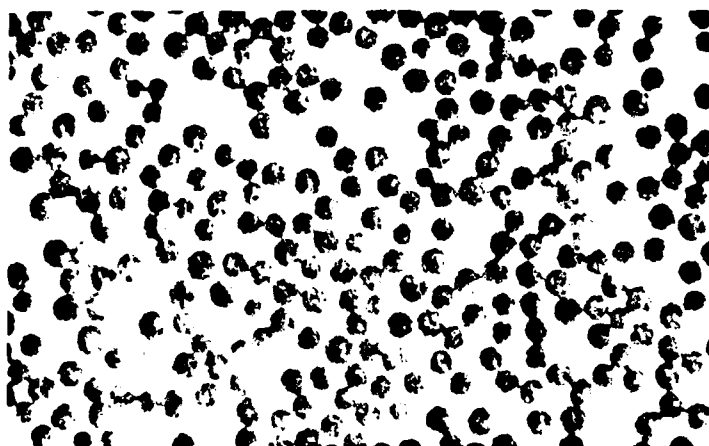
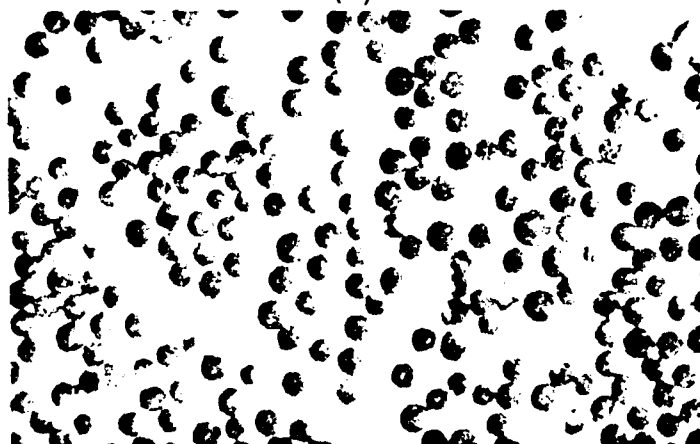


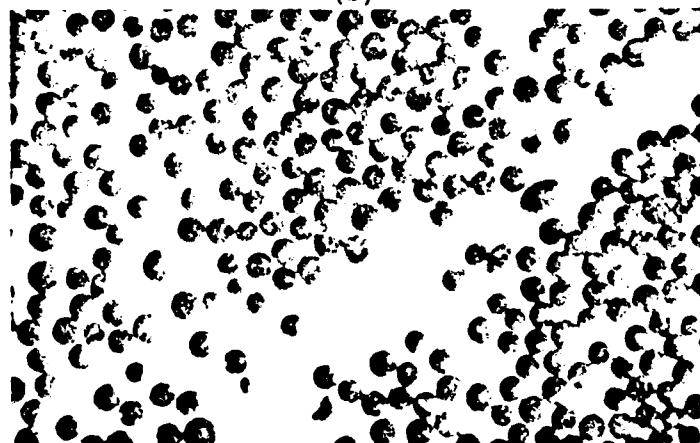
Figure 63. Micrographs of FP/Mg Specimen 6-2 (nonuniform fiber distribution):
 (a) 5X, (b) 12X, and (c) 24X magnification.



(a)



(b)



(c)

Figure 64. Micrographs (200X) of FP/Mg Specimen 6-2 (nonuniform fiber distribution) at three section locations: (a) Location 6-2-1, (b) Location 6-2-2, and (c) Location 6-2-3.

(Figure 64b) and the other micrographs (Figures 64a and 64c) is that there is a greater percentage of the matrix visible. This is exactly what was expected since the area of nonuniform fiber distribution was created by removing two fiber plies from the laminate in the circular area indicated in the C-scans (Figures 57 and 58).

3.6.8 Comparison of Inspection Procedures

Of the NDE procedures used to evaluate Specimen 6-2, ultrasonic inspection, wave propagation velocity, wave attenuation, and X-ray radiography indicated the presence of an area of nonuniform fiber distribution. Both C-scan types showed the location and extent of the flawed area and interpretation of the A-scans yielded important information about the through-the-thickness position and attenuative nature of the flawed area. Wave propagation velocity data and calculated material attenuation theory in differentiating unflawed from flawed areas of the specimen. X-ray radiography showed that the shape and extent of the area of nonuniform fiber distribution could be determined by a method other than ultrasonic inspection.

Ultrasonic backscattering provided virtually no information as to the state of material integrity of Specimen 6-2.

3.7 TYPE 7 SPECIMEN

The representative specimen for the Type 7 group, with matrix fracture, is Specimen 7-2.

3.7.1 Physical Properties

The pertinent physical properties for Specimen 7-2 are as follows:

$$\begin{aligned}L_{7-2} &= 12.80 \text{ cm (5.039 in.)} \\W_{7-2} &= 3.83 \text{ cm (1.506 in.)} \\T_{7-2} &= 0.59 \text{ cm (0.232 in.)} \\M_{7-2} &= 81.0807 \text{ g (0.178 lb)} \\ \rho_{7-2} &= 2.80 \text{ g/cm}^3 \text{ (0.101 lb/in}^3\text{)} \\C_{337-2} &= 6209 \text{ ms}^{-1} \text{ (244,400 in/sec).}\end{aligned}$$

The physical properties of ρ_{7-2} and C_{337-2} are within an acceptable tolerance of $\pm 5\%$ from the baseline values.

3.7.2 Ultrasonic Inspection

Figures 65 and 66 are pen-lift and analog C-scans, respectively, of Specimen 7-2. Both C-scans were generated using a 5 MHz, immersion, compression wave transducer operated in the pulse-echo mode with the specimen held in the special fixture.

Both C-scans give a clear indication of the presence of a flawed area within Specimen 7-2. The C-scans agree very well with respect to the location and extent of the flawed area. Figure 67 shows an A-scan photograph at an unflawed location (Figure 67a) and within the area of apparent matrix fracture (Figure 67b). Figure 67a is a typical A-scan of a location of unflawed FP/Mg material. There is a well-defined front and back-face reflection which is, once again, very similar to the A-scan (Figure 22a) of Specimen 1-1 with no intentional flaws.

Figure 67b shows a pronounced change in the shape of the front-face reflection and the amplitude of the back-face reflection of the ultrasonic waveform within the area of matrix fracture. The front-face reflected pulse shape is unique to any of the others shown previously for flawed locations of the FP/Mg composite material. A visual inspection of Specimen 7-2 did not reveal any surface irregularities which could have caused the change of the front-face reflection. This indicates that the matrix fracture was located near the front-face of the specimen through-the-thickness and was wave energy dissipative. The wave energy dissipation conclusion is based on the reduction of amplitude of the front and back-face pulses.

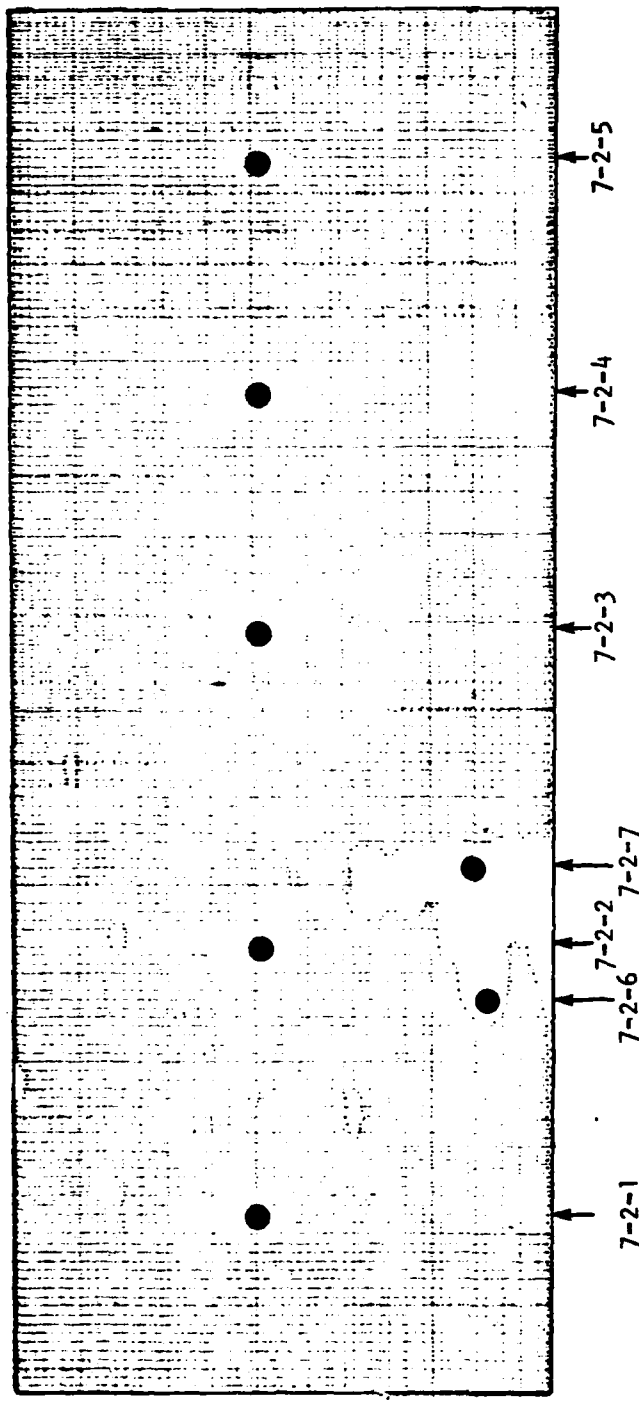
For Specimen 7-2, ultrasonic inspection gives an indication of the presence, location, and extent of an area of matrix fracture.

3.7.3 Wave Propagation Velocity

Table 14 shows the wave propagation velocities for the seven inspection locations shown in Figure 65.

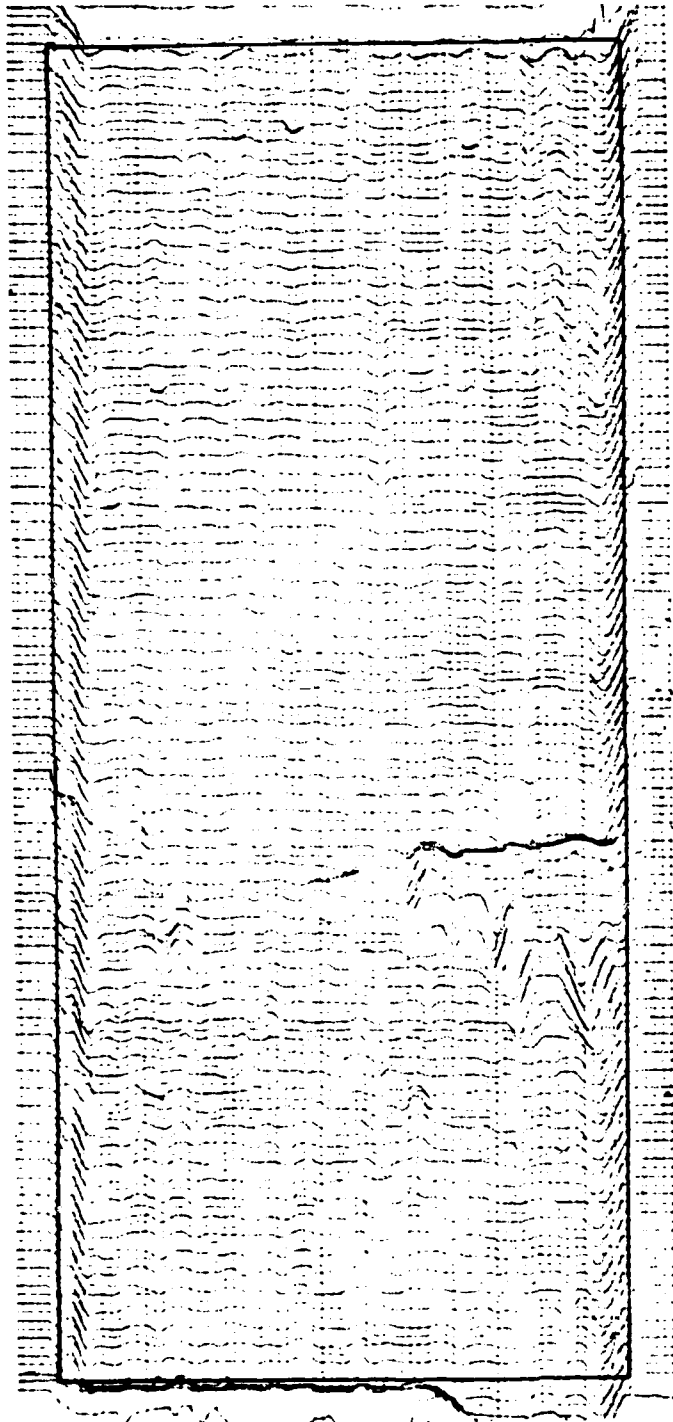
The wave propagation velocities for inspection locations 7-2-1 through 7-2-5 (apparently unflawed area) are very consistent with one another and the average propagation velocity of those five measurements is within 1% of the empirical average propagation velocity of 6466 ms^{-1} for Specimen 1-1. This indicates that the material integrity of Specimen 7-2 at locations 7-2-1 through 7-2-5 is comparable to that of Specimen 1-1, i.e., has no flaws.

IIT RESEARCH INSTITUTE



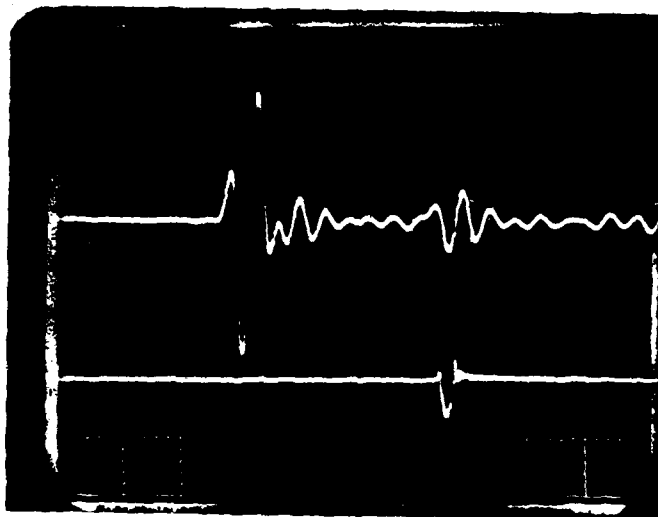
Repetition Rate	2K	Hz	Gated RF	Medium	/ Low
Damping Variable/Maximum	4	Ohms	Frequency	Less Than 8	MHz
Energy			Peak Polarity	Negative	
Receiver Attenuation	0	dB	Gain	x10	
High Pass Filter	1.0	MHz	Gain	20	dB
Marked RF	Interface				

Figure 65. Pen-lift C-scan of FP/Mg Specimen 7-2 (matrix fracture), 5 MHz transducer in pulse-echo mode.

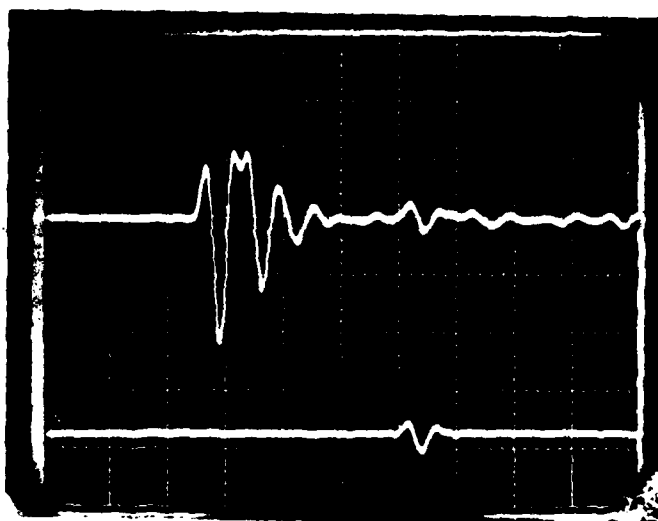


Repetition Rate	2K	Hz	Gated RF	Medium / Low
Damping	Variable/Maximum	Ohms	Frequency	Less Than 8 MHz
Energy	4		Peak Polarity	Negative
Receiver Attenuation	0	dB	Gain	x10
High Pass Filter	1.0	MHz	Gain	20 dB
Marked RF	Interface			

Figure 66. Analog C-scan of FP/Mg Specimen 7-2 (matrix fracture), 5 MHz transducer in pulse-echo mode.



(a)



(b)

Figure 67. Amplitude-time records (A-scans) of ultrasonic pulse at two locations of Specimen 7-2 (matrix fracture). (a) Unflawed location, (b) flawed location. (0.5 V/div, 0.5 μ s/div.) 5 MHz transducer in pulse-echo mode.

IIT RESEARCH INSTITUTE

TABLE 14. WAVE PROPAGATION VELOCITY ACROSS
THE THICKNESS AT VARIOUS LOCATIONS
ALONG SPECIMEN CENTERLINE (SPECIMEN 7-2)

<u>Inspection Location</u>	<u>Velocity, ms⁻¹ (10⁵ in/sec)</u>
7-2-1	6464 (2.544)
7-2-2	6463 (2.543)
7-2-3	6393 (2.516)
7-2-4	6380 (2.511)
7-2-5	6451 (2.539)
Average 7-2-1 to 7-2-5	6430 (2.531)
7-2-6	6163 (2.426)
7-2-7	6151 (2.421)
Average 7-2-6, 7-2-7	6157 (2.423)

TABLE 15. ULTRASONIC WAVE ATTENUATION COEFFICIENTS (SPECIMEN 7-2)

<u>Inspection Location</u>	<u>Attenuation (α), dB</u>		<u>Specimen Thickness d_1, cm (in.)</u>	<u>Material Attenuation (α), dB/cm (dB/in.)</u>	
	<u>Water Delay Line</u>	<u>Contact Transducer</u>		<u>Water Delay Line</u>	<u>Contact Transducer</u>
7-2-1	0.236	0.254	0.59 (0.232)	0.40 (1.02)	0.43 (1.09)
7-2-2	0.248	0.242	0.59 (0.232)	0.42 (1.07)	0.41 (1.04)
7-2-3	0.236	0.224	0.59 (0.232)	0.40 (1.02)	0.38 (0.97)
7-2-4	0.230	0.254	0.59 (0.232)	0.39 (0.99)	0.43 (1.09)
7-2-5	0.248	0.260	0.59 (0.232)	0.42 (1.07)	0.44 (1.12)
7-2-6	0.419	0.472	0.59 (0.232)	0.71 (1.81)	0.80 (2.03)
7-2-7	0.443	0.449	0.59 (0.232)	0.75 (1.91)	0.76 (1.94)

The wave propagation velocities for inspection locations 7-2-6 and 7-2-7 are noticeably lower than those mentioned above. This indicates that the flawed area, shown in Figures 65 and 66, is modestly wave energy dissipative.. This corresponds well with the conclusions drawn from ultrasonic inspection.

For Specimen 7-2, wave propagation velocity gives an indication of the presence of an area of matrix fracture.

3.7.4 Wave Attenuation

Table 15 shows the material attenuation coefficients calculated for Specimen 7-2 from measurements taken using the water delay line and contact transducer techniques. The inspection locations indicated in Table 15 correspond to those shown on Figure 65.

The material attenuation coefficients at all the unflawed (7-2-1 through 7-2-5) inspection locations, for both inspection techniques, show very good agreement with one another. These coefficients favorably agree with similar coefficients for Specimen 1-1. This again indicates that the material integrity at inspection locations 7-2-1 through 7-2-5 was of a uniform nature and similar to that of the unflawed Specimen 1-1.

The material attenuation coefficients at the flawed (7-2-6 and 7-2-7) inspection locations also show very good agreement with one another (for both techniques). These attenuation coefficients are appreciably higher than those for the unflawed inspection locations, which indicates the presence of an attenuative defect such as matrix fracture. Matrix fracture decreases the local modulus of a composite and means the ultrasound does not pass through a continuous material. Both of these results is an increase in the wave attenuation coefficient on a local basis.

For Specimen 7-2, wave attenuation coefficients give an indication of the presence of matrix fracture.

3.7.5 X-Ray Radiography

Figure 68 shows the X-ray radiograph for Specimen 7-2. This radiograph has a definite contrast change, corresponding to the flawed area of Figure 65 and indicating the presence of an area of matrix fracture. It is very possible that an enhancement medium could be used to improve the contrast



Figure 68. X-ray radiograph of FP/Mg specimen with matrix fracture (Specimen 7-2).

difference of Figure 68 since the area of matrix fracture is open to a free surface of the specimen.

For Specimen 7-2, X-ray radiography gives an indication of the presence of an area of matrix fracture.

3.7.6 Ultrasonic Backscattering

Figure 69 is a backscatter curve of Specimen 7-2. The incident angle () of the 5 MHz immersion transducer operated in the pulse-echo mode was 20° with respect to a line normal to the front-face surface plane of the specimen.

This curve gives no indication of the presence of an area of matrix fracture beyond the decrease of the amplitude of the reflected pulse. The only activity on the curve occurs when the transducer focal axis sweeps near and through the plane normal to the fiber orientation.

For Specimen 7-2, ultrasonic backscattering does not appear to give any appreciable indication of the presence of an area of matrix fracture.

3.7.7 Micrographic Inspection

Figures 70 and 71 show four micrographs each of sections cut and polished from Specimen 7-2. The section locations (7-2-1 through 7-2-4) indicated on Figure 70 correspond to inspection locations 7-2-1 through 7-2-4, respectively, on Figure 65.

The low magnification micrographs shown in Figure 70 do not indicate the presence of the defect shown in the ultrasonic C-scans. Some trace of the

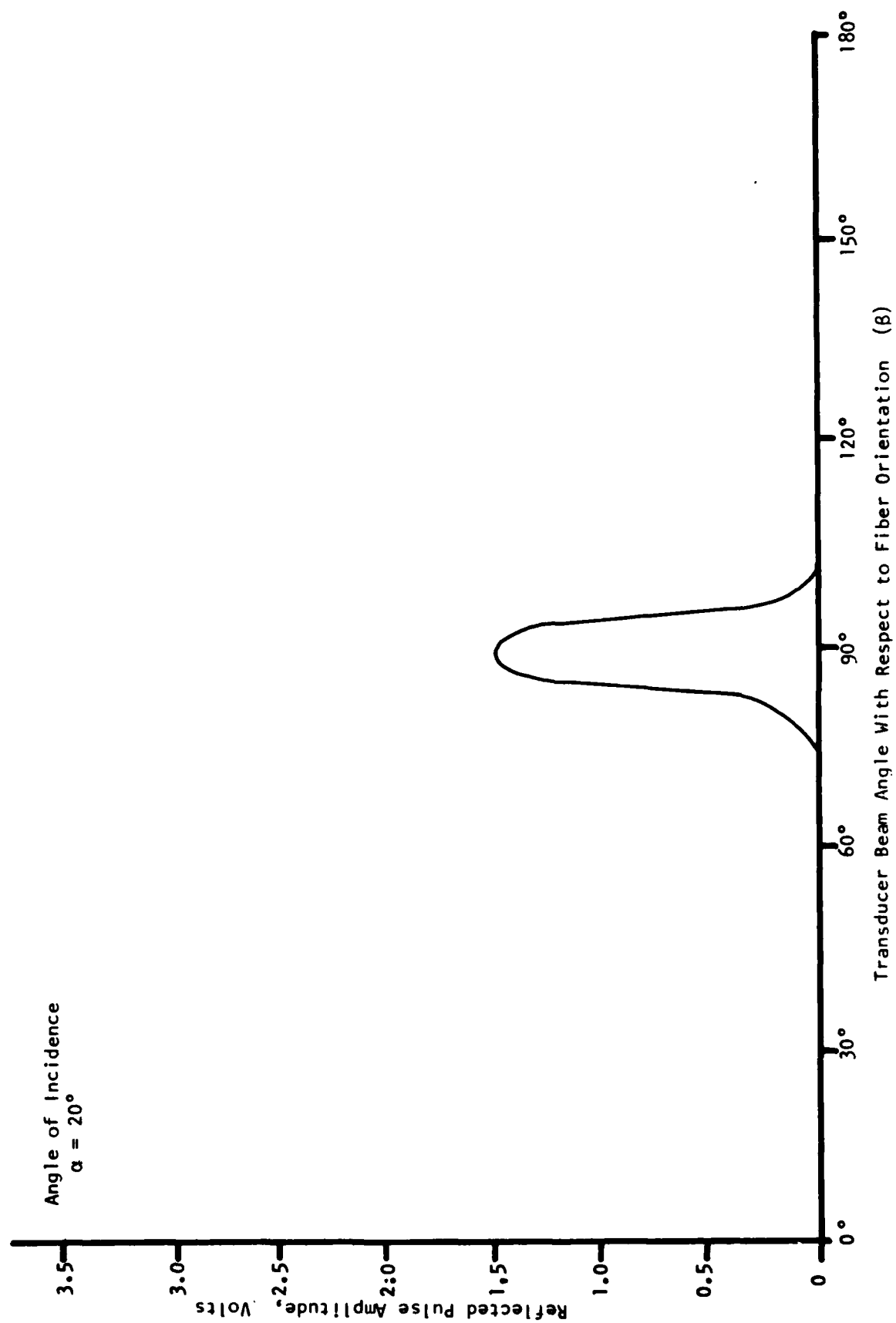
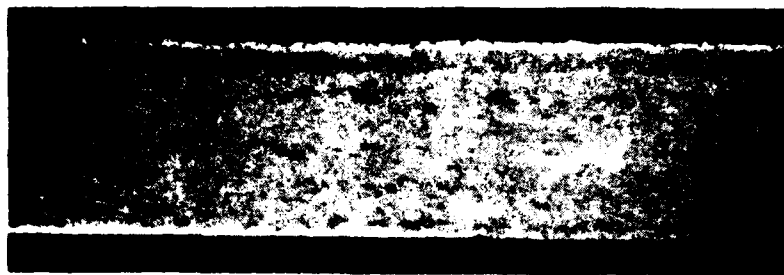


Figure 69. Ultrasonic backscattering curve of FP/Mg specimen with matrix fracture (Specimen 7-2)



(a)



(b)



(c)



(d)

Figure 70. Micrographs of FP/Mg Specimen 7-2 (matrix fracture) at four section locations: (a) Location 7-2-1, (b) location 7-2-2, (c) location 7-2-3, and (d) location 7-2-4.

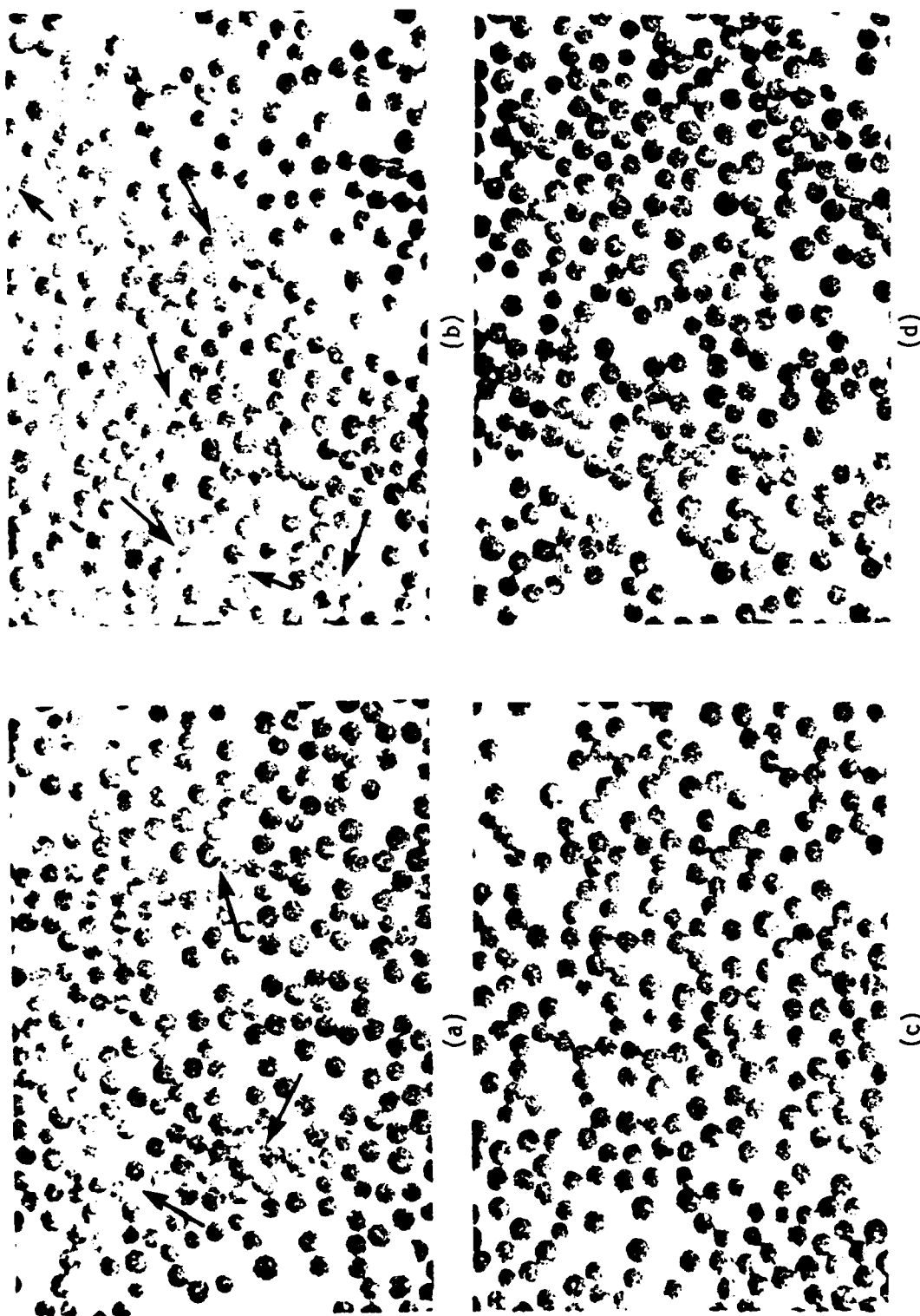


Figure 71. Micrographs (200X) of FP/Mg Specimen 7-2 (matrix fracture) at four section locations:
 (a) Location 7-2-1, (b) Location 7-2-2, (c) Location 7-2-3, and (d) Location 7-2-4.

matrix fracture should have been visible in Figure 70b since the section was cut through the flawed area indicated on Figure 65.

The 200X micrographs shown in Figure 71 indicate the presence of a material discontinuity which may be matrix fracture. The discontinuities (highlighted with arrows) can be seen to some extent in Figure 71a, but to a much greater extent in Figure 71b. The discontinuity appears as tendrils in the matrix connecting adjoining fiber bundles. This is the form that matrix fracture would be expected to take; therefore, it may be concluded that the area shown in micrograph Figure 71b contains matrix fracture.

3.7.8 Comparison of Inspection Procedures

Of the NDE procedures used to evaluate Specimen 7-2, ultrasonic inspection, wave propagation velocity, wave attenuation, and X-ray radiography indicated the presence of an area of matrix fracture. Both C-scan types showed the location and extent of the flawed area and interpretation of the A-scans yielded information about the through-the-thickness position and attenuative nature of the flawed area. Wave propagation velocity data and calculated material attenuation coefficients agreed very well with the C-scans and ultrasonic attenuation data in differentiating unflawed from flawed areas of the specimen. X-ray radiography showed that the shape and extent of the area of matrix fracture could be determined by a method other than ultrasonic inspection.

Ultrasonic backscattering provided virtually no information as to the state of material integrity of Specimen 7-2.

3.8 SUMMARY OF RESULTS

Table 16 summarizes the results presented in the preceding subsections. The ultrasonic inspection and wave propagation velocity techniques were more widely applicable to different flaw types than were the wave attenuation, X-ray radiography, and ultrasonic backscattering techniques. The only flaw type which ultrasonic inspection or wave propagation velocity could not detect was the misaligned fibers, a defect which only ultrasonic backscattering could determine. Since ultrasonic inspection is the only technique which gives a pictorial representation (C-scans) of the material flaw pattern within a specimen, and since it was applicable to the most flaw types, it is the conclusion

TABLE 16. SUMMARY OF RESULTS ON NDE TECHNIQUES FOR DETECTION OF FLAWS

Specimen	Ultrasonic Inspection			Wave Attenuation			X-Ray Radiography		Ultrasonic Backscattering
	Pen-Lift	C-Scan Analog	A-Scan	Wave Propagation	Water Delay Line	Contact Transducer	Unenhanced	Enhanced	
1-1	OK	OK	OK	OK	OK	OK	OK	OK	OK
2-1	Y	Y	Y	Y	N	N	Y	P	N
3-1	Y	Y	Y	Y	Y	Y	N	P	N
4-1	N	N	N	N	N	N	N	P	Y
5-1	N (P)	Y	Y	Y	Y	Y	N	P	N
6-2	Y	Y	Y	Y	Y	Y	Y	N	N
7-2	Y	Y	Y	Y	Y	Y	Y	P	N

OK - Show further applicability of the inspection technique based on the results of inspection of specimen 1-1.

Y - Provided a positive indication of the presence of the flaw type in the specimen indicated.

N - Did not provide any indication of the presence of the flaw type in the specimen indicated.

P - Indicates that an equipment or procedure change may make the inspection applicable for the detection of the flaw type in the specimen indicated.

of this investigation that the ultrasonic inspection technique is the best of the NDE techniques evaluated for determining the material integrity of FP/Mg composites. It is also concluded that amplitude-time records (A-scans), wave propagation velocities, and wave attenuation coefficients provide valuable information about the through-the-thickness characteristics and physical nature of flaws detected by ultrasonic inspection. It is apparent from the data generated during this program that no single NDE technique that was evaluated can provide all the information required to adequately define the state of material integrity of FP/Mg composites.

Based on the results and conclusions of this investigation, it is recommended that additional work be conducted in evaluating the applicability of NDE to metal matrix composites. Suggestions for additional work include the use of higher frequency (greater than 15 MHz) transducers in ultrasonic inspection or frequency distribution analyses. Also, it is recommended that NDE be applied to FP/Mg specimens subjected to an "in service" simulation of applied loads. This type of investigation would indicate which NDE techniques could map increases in flaw size as a function of load application.

4. SUMMARY AND CONCLUSIONS

The objective of this program was to apply nondestructive evaluation methods to assess the integrity of FP/magnesium composites.

The program was performed using an existing ultrasonic detection and recording system using compression wave transducers operated in the pulse-echo mode at five frequencies of 1, 2.25, 5, 10, and 15 MHz. Additionally, low energy X-ray radiography was done with a commercially available X-ray unit.

It was found that ultrasonic inspection with a 15 MHz transducer generating an analog C-scan gave the best pictorial representation of the presence of a majority of the flaw types investigated. Pen-lift C-scans were comparable to analog C-scans for most of the flaw types investigated and, where they were not comparable, an increase in transducer frequency could be expected to make them comparable to the analog C-scans. A-scans, wave propagation velocities, and wave attenuation coefficients corresponded very well with the C-scans, but since they are point inspection procedures, they are difficult to use to map the extent of flaws. Unenhanced X-ray radiography was applicable to approximately half of the flaw types investigated, and indications are that the use of enhancement media would considerably increase the applicability of X-ray radiography. Although used only cursorily, ultrasonic backscattering gave little indication of applicability to more than one specific flaw type. An encouraging result of this program is that although the FP/Mg composite is a relatively sophisticated material to fabricate and use, its integrity can be determined without using exotic inspection techniques or equipment. This is impressive in the light of the number of specimens and number of flaw types investigated.

5. ACKNOWLEDGEMENT

The IIT Research Institute would like to thank Drs. Alan Champion and Hank Nusbaum of E. I. DuPont's Textile Fibers Department of the Pioneering Research Laboratory for their cooperation in the specification and fabrication of metal matrix composite specimens used in this project.

IIT RESEARCH INSTITUTE

REFERENCES

1. Hybrid and Select Metal Matrix Composite, Ed. by W.J. Renton, American Institute of Aeronautics and Astronautics, New York, NY, 1977.
2. McMaster, R. C., Ed., Nondestructive Testing Handbook, The Ronald Press, New York, NY, 1963.
3. Krautkramer, J. and Krautkramer, H., Ultrasonic Testing of Materials, Springer-Verlag, Inc., New York, 1969.
4. Fredric, J. R., Ultrasonic Engineering, John Wiley & Sons, Inc., New York, 1965.
5. Rose, J. L., Carson, J. M* and Leidel, D. J., "Ultrasonic Procedures for Fibers and Composites, ASTM STP 521, 1973, pp. 311-325.
6. Gericke, O. R., "Ultrasonic Spectroscopy," Research Techniques in Non-destructive Testing, Sharpe, R. S., Ed., Academic Press, New York, 1970, pp. 31-61.
7. Chang, F. H., Kline, R. A. and Bell, J. R., "Ultrasonic Evaluation of Adhesive Bond Strength Using Spectroscopic Techniques," General Dynamics, Fort Worth Division, Proceedings ARPA/AFML Review of Progress in Quantitative NDE, Scripps Institution of Oceanography, La Jolla, CA, July 18-21, 1978.
8. "Interdisciplinary Program for Quantitative Flaw Detection," Rockwell International Science Center, Contract No. F33615-74-C-5180, for ARPA/AFML, September, 1975.
9. Mucciardi, A. N., et.al., "Adaptive Nonlinear Signal Processing for Characterization of Ultrasonic NDE Waveforms," Task 2, Measurement of Subsurface Fatigue Crack Size, Technical Report AFML-TR-76-44, April 1976.
10. Bar-Cohen, Y. and Crane, R. L., "Nondestructive Evaluation of Fiber-Reinforced Composites with Backscattering Measurements."
11. Dhingra, A. K., "Inorganic Alumina Fibers for Reinforcement of Metal Castings," E. I. DuPont De Nemours & Co., Inc., p. 19.
12. "Advanced Composite Serviceability Program," IIT Research Institute sub-contract to Rockwell International, Air Force Materials and Flight Dynamics Laboratories, Contract NO. F33615-76-C-5344.
13. "Test System for Conducting Biaxial Test of Composite Laminates," Air Force Flight Dynamics Laboratories, Contract No. F33615-77-3014.
14. "Sensitivity of Ultrasonic Detection of Delaminations and Disbonds in Composite Laminates and Joints," David W. Taylor Naval Ship R&D Center, Contract No. N00167-78-C-0085.

IIT RESEARCH INSTITUTE

APPENDIX

PROCEDURES USED TO GENERATE SPECIMEN DEFECTS

IIT RESEARCH INSTITUTE

PROCEDURES USED TO GENERATE SPECIMEN DEFECTS

The following is a brief description of the procedures used to generate the defects in the metal matrix specimens used in this project.

- o Type 1: No intentional flaws (self explanatory).
- o Type 2: Fiber Matrix Debonding. The flaws were obtained by applying a release agent (boron nitride) to the two middle plies of the FP fiber stack before the magnesium alloy was introduced. The release agent prevented the matrix material from wetting the fibers.
- o Type 3: Porosity. Porosity was produced by controlling the cooling rate and amount of make-up material added to the casting mold. By accelerated cooling and depriving the mold of make-up material, shrinkage voids, but not cracks, could be generated in the matrix.
- o Type 4: Fiber Misalignment. Fiber misalignment was created by cutting the middle two plies in such a way that the fibers were oriented at 10-deg with the longitudinal axis of the specimen.
- o Type 5: Fiber Fracture. Fiber fracture was generated by cutting the second, fourth, and sixth fiber plies at staggered positions along the length of the specimen. When the fiber plies were stacked, the cut plies were separated by approximately 0.32 cm (0.13 in.) providing a migration path for the matrix material.
- o Type 6: Nonuniform Fiber Distribution. In two of the specimens, nonuniform fiber distribution was created by removing a 1.3 cm (0.5 in.) wide strip of fibers from the fourth and fifth plies of the laminate parallel to the longitudinal axis of the specimen. In the third specimen, a 1.3 cm (0.5 in.) diameter hold was cut in the fourth fiber ply near the center of the specimen.
- o Type 7: Matrix Fracture. Matrix fracture was created by quenching the cooling casting in a liquid nitrogen bath.

NONDESTRUCTIVE EVALUATION OF METAL MATRIX COMPOSITES

Final Report

(Unclassified)

Contract DAAG46-80-C-0070
Work Unit D/A Project: IL2611027071

ITT Research Institute
May 1982

ABSTRACT: The objective of the program was to apply nondestructive evaluation (NDE) methods to assess the integrity of P/magnesium composites. The material investigated was ZEK1A magnesium alloy reinforced with P (aluminum oxide) fibers. The 21 specimens (three specimens of each of six flaw types and three unfilled specimens) were evaluated using ultrasonic scanning, wave propagation velocity, wave attenuation, and X-ray radiograph inspection techniques. The specimens evaluated were 12.7 cm (5 in.) long x 3.8 cm (1.5 in.) wide x 0.6 cm (0.25 in.) thick, with a fiber volume fraction of 0.50. After the NDE inspections were completed, a representative specimen from each of the seven groups was sectioned and micrographs were made for comparison with the NDE results. It was found that ultrasonic scanning using a 15 MHz compressional wave, focused transducer operated in the pulse-echo mode generating an analog C-scan gave the best results. The wave attenuation and wave propagation velocity measurements were found to be very consistent with the ultrasonic C-scans, but X-ray radiography was useful only at locations of gross material defect.

NONDESTRUCTIVE EVALUATION OF METAL MATRIX COMPOSITES

Final Report

(Unclassified)

Contract DAAG46-80-C-0070
Work Unit D/A Project: IL2611027071

ITT Research Institute
May 1982

ABSTRACT: The objective of the program was to apply nondestructive evaluation (NDE) methods to assess the integrity of P/magnesium composites. The material investigated was ZEK1A magnesium alloy reinforced with P (aluminum oxide) fibers. The 21 specimens (three specimens of each of six flaw types and three unfilled specimens) were evaluated using ultrasonic scanning, wave propagation velocity, wave attenuation, and X-ray radiograph inspection techniques. The specimens evaluated were 12.7 cm (5 in.) long x 3.8 cm (1.5 in.) wide x 0.6 cm (0.25 in.) thick, with a fiber volume fraction of 0.50. After the NDE inspections were completed, a representative specimen from each of the seven groups was sectioned and micrographs were made for comparison with the NDE results. It was found that ultrasonic scanning using a 15 MHz compressional wave, focused transducer operated in the pulse-echo mode generating an analog C-scan gave the best results. The wave attenuation and wave propagation velocity measurements were found to be very consistent with the ultrasonic C-scans, but X-ray radiography was useful only at locations of gross material defect.

NONDESTRUCTIVE EVALUATION OF METAL MATRIX COMPOSITES

Final Report

(Unclassified)

Contract DAAG46-80-C-0070
Work Unit D/A Project: IL2611027071

ITT Research Institute
May 1982

ABSTRACT: The objective of the program was to apply nondestructive evaluation (NDE) methods to assess the integrity of P/magnesium composites. The material investigated was ZEK1A magnesium alloy reinforced with P (aluminum oxide) fibers. The 21 specimens (three specimens of each of six flaw types and three unfilled specimens) were evaluated using ultrasonic scanning, wave propagation velocity, wave attenuation, and X-ray radiograph inspection techniques. The specimens evaluated were 12.7 cm (5 in.) long x 3.8 cm (1.5 in.) wide x 0.6 cm (0.25 in.) thick, with a fiber volume fraction of 0.50. After the NDE inspections were completed, a representative specimen from each of the seven groups was sectioned and micrographs were made for comparison with the NDE results. It was found that ultrasonic scanning using a 15 MHz compressional wave, focused transducer operated in the pulse-echo mode generating an analog C-scan gave the best results. The wave attenuation and wave propagation velocity measurements were found to be very consistent with the ultrasonic C-scans, but X-ray radiography was useful only at locations of gross material defect.

NONDESTRUCTIVE EVALUATION OF METAL MATRIX COMPOSITES

Final Report

(Unclassified)

Contract DAAG46-80-C-0070
Work Unit D/A Project: IL2611027071

ITT Research Institute
May 1982

ABSTRACT: The objective of the program was to apply nondestructive evaluation (NDE) methods to assess the integrity of P/magnesium composites. The material investigated was ZEK1A magnesium alloy reinforced with P (aluminum oxide) fibers. The 21 specimens (three specimens of each of six flaw types and three unfilled specimens) were evaluated using ultrasonic scanning, wave propagation velocity, wave attenuation, and X-ray radiograph inspection techniques. The specimens evaluated were 12.7 cm (5 in.) long x 3.8 cm (1.5 in.) wide x 0.6 cm (0.25 in.) thick, with a fiber volume fraction of 0.50. After the NDE inspections were completed, a representative specimen from each of the seven groups was sectioned and micrographs were made for comparison with the NDE results. It was found that ultrasonic scanning using a 15 MHz compressional wave, focused transducer operated in the pulse-echo mode generating an analog C-scan gave the best results. The wave attenuation and wave propagation velocity measurements were found to be very consistent with the ultrasonic C-scans, but X-ray radiography was useful only at locations of gross material defect.

MEI
8